

DIGITALLY-TUNABLE SURFACE ACOUSTIC WAVE RESONATOR

by

Robert Russell Hay

A dissertation

submitted in partial fulfillment

of the requirements for the degree of

Doctor of Philosophy in Electrical and Computer Engineering,

Boise State University

June 2009

© 2009

Robert R. Hay

ALL RIGHTS RESERVED

BOISE STATE UNIVERSITY GRADUATE COLLEGE

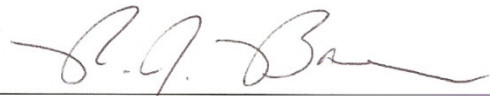
DEFENSE COMMITTEE APPROVAL

of the dissertation submitted by

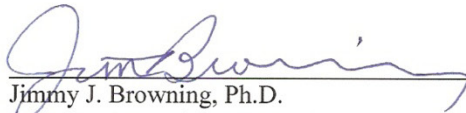
Robert Russell Hay

We have read and discussed the dissertation submitted by student Robert Russell Hay, and we have evaluated his presentation and response to questions during the final oral examination. We find that the student has passed the final oral examination. The dissertation is satisfactory for a doctoral degree and ready for any final modifications that we may explicitly require.

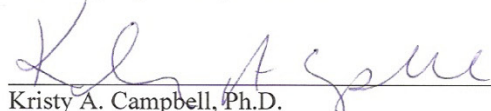
6/8/09
Date


R. Jacob Baker, Ph.D.
Chair, Supervisory Committee

6/8/09
Date


Jimmy J. Browning, Ph.D.
Member, Supervisory Committee

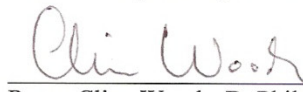
6/8/09
Date


Kristy A. Campbell, Ph.D.
Member, Supervisory Committee

06/08/09
Date


Wan Kuang, Ph.D.
Member, Supervisory Committee

06/08/09
Date


Roger Clive Woods, D.Phil., D.Sc.
External Examiner

BOISE STATE UNIVERSITY GRADUATE COLLEGE

FINAL READING APPROVAL

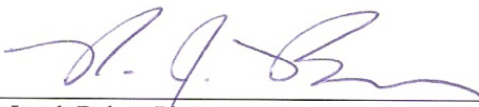
of the dissertation submitted by

Robert Russell Hay

To the Graduate College of Boise State University:

I have read the dissertation of Robert Russell Hay in its final form and have found that (1) the modifications required by the defense committee are complete; (2) the format, citations, and bibliographic style are consistent and acceptable; (3) the illustrative materials including figures, tables, and charts are in place; and (4) the final manuscript is ready for submission to the Graduate College.

6/15/09
Date



R. Jacob Baker, Ph.D.
Chair, Supervisory Committee

Approved for the Graduate College:

Date

John R. Pelton, Ph.D.
Dean of the Graduate College

DEDICATION

To Anne.

ACKNOWLEDGMENTS

I am deeply indebted to my advisor Dr. Jake Baker for the guidance and encouragement he has provided during my student and faculty experience at BSU. His energy and terrific desire to instill quality in the educational and research processes are characteristics I can only hope to emulate. I would like to also thank the other members of my dissertation committee who devoted their time and effort to this project and provided considerable advice throughout the process – Dr. Kris Campbell, Dr. Jim Browning, and Dr. Wan Kuang. Dr. Campbell deserves special thanks for the help she and her team provided on material processing issues. Dr. Thad Welch, as department chair, was very helpful in working to arrange my teaching schedule to permit time for this research.

I also owe a debt of gratitude to the other ECE Faculty members who have provided help in many ways – Dr. Elisa Barney-Smith who among other things taught the first graduate class I took at BSU, as well as Dr. Scott Smith and Dr. Said Ahmed-Zaid who have played major roles in helping with many academic endeavors. I also appreciate the insight that Dr. Bill Knowlton and Dr. Will Hughes provided regarding the material science matters.

AUTOBIOGRAPHICAL SKETCH OF THE AUTHOR

Robert (Bob) Hay attended Carnegie Institute of Technology where he received his B.S.E.E degree and received his M.S.E.E. degree a year later from the newly renamed Carnegie-Mellon University. In the summers between these academic sessions he had the opportunity to serve as summer intern at various organizations including Square D Company (Cleveland, OH)), Westinghouse Air Brake (WABCO) (Pittsburgh, PA), and Johns Hopkins Applied Physics Laboratory (Silver Spring, MD). Following graduation he began a career at Hewlett-Packard Company that spanned nearly 29 years of involvement in three R&D efforts of approximately equal durations. The first third of his career involved the development of RF and microwave instrumentation in Palo Alto. During this period he also earned an MBA degree at Santa Clara University. This period was followed by a move to HP's new facility in Boise and a stint in printing technology that included development of HP's first laser printer and early involvement in the development of HP's thermal inkjet technology. The final third of his career at HP involved development and sourcing of magnetic recording technology (heads, media, and channels) for HP's disk drive business. Nearly all of the work at HP was done in the role of project manager, a position which provided an excellent combination of technology involvement along with management experience. The breadth of experience derived from involvement in these diverse and interdisciplinary development efforts has been very useful to provide insights related to a wide variety of technical challenges. An

ancillary role at HP involved campus recruiting at various universities, finally serving as campus manager for CMU. These experiences along with in-plant interviewing provided interesting insight into factors that led to student success.

In 1997, following the closure of HP's disk memory division (DMD), he explored various business and technology options and decided to launch a small consulting business (AlloSys Corporation) in the area of wireless technology design and testing. This activity built on his original career of RF and microwave development at HP along with his management experience and coincided with a period of rapid growth in the wireless business. Clients included companies involved in RFID technology as well as wireless LAN and Bluetooth product development and testing. It was during this time that the concept of the digitally tunable SAW oscillator was hatched. It was also during this time that the appreciation he and his wife Anne shared for the performing arts led to supporting the Idaho Shakespeare Festival in the role of member of the Board of Trustees, a 3-month effort to complete a database conversion to a new SQL-based patron/donor database, and a one-year stint as Board President.

His involvement with BSU began with a conversation with Jake Baker at a state technology conference that led in short order to taking a graduate class followed by an adjunct role in teaching a graduate RF Design class, followed by admission to the new Ph.D. program in the Fall of 2006 and a role as special instructor that has included teaching linear systems, senior design, and introduction to circuits.

ABSTRACT

Surface acoustic wave (SAW) technology has been utilized in numerous research and commercial devices since the practical implementation was enabled by the availability of suitable photolithographic techniques in the 1970s. With the traditional approach to implementing these devices the frequency response is established during manufacture. This dissertation proposes a different approach to implementing a SAW device. The SAW structure is added to the top of an integrated circuit so that the frequency response can be digitally controlled and the peak resonant frequency can be varied. The approach is based on implementing a phase-controlled interface between the SAW transducer fingers and the input and output signals. The methods described can be applied to SAW resonators used for applications such as filters, oscillators, signal processing, and material sensing where frequency agility is a benefit.

Two design architectures are proposed and verified with simulations, with one offering somewhat more predictable performance while the other offers the potential benefit of lower-power operation. The simulations are performed using a combination of SPICE and MATLAB whereby the MATLAB code translates a desired frequency to a set of phase assignments for the SAW fingers and launches the SPICE application to simulate the performance. The SPICE application uses a lossy transmission line as a coupled-mode electromagnetic system to simulate the piezoelectric electroacoustic system. Simulations were done with center frequencies of 200 MHz and 800 MHz.

Theory predicts, and simulations verify, that using a 500nm CMOS process an oscillator can be implemented with frequencies up to 1 GHz and a resulting Q of approximately 600. Theory supports the possibility of operation up to 50 GHz with advanced circuits and finger widths of 45 nm.

TABLE OF CONTENTS

Dedication	v
Acknowledgments.....	vi
Autobiographical Sketch of the Author	vii
Abstract	ix
List of Tables	xiii
List of Figures.....	xiv
List of Abbreviations and Symbols.....	xviii
Chapter 1 Introduction	1
1.1 Overview of Conventional SAW Device Design	1
1.2 Overview of Typical Piezoelectric Materials	4
Chapter 2 SAW Applications.....	8
2.1 Oscillator Resonator.....	8
2.2 Oscillator Phase Noise	17
Chapter 3 Research Concept and Implementation Options	27
3.1 Concept	27
3.2 Ideal Implementation	31
3.3 Practical Implementation Options.....	35
3.4 Implementations Presented in this Dissertation	40
3.5 Material and Fabrication Options	42
3.6 RF Considerations.....	46
3.7 Additional Phase Noise Considerations.....	47
Chapter 4 Prior and Current Art.....	49

Chapter 5 Simulation	52
5.1 Simulation Approach	52
5.2 Simulated Designs	55
5.2.1 Design Case 1	55
5.2.2 Design Case 2	64
5.3 Simulation Algorithms.....	76
5.3.1 Determining the phase shift between IDT fingers.....	76
5.3.2 Determining target phase of the signal to each finger	76
5.3.3 Determining available phases of the input signal	77
5.3.4 Assigning input signal phases to the fingers	79
5.3.5 Estimating the launch angle.....	81
5.3.6 Estimating the receive angle.....	83
5.3.6 Assigning phase delays to the receiving fingers.....	84
5.4 Simulation Results	88
5.4.1 General Simulation Observations	88
5.4.2 Design Case 1 Simulation Results.....	92
5.4.3 Design Case 1a Simulation Results.....	98
5.4.4 Design Case 2 Simulation Results.....	100
Chapter 6 Conclusions and Future Work.....	105
6.1 Conclusions.....	105
6.2 Future work.....	106
References Cited.....	107

LIST OF TABLES

Table 1.	SAW properties of piezoelectric substrates.....	6
Table 2.	Number of phase combinations vs. number of fingers.....	38
Table 3.	General SPICE simulation device parameters.....	55
Table 4.	SPICE directives for IDT transmission lines.....	60
Table 5.	Algorithm to determine finger phases	87
Table 6.	Summary of simulation results.....	95

LIST OF FIGURES

Figure 1.	Conventional SAW device design.....	2
Figure 2.	Typical oscillator design.....	9
Figure 3.	Oscillator circuit with loop broken.....	10
Figure 4.	Contributions to Q from delay and path loss at different frequencies.....	12
Figure 5.	Effective Q resulting from the two contributors.....	13
Figure 6.	Case with insufficient selectivity to support the desired value of N.	15
Figure 7.	Case with selectivity increased by doubling the number of fingers.	16
Figure 8.	Leeson's oscillator noise model.....	18
Figure 9.	Example of a commercial SAW oscillator.	22
Figure 10.	Phase noise of OCXO, SAW, and YIG oscillators.....	23
Figure 11.	Phase noise of composite oscillator compared with two Agilent sources. .	24
Figure 12.	Effect of phase noise on communication signal.	25
Figure 13.	Piezoelectric potential vs. position for conventional SAW device.....	28
Figure 14.	Piezoelectric potential vs. position with independent finger control.....	29
Figure 15.	CSAW device with individual finger phase control.	30
Figure 16.	Ideal implementation of send finger control.....	32
Figure 17.	Method for adjusting gains to achieve desired sender rotation.....	33
Figure 18.	Ideal implementation of receiving finger control.	33
Figure 19.	Method for adjusting gains to achieve desired receiver rotation.	34
Figure 20.	Maximum frequency vs. finger width.....	35
Figure 21.	Phase rotation possibilities.....	37

Figure 22	Cross-section view of a thin-film piezoelectric material on Si.....	43
Figure 23	Top view of possible layout of circuits and SAW device.....	45
Figure 24	Tuning noise source for analog-tuned broadband oscillator.....	47
Figure 25	SNR comparison of conventional SAW vs. CSAW.....	48
Figure 26.	Input simulation source.....	56
Figure 27.	Inverters used to generate four phases from the two quadrature phases.....	56
Figure 28.	Sending finger control element.....	57
Figure 29.	Inverter design.....	57
Figure 30.	Transmission gate circuit.....	59
Figure 31.	Lossy transmission line segments simulating IDT portion.....	59
Figure 32.	Eight-finger sending module.....	61
Figure 33.	Eight-finger receiving module and intra-IDT delay line.....	62
Figure 34.	Lossy transmission line segments simulating receive IDT line.....	62
Figure 35.	Receive finger control element.....	62
Figure 36.	Buffer elements driven by the receive element signals.....	63
Figure 37.	Quadrature combiner for the receive fingers.....	64
Figure 38.	Signal Generation Circuit.....	66
Figure 39.	Analog buffer.....	66
Figure 40.	AinvG Input inverter.....	67
Figure 41.	AinvW Wide analog inverter.....	67
Figure 42.	InvBuf Inverting buffer design.....	68
Figure 43.	Eight-finger sending module.....	69
Figure 44.	Switching modules controlling the fingers.....	70
Figure 45.	Detail of the finger control elements.....	70

Figure 46.	Receiving module switching array.....	71
Figure 47.	Receiving summing and shifting module.	72
Figure 48.	Low input impedance amplifier stage.....	73
Figure 49.	Gain of the amplifier in Figure 48	74
Figure 50.	Input impedance of amplifier in Figure 48	75
Figure 51.	Mini-Circuits model “QCN-3+” 90° splitter “phase unbalance.”.....	78
Figure 52.	Phases of sending fingers for conventional SAW device.	79
Figure 53.	Sending finger phases for $f_D > f_C$	80
Figure 54.	Sending finger phases for $f_D < f_C$	81
Figure 55.	Receiving finger phases.....	85
Figure 56.	Acoustic amplitude of desired and image components vs. position	90
Figure 57.	Results for a desired frequency of 160 MHz.	93
Figure 58.	Results for a desired frequency of 200 MHz.	93
Figure 59.	Results for a desired frequency of 240 MHz.	94
Figure 60.	Phase at desired frequency for DC1.....	96
Figure 61.	Frequency error for DC1.....	97
Figure 62.	Amplitude response vs. frequency for DC1.....	98
Figure 63.	Results at 500 MHz for the high-frequency DC1a case.	99
Figure 64.	Results at 1 GHz for the high-frequency DC1a case.	100
Figure 65.	Results for a desired frequency of 160 MHz.	101
Figure 66.	Results for a desired frequency of 200 MHz.	101
Figure 67.	Results for a desired frequency of 240 MHz.	102
Figure 68.	Phase at desired frequency for DC2.....	103
Figure 69.	Frequency error for DC2.....	103

Figure 70. Amplitude response vs. frequency for DC2..... 104

LIST OF ABBREVIATIONS AND SYMBOLS

ACT	Acoustic Charge Transfer
ALD	Atomic Layer Deposition
AlN	Aluminum Nitride
BAW	Bulk Acoustic Wave
COM	Coupling of Modes
CSAW	Configurable SAW
CVD	Chemical Vapor Deposition
DLC	Diamond-Like Carbon
DRO	Dielectric Resonator Oscillator
ECR	Electron Cyclotron Resonance
EVM	Error Vector Magnitude
GSQW	Generalized SAW wave
HVPSAW	High-Velocity Pseudosurface Wave
IDT	Interdigitated Transducer
LiNbO ₃	Lithium Niobate
LiTaO ₃	Lithium Tantalate
MBE	Molecular Beam Epitaxy
OCXO	Oven-Controlled Crystal Oscillator
PGA	Programmable Gain Amplifier

PLL	Phase-Locked Loop
PPM	Parts Per Million
PSAW	Pseudosurface Wave
PTDL	Programmable Tapped Delay Line
PZT	Lead Zirconate Titanate
Q	Quality Factor
QAM	Quadrature Amplitude Modulation
RF	Radio Frequency
SAW	Surface Acoustic Wave
SBAW	Shallow Bulk Acoustic Wave
SC	Stress Compensated
SPUDT	Single-Phase Unidirectional Transducer
SSB	Single Side Band
SSBW	Surface Skimming Bulk Wave
TG	Transmission Gate
YIG	Yttrium Iron Garnet
ZnO	Zinc Oxide

CHAPTER 1 INTRODUCTION

1.1 Overview of Conventional SAW Device Design

Surface Acoustic Wave (SAW) Devices emerged from the confluence of piezoelectricity discovered in 1880 by the brothers Pierre and Jacques Curie [1] and the theory of plane surface waves postulated in 1885 by Lord Rayleigh [2] and enabled by the availability of photolithographic technology to support the necessary metallic geometries for a practical implementation. The first disclosed SAW devices were made in 1965 [3].

These devices are frequently used as filters, signal processing components, and as the resonating components of oscillators for generating sinusoid signals. Utilization of these devices is typically limited to applications where the frequency response is fixed or slightly tunable to the minor extent that substrate geometry or propagation velocity can be modified. Variations of these parameters on the order of 100 ppm would generally be considered a typical range.

In contrast to a Bulk Acoustic Wave (BAW) device where the resonant frequency is generally determined almost exclusively by the physical properties and geometry of the piezoelectric material, the frequency and propagation delay properties of a SAW device are influenced both by the mechanism by which signals are applied to and extracted from

the piezoelectric substrate as well as by the material properties. The SAW device can be thought of as a frequency-selective delay line. A simplified functional diagram of a typical SAW device consisting of a pair of interdigitated transducer (IDT) comb electrodes that serve to transmit and receive the acoustic wave is shown in Figure 1 [4].

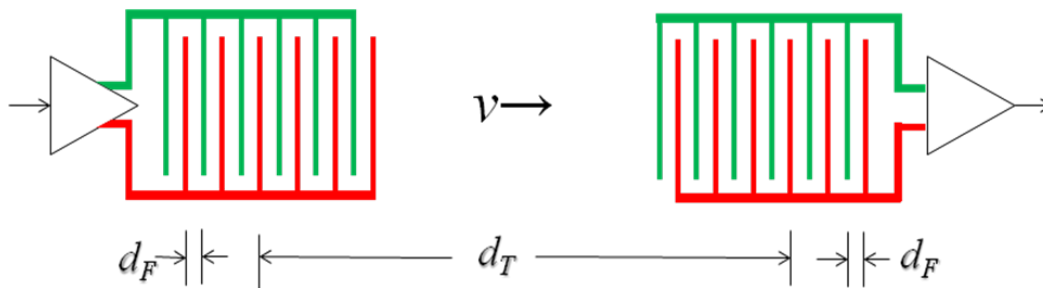


Figure 1. Conventional SAW device design.

The sending set of electrodes (or fingers) on the left end of the figure creates an acoustic vibration in the substrate due to the inverse piezoelectric effect. This acoustic vibration travels in both directions at the acoustic propagation velocity v with the desired energy traveling toward the receptor electrodes on the right side of the drawing. The undesired energy launched in the opposite direction is largely absorbed by structures not shown. The vibration appearing under the receiving set of electrodes on the right side induces a voltage on the receiving fingers via the piezoelectric effect.

The frequency selectivity is influenced by the characteristics of the sending and receiving interdigitated transducer (IDT) comb electrodes in the following manner. Adjacent fingers which are driven by opposite phases of the input signal will create

constructive interference at signal frequency f if the spacing $d_F = \frac{\lambda}{2}$ where the acoustic wavelength $\lambda = \frac{v}{f}$ and where v is the acoustic velocity. Therefore, the maximum acoustic energy will be injected into the substrate when $f = \frac{v}{2d_F}$. Thus for a typical filter design the bandpass center frequency is

$$f_c = \frac{v}{2d_F} \quad (1)$$

The width and length of the fingers will determine the amount of energy injected into the substrate as well as the differential impedance of the transducer but will have only a secondary effect on the center frequency response of the device. Variations of finger length within an IDT, a technique referred to as apodization [5], will cause changes in the shape of the frequency response. Note that the signal travels through the metallization at electromagnetic speeds or velocities and through the substrate at a much slower acoustic velocity.

The spacing d_T between the fingers of the same polarity at the approximate centers of the transducer pair influences the propagation delay τ_d between the input and output signal. The propagation delay can be represented as

$$\tau_D = \frac{d_T}{v} \quad (2)$$

The benefit of using a device utilizing acoustic propagation rather than electromagnetic propagation derives from the fact that typical acoustic propagation velocities V as shown in Table 1 are on the order of 3 – 5 km/sec, or about 4 to 5 orders of magnitude lower than the velocity of an electrical signal through a typical

electromagnetic transmission medium. This approach enables a relatively small physical size for critical parameters such as the value of the finger spacing $\frac{\lambda}{2}$ and the propagation delay τ_D .

Acoustic wave propagation can occur in several forms [6]. These include the Rayleigh wave, the Generalized SAW (GSQW) wave, the Leaky SAW wave, the Shallow Bulk Acoustic Wave (SBAW), the Surface Skimming Bulk Wave (SSBW) [7], the Pseudosurface SAW (PSAW) wave [8], and the High Velocity Pseudosurface Waves (HVPSAW). The propagation mode depends on a variety of substrate and metallization properties. The velocities of the Pseudosurface waves can be 40% (PSAW) to 100% (HVPSAW) higher than the standard Rayleigh wave devices [9]. As will be seen shortly, higher propagation velocities offer benefits for higher frequency applications.

1.2 Overview of Typical Piezoelectric Materials

Properties of numerous piezoelectric materials are discussed in the literature [10], [11]. The SAW properties of some of the most commonly used materials are shown in Table 1 where “ V ” is the acoustic velocity, “ K^2 ” is the coupling constant, “Loss” is the acoustic attenuation, “Leaky” is the loss of the pseudo-SAW (PSAW) propagation, and “ TCD ” is the temperature coefficient of the delay. As can be seen in the table, quartz offers relatively low temperature coefficients but has a low coupling constant and high loss. LiNbO_3 offers a relatively high coupling constant and low loss and therefore

somewhat better efficiency. Most SAW RF filters and duplexers use LiTaO_3 due to the optimum coupling factor [12].

The observation can be made that most piezoelectric materials are not semiconductors and that most semiconductors do not possess piezoelectric properties. However, there are exceptions, with one of the more interesting ones being GaAs, whose acoustic properties are included in Table 1 [13]. This dual property has been the subject of various research efforts [14] [15] [16].

Ceramic materials such as lead zirconate titanate (PZT) are highly effective piezoelectric materials but are not listed here because their attenuation becomes unacceptable at frequencies above 50 MHz [17]. An alternative hybrid approach to integrating piezoelectric and semiconducting material properties involves the application of a thin film of piezoelectric material to substrates such as silicon. Additional discussion of thin film materials is presented in section 3.4.

Table 1. SAW properties of piezoelectric substrates.

Material	Cut	V (m/sec)	K^2	Loss* (dB/cm)	Leaky (dB/ λ)	TCD ppm/ $^{\circ}C$
Quartz	YX	3159	0.18	8.2		24
	ST	3158	0.12	9.8		~ 0
	ST-PSAW	5078	0.033		$7.8e-2$	
	ST-HVPSAW	5745	0.011		$1.2e-3$	
Lithium Tantalate LiTaO ₃	YZ	3230	0.72	3.5		-35
	112YX	3288	0.6	3.3		-18
	36YZ PSAW	4227	5.6		$2.1e-4$	
	36YX HVPSAW	6978	21.1		0.12	
Lithium Niobate LiNbO ₃	YZ	3488	4.5	3.1		-94
	128YX	3992	5.3	2.7		-75
	64 YX PSAW	4692	10.8		$5.2e-2$	
	41 YX PSAW	4752	17.2		$2.4e-4$	
Gallium Arsenide	(001)(110)	2868	0.072	14.0		-52
Cadmium Sulphide	(001)(100)	1725	0.47	20.0		
Zinc Oxide	(001)(100)	2690	1.0	9.5		-37
Lithium Tetraborate	XZ	3542	1.0			~ 0
SiO ₂ /LiTaO ₃	YZ(SiO ₂)-TF LiTaO ₃	3435	.3	17		~ 0
Langasite		2600	0.3			~ 0
Bismuth Germanium Oxide	(001)(110)	1681	1.4	12.0		-120

*Loss is in air at 1 GHz.

While it is important that the transducer fingers are effective at injecting and receiving a signal from the piezoelectric substrate, it is also important that they do not play a role in excessively attenuating the acoustic signal passing by them. Avoiding this excess attenuation generally requires that the width w of the fingers be $w \leq \frac{\lambda}{4}$ and preferably $w \leq \frac{\lambda}{8}$ [18]. It is clear from this relationship that as frequencies increase, the upper limit of finger width decreases. At some point these finger widths become smaller than typical processes can support. A solution to this limitation is to select a substrate

with a higher propagation velocity. For example, there are reported velocities as high as 12km/s [19] on AlN/Diamond substrates supporting operation as high as 8GHz [20].

CHAPTER 2 SAW APPLICATIONS

SAW technology is most commonly used in bandpass filters, oscillators, signal processing devices including correlators and dispersive delay lines, and as a component for characterizing material properties such as viscosity and density.

The primary benefit of using traditional SAW technology for a filter application is the high Q capability combined with the small size and the flexibility available to tailor the frequency response [21], [22]. In the case where the device is used as a bandpass filter, it is generally not desirable to incorporate a long distance d_T between the transducer pair as the associated delay τ_D generally provides no benefit. The design of a SAW filter includes many considerations related to IDT geometry and additional components to deal with parasitic effects such as triple transit reflections [23]. In some cases the finger lengths are chosen to be non-uniform to provide for different weighting using an apodization or similar function chosen to provide the desired filter response [24], [25].

2.1 Oscillator Resonator

In the case where the device is used as a resonator element for an oscillator, the SAW resonator can be thought of as a delay-line with propagation delay τ_d combined with a pair of IDT comb electrodes that serve simultaneously to transmit and receive the acoustic wave as well as an intrinsic bandpass filter whose purpose will be discussed

shortly. Oscillators using SAW resonators were introduced in 1969 [26] and have found limited commercial application in certain areas where low phase noise is an important consideration [27] [28]. A typical oscillator constructed with a SAW device as a resonator combined with appropriate gain blocks and an optional variable phase delay to provide for tuning over a narrow frequency range is shown in Figure 2.

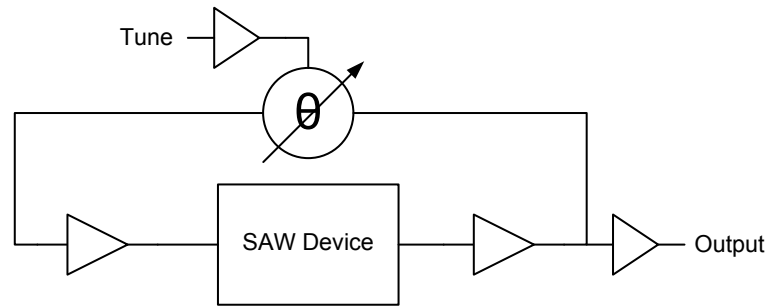


Figure 2. Typical oscillator design.

For the purposes of this discussion the total loop propagation delay τ_T can be assumed to be the sum of the SAW propagation delay τ_D and the external delays through the gain stages, phase delay block, and other intrinsic delays. If the loop is broken, the circuit is simplified by removing the phase-shifting component, and a signal source is inserted as shown in Figure 3. The open loop gain could be defined as

$$G = \left| \frac{V_{out}}{V_{in}} \right| \quad (3)$$

and

$$\phi = \angle V_{out} - \angle V_{in} \quad (4)$$

as measured in radians. It should also be noted that

$$\phi = -\omega_{OSC}\tau_T + 2N\pi \quad (5)$$

where ω_{osc} is the radian frequency of the stimulus in Figure 3 and N is the number of surface acoustic wavelengths of the signal ω_{osc} ,

$$N = \text{int} \left(\frac{\omega_{osc} \tau_T}{2\pi} \right) \quad (6)$$

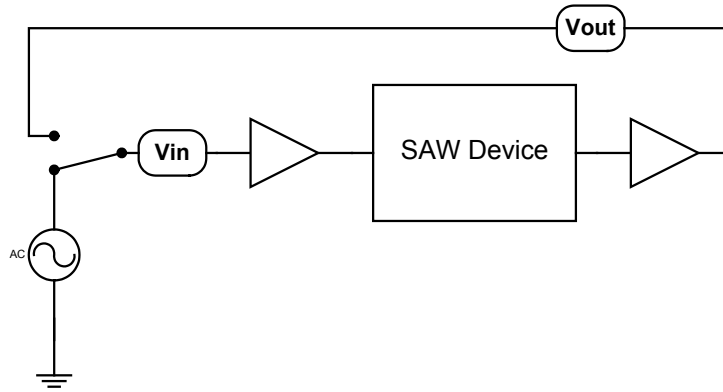


Figure 3. Oscillator circuit with loop broken.

From Equation (5) it can be seen that the change in the phase shift with frequency is a constant delay equal to the transit time through the structure.

$$\frac{d\phi}{d\omega_{osc}} = -\tau_T \quad (7)$$

In order for a resonant system to oscillate when the loop is closed (the switch in Figure 3 is flipped to the up position), it is necessary that

- a): the value of G in Equation (3) be such that $G > 1$, and
- b): the value of ϕ in Equation (4) be such that $\phi = 0$.

These two requirements are known as the Barkhausen criteria for oscillation. In order to meet condition b) it can be seen from (5) that

$$\omega_{osc} \tau_T = 2N\pi \quad (8)$$

where N is an integer representing the number of cycles of delay in the loop.

A good resonator for an oscillator is one that creates a very stable frequency. In order for a resonator to do this well, it must have a high Quality Factor, or Q value. While the standard definition of Q is the ratio of energy stored to the energy dissipated in a half cycle in a resonator, this view gets more complicated when analyzing a resonator where there are two primary components which contribute to what is generally referred as the unloaded Q . One contributor is the delay of the resonator where it can be shown that the delay component Q_D can be estimated as [29]

$$Q_D = -0.5\omega_{OSC} \frac{d\phi}{d\omega_{OSC}} \quad (9)$$

which implies from (7) that

$$Q_D = 0.5\omega_{OSC}\tau_T \quad (10)$$

and from (8) that

$$Q_D = N\pi \quad (11)$$

This suggests that a high Q is achieved with a large value for τ_i . However, increasing the value of τ_i creates several problems. First, it turns out that the resonator Q is also limited by the attenuation of the transmission line which causes a reduction of the received signal (and thus SNR at the receiver) and results in a lower effective resonator Q . In reality this attenuation tends to increase with the square of the frequency [30] on quartz substrates, and this dependence is likely to be typical of most substrates. If Q_L is defined as the component's loaded Q due to the of loss in this transmission line, then the effective Q [31] can be described as

$$\frac{1}{Q_{EFF}} = \frac{1}{Q_D} + \frac{1}{Q_L} \quad (12)$$

The effects of these two components of Q_{EFF} are shown in Figure 4 where the rising lines are the contributions due to the delay element and the falling lines are the contributions due to the loss, and the results are shown at frequencies from 100 MHz to 9000 MHz.

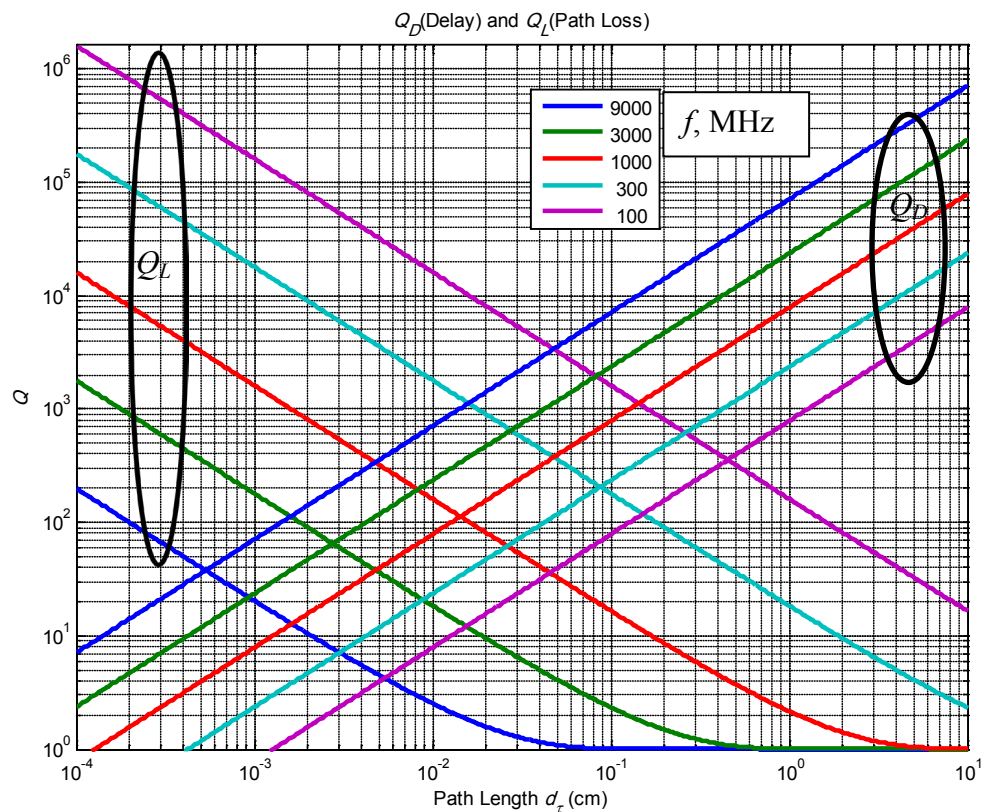


Figure 4. Contributions to Q from delay and path loss at different frequencies.

Combining the two contributions as described in Equation (12) produces the result shown in Figure 5. This result is very similar to that described by Lewis [32] and provides some insight regarding the optimal length of the device and the associated propagation

delay for maximum Q_{EFF} . From Figure 5 it can be estimated that, in the region of path lengths that represent the rising portion of Q_{EFF} , its value is approximately

$$Q_{EFF} = N\pi \quad (13)$$

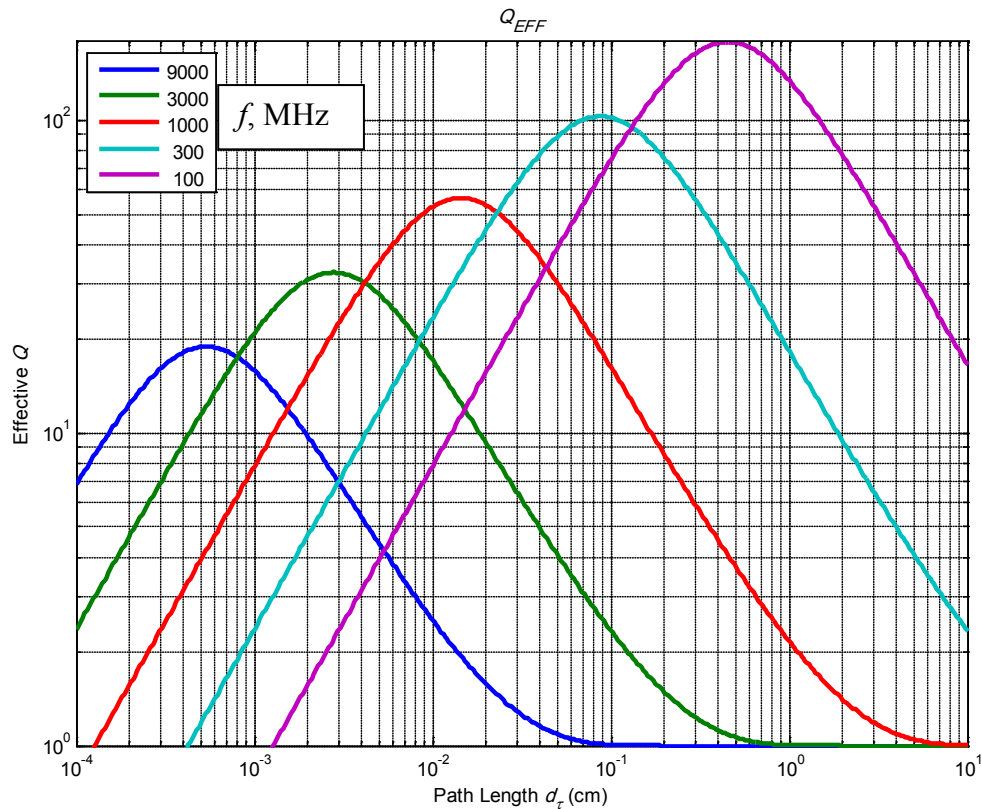


Figure 5. Effective Q resulting from the two contributors.

Another important factor affects maximum path length, which is proportional to N at any given frequency. The frequency range met by the gain portion of the Barkhausen criteria, $G > 1$, is determined by the bandpass filtering capability of the IDT pair mentioned previously.

It is apparent that through efforts to increase Q by increasing the value of τ_i (or equivalently, N) multiple values of N (and thus multiple values of frequency) will lead to meeting the conditions of both Barkhausen criteria. Avoiding this frequency ambiguity requires that both criteria be met for only one value of N . In order to ensure this non-ambiguity, it is important that the selectivity of the filter be consistent with the value of N (and τ_i). An example of this problem is shown in Figure 6 where the green line shows the phase shift and the green dots show each point at which $\phi = 2N\pi$, which indicates a potential frequency of oscillation if there is sufficient G . The blue line indicates the relative gain vs. frequency, recognizing that in this case additional loop gain would have to be supplied to support oscillation. The red dots on the blue line correspond to the frequencies represented by the green dots, indicating a potential frequency for oscillation. This result poses the problem that with only about 1.5 dB of separation between the gain for the three candidate frequencies, it is highly likely that a spurious oscillation will occur at an undesired frequency. Because of the nonlinearity of oscillator gain stages, it is frequently the case that an oscillator once excited at a frequency with sufficient gain will continue to oscillate at this initially excited spurious frequency and ignore other resonances that meet the Barkhausen criteria.

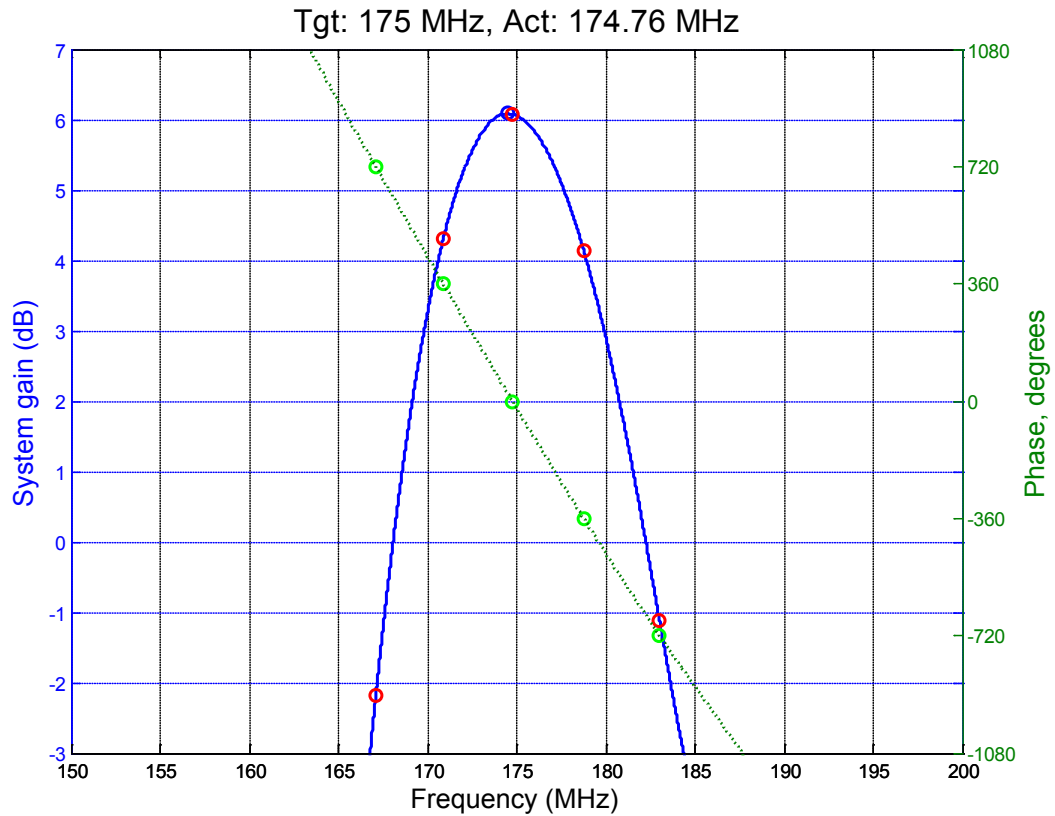


Figure 6. Case with insufficient selectivity to support the desired value of N .

The general approach to increasing filter selectivity is to increase the number of fingers in the IDT. In the case of Figure 7 the number of fingers per IDT was doubled from 32 to 64 and the result was an increase of gain separation to a little over 4 dB. This change may still be insufficient, depending on the gain control available, but clearly indicates the relationship between N , the number of cycles of delay, and M , the number of fingers in the IDTs. The 4-dB bandwidth can be generally approximated as $BW_{4dB} \approx \frac{1}{T}$ where T is the propagation length of an IDT represented in seconds [33.]

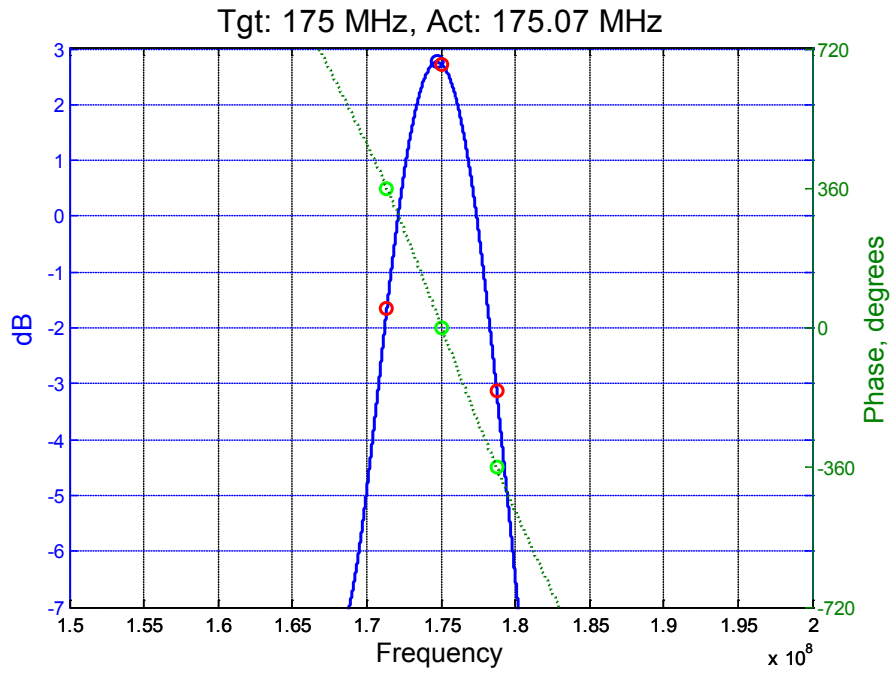


Figure 7. Case with selectivity increased by doubling the number of fingers.

2.2 Oscillator Phase Noise

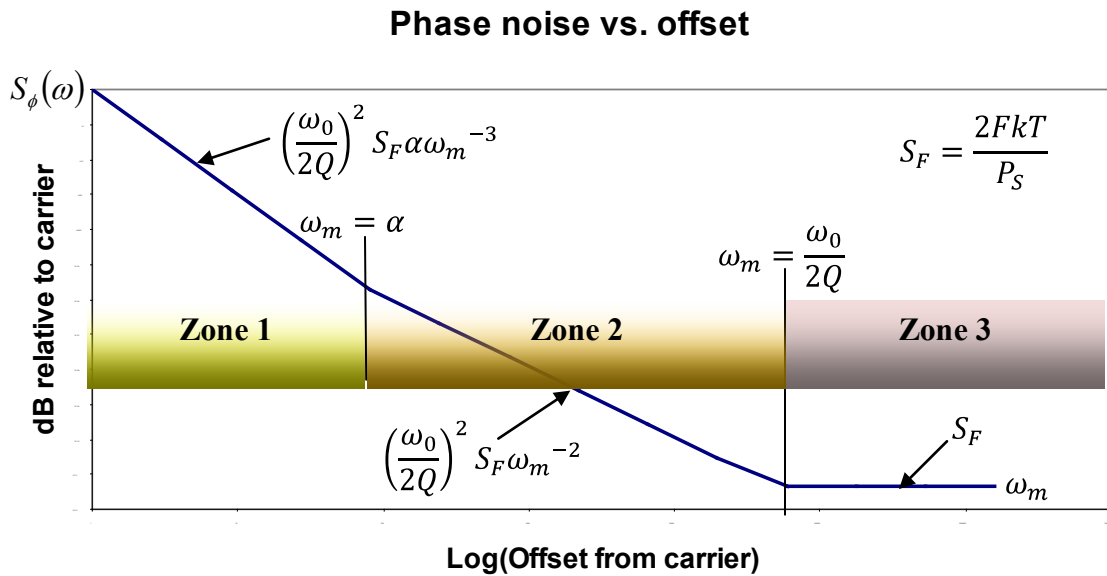
Phase noise in oscillators is a very important measure of quality. The well-known Shannon-Hartley theorem, derived largely from Shannon's Theorem [34], posits that the maximum channel capacity using ideal coding techniques can approach the upper limit

$$C = B \log_2 \left(1 + \frac{S}{N} \right) \quad (14)$$

where C is the channel capacity in bits per second, B is the channel bandwidth in Hz, and S and N are signal and noise power respectively. When an oscillator is used for up converting or down converting between a baseband and a carrier signal, its noise adds directly to the signal, thus reducing channel capacity according to (14). Oscillator phase noise creates an additional problem due to the fact that noise components mix with adjacent channel signals that may be larger than the desired signal, creating a noise component that is considerably larger than would be attributed to the phase noise component alone. Because of the limiting behavior of the gain stages of oscillators, much of the inherent amplitude noise is suppressed so the phase noise is the dominant noise source.

A model of oscillator phase noise was proposed in 1966 by D. B. Leeson [35] in which it was postulated that there are three regions of noise as noted in Figure 8. Here Q is the loaded Q of the resonator, ω_0 is the carrier frequency, ω_m is the offset (modulation) frequency, k is Boltzmann's constant, T is absolute temperature, P_s is the power entering the resonator, F is the oscillator noise factor, and α is a constant related to the

frequency where the $\frac{1}{f}$ noise becomes dominant.



It is customary to characterize the phase noise as the spectral density of the noise in a 1 Hz bandwidth relative to the carrier power. Since the noise is actually the result of phase modulation in units of RMS radians, it scales with $\sqrt{\text{bandwidth}}$. In the model shown, Zone 1 is the frequency range where the $\frac{1}{f}$ noise due to the active device in the oscillator dominates. Zones 2 and 3 include the frequency range where the amplifier thermal noise dominates. Both Zones 1 and 2 are inside the half-bandwidth of the resonator so that their noise modulates the frequency of the system which when integrated becomes phase noise with an additional $\frac{1}{f^2}$ power slope. Zone 3 is outside the resonator bandwidth, so the noise is primarily thermal noise determined by the properties of the amplification system.

Important observations that can be made from this model include:

- Increasing Q reduces the noise power in zones 1 and 2.
- Increasing the carrier power improves the noise performance in all zones. This observation is not quite accurate in the sense that for many resonators, an increase in carrier power will increase aging rate, thus causing deterioration in extremely close-in noise.
- Increasing carrier frequency causes noise to increase at the rate of 20 dB per decade in zones 1 and 2 and extends the offset range for Zone 2.
- The power spectral density is generally lower at greater offsets from the carrier in zones 1 and 2.

The Leeson model is conceptually useful but various complications limit its capability to lead to design improvements. As has been suggested in the literature [36], [37] some of these limitations are related to the fact that the SAW resonators often have a flicker noise of their own, that amplifiers add phase variation throughout the chain so that the noise factor which emphasizes the noise contribution of the first stage may not be a valid measure, and that the quality of matching to the complex impedance of the SAW resonator can change performance considerably and make the characterization of loaded Q very difficult.

There are some other fundamental relationships that are important to consider.

- Multiplying the frequency of the oscillator output will change the noise across the entire spectrum at a rate proportional to the multiplication factor. For example,

doubling the frequency will increase the phase noise by 6dB at all frequencies including frequencies associated with the noise floor.

- Using an oscillator as a reference in a PLL will have exactly the same effect as multiplying the frequency but only approximately within the unity-gain bandwidth of the PLL.
- Dividing the frequency of an oscillator output will decrease the noise across the entire spectrum proportional to the division factor except that the noise floor is controlled by the noise floor of the divider and its thermal (kT) noise.

Because of these relationships it is customary to design a frequency source as a composite system of two or more oscillators. The reference oscillator may use a quartz BAW resonator operating at a frequency of 10 MHz. Ideally it would be an oven controlled crystal oscillator (OCXO) using a stress compensated (SC-cut) [38] quartz resonator operating at 70°C so that minimal capacitive tuning (which degrades the Q) is necessary to maintain the specified frequency. The operating power of the quartz resonator must be chosen to achieve the desired stability tradeoff. Operation at low power will reduce aging effects and enhance its long-term (close-in) stability. From the Leeson model, however, low resonator power will cause an increase in far-out phase noise.

Assuming that the application required an actual operating frequency of around 1 GHz, the reference frequency would effectively be multiplied by 100, causing its noise levels to increase by 40 dB at all offset frequencies. For close-in noise (small offsets) this increase may not be a problem because for a constant Q the noise would increase

with frequency with any oscillator, so the end result would still be an acceptable level of phase noise. Due to multiplication of the noise far from the carrier of the low-frequency reference oscillator, a low phase noise system will require the addition of a higher-frequency oscillator which is optimized for a low level of far-out noise and is phase locked to the master oscillator with a relatively narrow loop bandwidth to benefit from its close-in noise but avoid its multiplied far-out noise.

SAW resonators have the capability of producing oscillators with very competitive phase noise. An example of the phase noise performance of a commercial SAW oscillator is shown in Figure 9 [39]. An example of slightly more impressive phase noise performance is provided by work done by Montress, Parker, and Andres [40] with the results shown in cited reference's Figure 8.

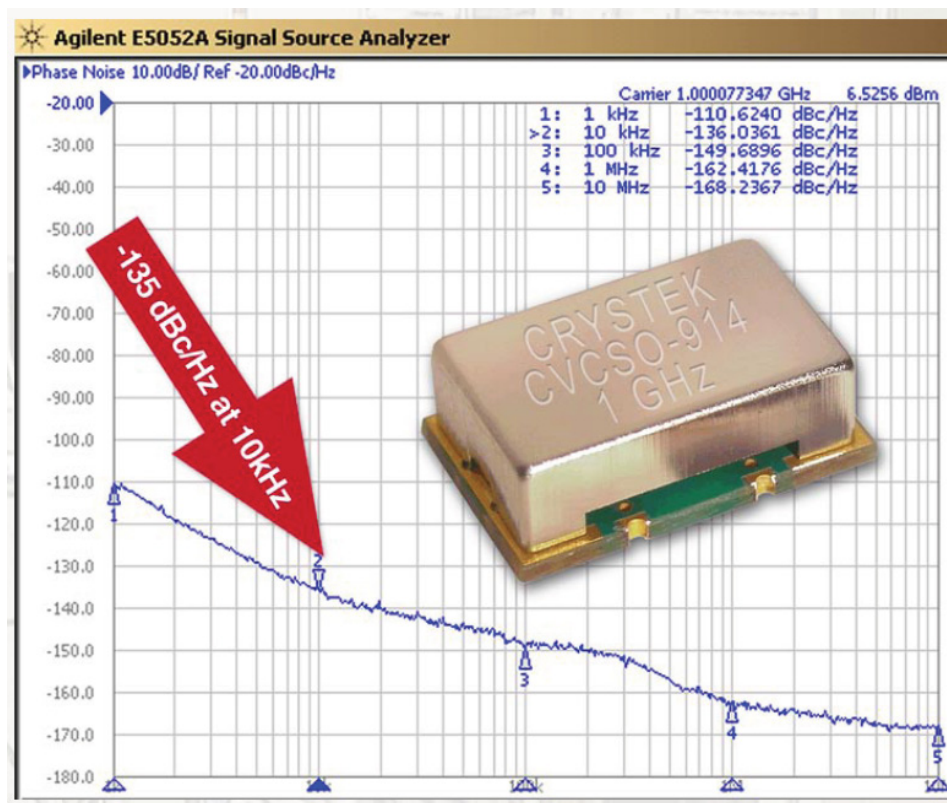


Figure 9. Example of a commercial SAW oscillator.

Phase noise data from these two aforementioned SAW oscillators and two other oscillators are shown in Figure 10 – a Micro Lambda Wireless Inc. low-noise 3 GHz YIG oscillator [41] and a Bliley Technologies Inc. low-noise 10 MHz OCXO [42]. In all four cases the phase noise is normalized to a carrier frequency of 1 GHz using the conversion factor of $20\log_{10}\left(\frac{1\text{ GHz}}{f_{osc}}\right)$.

While commercial SAW oscillators exist as shown by the example in Figure 9, their limited tunability makes them unsuitable for applications requiring the wide tunable range provided by YIG technology. They are useful only in applications requiring narrow-band tuning capabilities where alternatives such as dielectric resonator oscillators

(DROs) may be preferred. Consequently, SAW-based oscillators are less commonly found in commercial applications than oscillators using other resonator technologies.

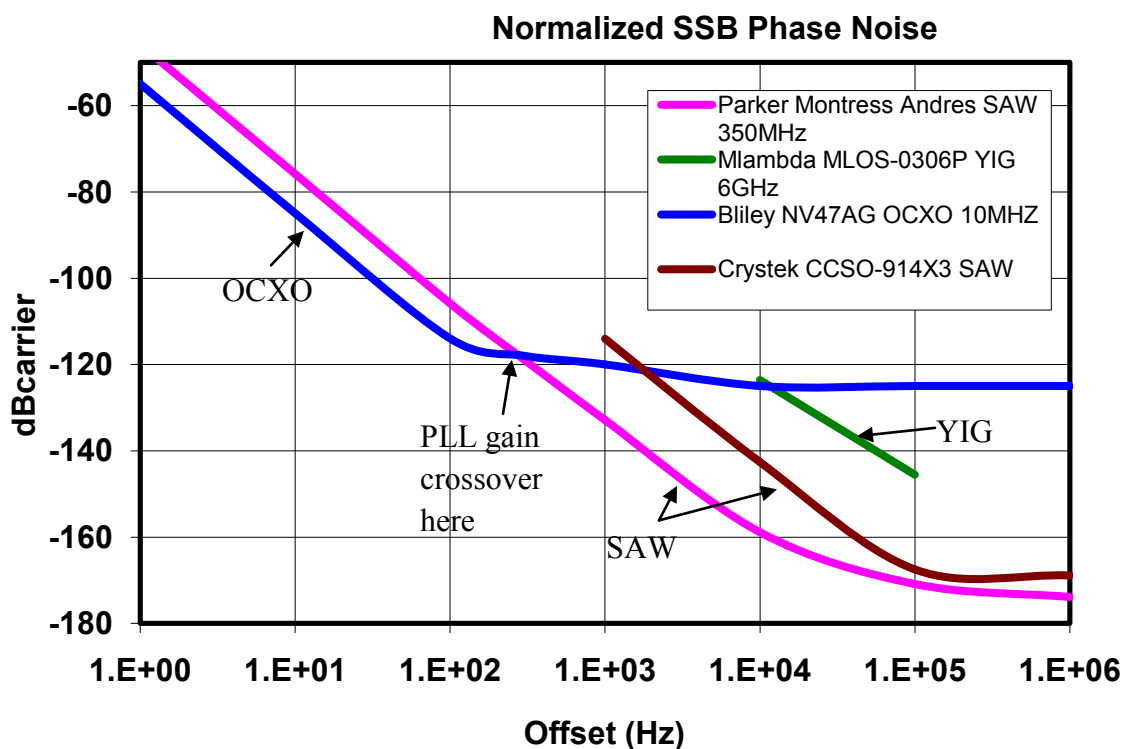


Figure 10. Phase noise of OCXO, SAW, and YIG oscillators.

Based on the phase noise performance shown in Figure 10 an oscillator system would ideally be constructed by using the SAW oscillator phase-locked to the OCXO with a PLL gain crossover in the vicinity of 300 Hz. This would limit the contribution of the elevated OCXO noise at frequencies offset by more than 300 Hz from the carrier.

Figure 11 shows the composite of the OCXO and the SAW oscillators assuming an ideal PLL can be created that yields the composite optimum of the phase noise of the two sources. Also included in this figure, for reference, are the specifications from two Agilent products that have excellent close-in phase noise performance – the Agilent

E5500 Phase Noise Measurement System [43] and the Agilent E8663B Analog Signal Generator [44]. Again, an important caveat is that it is very difficult to create an optimum synthesizer that tracks the maximum performance of multiple sources. However, the fundamental performance is very encouraging.

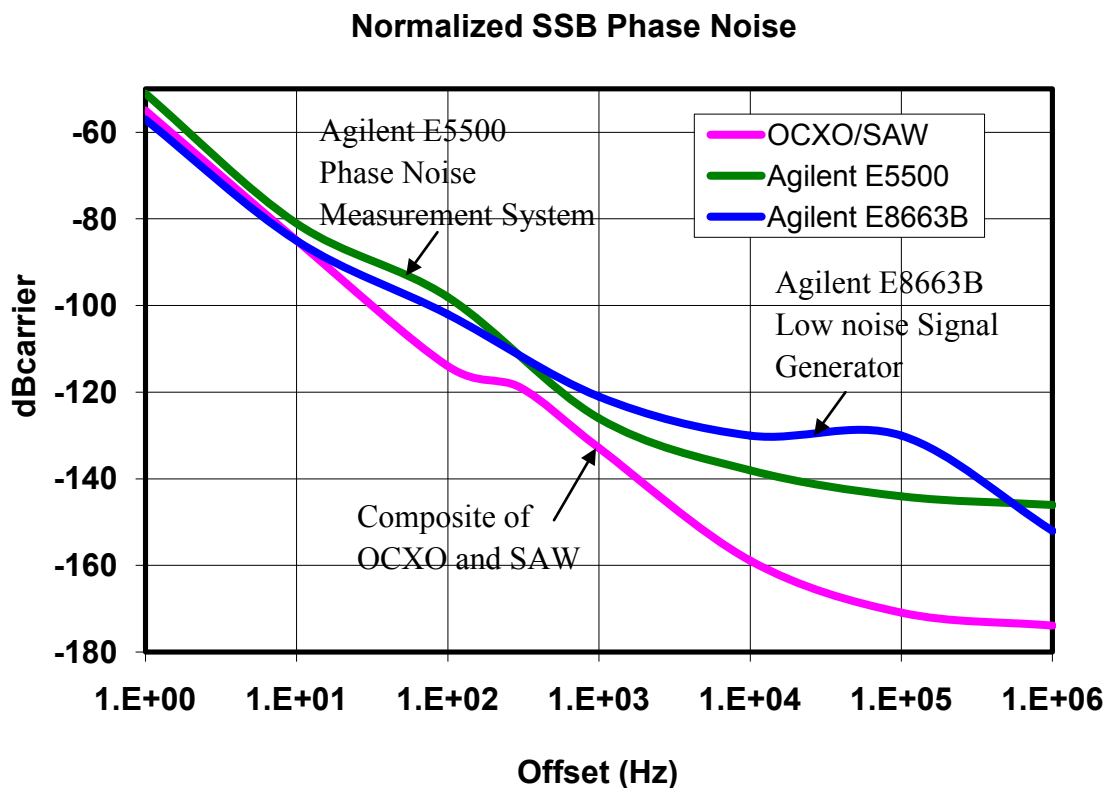
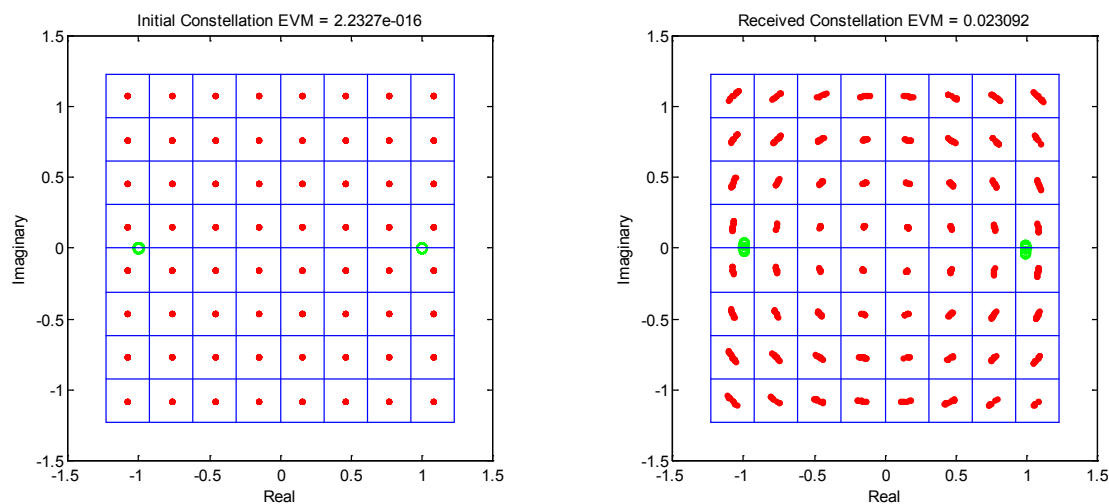


Figure 11. Phase noise of composite oscillator compared with two Agilent sources.

The noise discussion is concluded with a simple visual example of how phase noise can affect the quality of a received signal when converted to the baseband. As mentioned, when an oscillator is used as a local oscillator (LO) in a transmitter or receiver its phase noise adds directly to phase variation of the received baseband signal. Thus, its phase noise is a particularly important parameter in systems which incorporate

phase (or frequency) modulation. The effects of phase noise on a 64-QAM (Quadrature Amplitude Modulated) constellation are shown in Figure 12.

In practice phase noise which occurs at low rates is not a severe problem for communication systems where the pilot tones (the two green circles near either end of the real axis) are available for correcting for these errors. The receiver can de-rotate the signal by using the pilot tones as a reference and bring the Error Vector Magnitude (EVM) back to an acceptable value for phase noise components at offset frequencies much less than the inverse of the symbol time (about $4 \mu\text{s}$ in wireless LAN applications). However, for noise at higher frequency offsets from the carrier this correction does not provide much, if any, compensation for the noise.



Constellation prior to frequency conversion

Constellation after frequency conversion with minor phase noise.

Figure 12. Effect of phase noise on communication signal.

This example shows how coding can be used to improve error rate in a noisy environment and how good design can help a system to approach the Shannon limits.

However, as mentioned previously, oscillator phase noise in the presence of adjacent signals causes more problems than just phase rotation of the baseband signal.

CHAPTER 3 RESEARCH CONCEPT AND IMPLEMENTATION OPTIONS

3.1 Concept

This research involved the development of approaches to increase significantly the fundamental flexibility and adaptability of the response of SAW devices by incorporating individual control of the signal applied to or received from each of the fingers of the IDTs. The result, as demonstrated by the simulations and analyses, is a configurable SAW (CSAW) device capable of supporting the digital control of its response over a very wide frequency range.

The conventional SAW layout shown in Figure 1 can be viewed in a different perspective as shown in Figure 13. Here the horizontal axis of this plot represents position. The piezoelectric potential is shown on the vertical axis vs. position at an instant in time when the signal at the fingers is at its peak magnitude. In the case of the substrate area under the sending fingers, that voltage is due to the signal supplied to the sending fingers which induces vibration into the piezoelectric substrate due to the inverse piezoelectric effect. The vibration travels as a surface wave to the right on the substrate as shown, inducing a voltage on the surface which, when in contact with the receiving fingers, is collected and presented to the output.

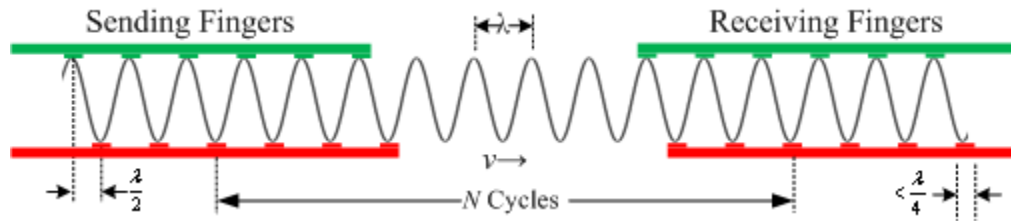


Figure 13. Piezoelectric potential vs. position for conventional SAW device.

Since the vertical position of the finger structures in this figure represent voltage on the substrate, the green and red fingers would be oscillating vertically in such a way that every half-cycle they would exchange places. This process works very effectively when the frequency of the signal is the center frequency f_C as defined in Equation (1) such that the adjacent fingers are spaced by exactly a half wavelength. However, at any other frequency the fingers would create destructive rather than constructive interference and the transmission level would be much lower. It is also apparent that increasing the number of fingers will lead to more attenuation for frequencies slightly offset from f_C due to additional phase shift in the longer IDT.

The focus of the remaining discussion addresses the case where it is desired to launch an acoustic wave at a frequency f_0 that is different from the frequency f_C . It can be readily noted that if such an acoustic wave were to be launched it would be periodic in time under each finger at frequency f_0 , but the phase relationship between the signals at adjacent fingers would be different from 180° . Clearly, then, if a signal were supplied to each finger of the transmitter IDT at frequency f_0 and with the proper phase relationship relative to the adjacent fingers, it would be possible to launch a signal at the desired frequency with constructive interference. Furthermore, if the phase relationships were

properly maintained, then the peak response of the filter would shift from f_C to f_0 .

Similarly, if the signal from each receiving finger could be appropriately phase shifted prior to summing, then an adjustable frequency response would be created at the receiving IDT.

This concept is illustrated in Figure 14 where, as opposed to the situation in Figure 13, the adjacent finger pairs may have a phase relationship that is different from 180° and consequently the alternate sets of fingers having the same color do not necessarily share the same potential. It follows that a major requirement for implementing this solution is to be able to individually control the signal phase shifts to each sending finger and from each receiving finger. More discussion of this phase relationship can be found in Section 5.3.

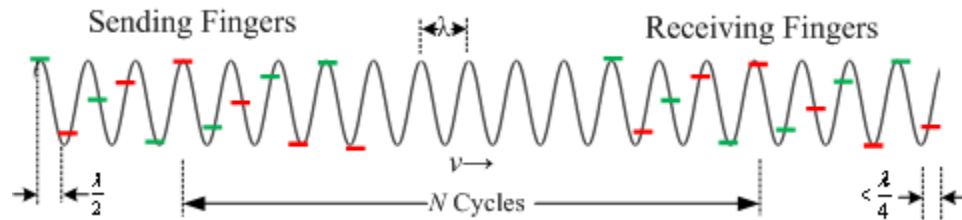


Figure 14. Piezoelectric potential vs. position with independent finger control.

It is important to note at this point that with this approach it is no longer necessary for the fingers of either IDT to have equal spacing. In fact, there may be some significant benefits to unequal spacing including increased directionality of the IDTs, wider tuning range, and more uniform performance across the frequency range as there would no longer be a frequency f_C which would exhibit some performance anomalies.

For an application such as an oscillator resonator where accurate control of phase delay is critical, an important additional capability of this design is the flexibility of the concept of the IDT spacing d_T . In Figure 1, d_T was the distance between the center finger of the sending IDT and the center finger of the same phase of the receiving IDT. If the resonator of Figure 1 is operating in a way in which the Barkhausen criteria are met, all fingers of the same polarity are of the same phase, leading to the conclusion that

$$d_T = N\lambda_{OSC} \quad (15)$$

where λ_{OSC} is the wavelength at the frequency of oscillation

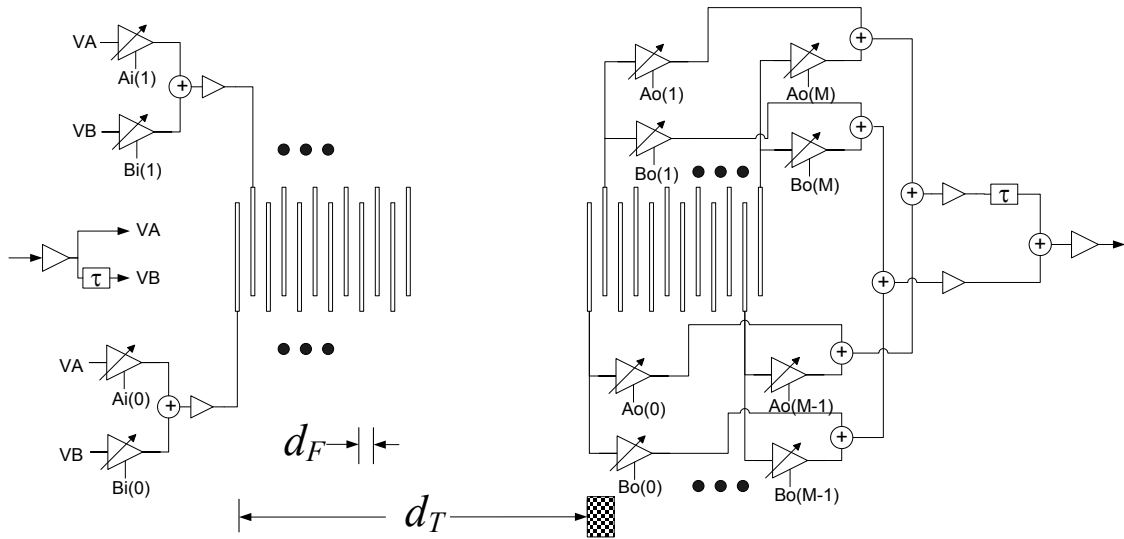


Figure 15. CSAW device with individual finger phase control.

In Figure 15 the phase of the signal will vary with each individual finger but the factors determining d_T remain the same as shown in Equation (15). However, due to this phase variation between fingers, the length of d_T is shown in Figure 15 as an approximate value as its actual value will vary with frequency. It is important for the algorithm that computes the phase shift of the receiving fingers to determine this value of d_T or,

equivalently, the phase of the wave arriving at the first receiving finger at the desired oscillation frequency f_{osc} .

The value of N in Equation (15) will naturally vary over the frequency range of oscillation according to (6) in order to limit the needed range of variation of d_T to λ_{osc} .

3.2 Ideal Implementation

In an ideal implementation of the concept the transmitter phase control may be accomplished through the use of programmable gain amplifiers (PGAs) whose gain can be varied over a range of approximately (-1 to +1). The signal applied to each finger is the sum of the output of two of these PGAs with one amplifying an in-phase signal and the other amplifying a phase-shifted (by $\phi \approx \frac{\pi}{2}$) quadrature signal. This implementation is shown in Figure 16 where the in-phase and quadrature gains for finger m are represented by $K_{1,m}A_1$ and $K_{2,m}A_1$ respectively. Note that the values of A_2 and B_2 in the figure represent the rotated voltage supplied to the finger and are derived based on the observed phase shift as shown in the figure.

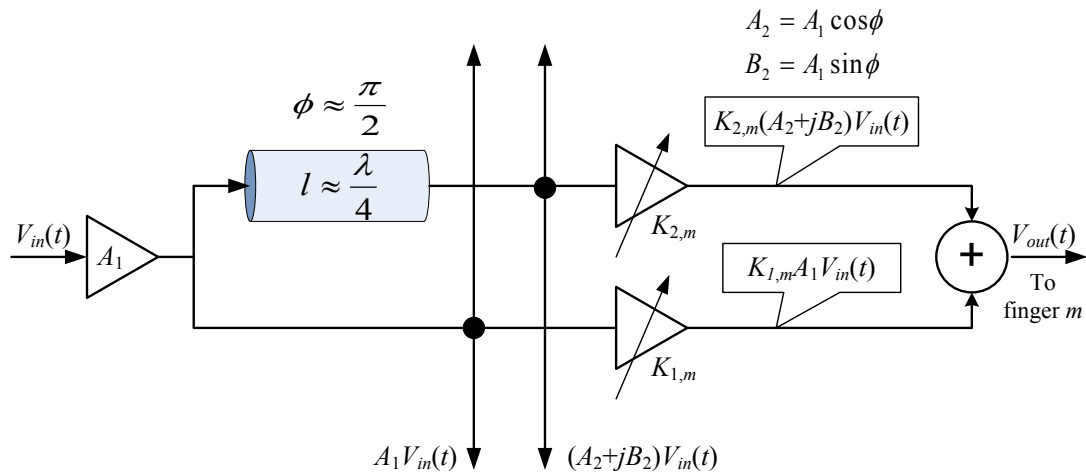


Figure 16. Ideal implementation of send finger control.

Note that for the purposes of computing the appropriate gains it is not necessary for the phase delay (as seen to create the signal VB) to be exactly $\phi = \frac{\pi}{2}$, but rather it is important for the phase delay to be known as a function of frequency and for the phase delay to be a reasonable distance from 180° in order to provide a useful quadrature signal component. As can be seen in Figure 17, where the phase delay is represented by the angle ϕ , it is possible to achieve any desired phase rotation. An example is represented by the red dot on the unit circle, where the proper gain coefficients were chosen. This approach works well even in the case shown where the phase shift is considerably more than $\frac{\pi}{2}$.

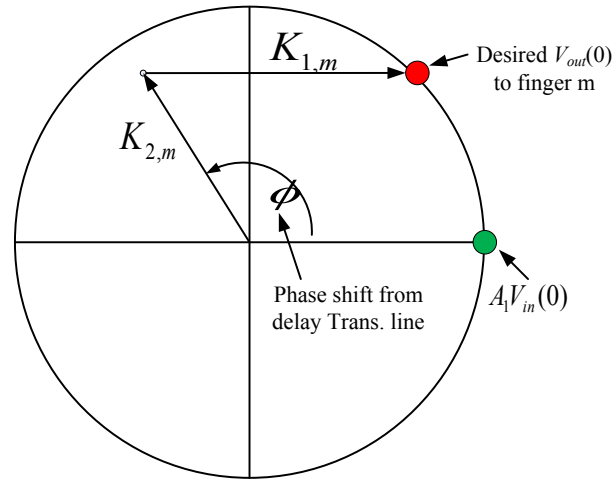


Figure 17. Method for adjusting gains to achieve desired sender rotation.

The implementation of the receiving IDT phase control is accomplished through a pair of PGAs where the output of one set of amplifiers is summed with the output of the other set when followed by a phase delay.

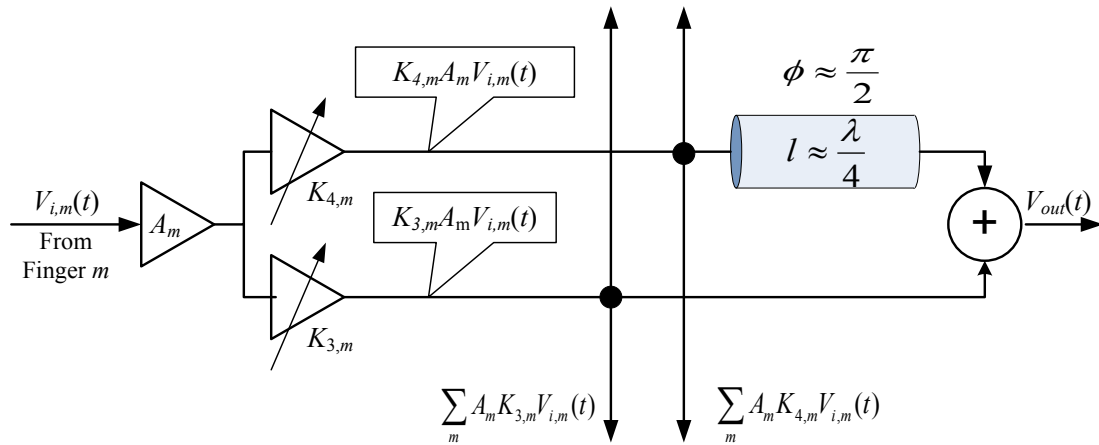


Figure 18. Ideal implementation of receiving finger control.

As previously indicated, the gains can be adjusted programmatically once the desired frequency, inter-finger delay time, and the angle ϕ is known. The method for determining these gains for a particular expected finger voltage is shown in Figure 19.

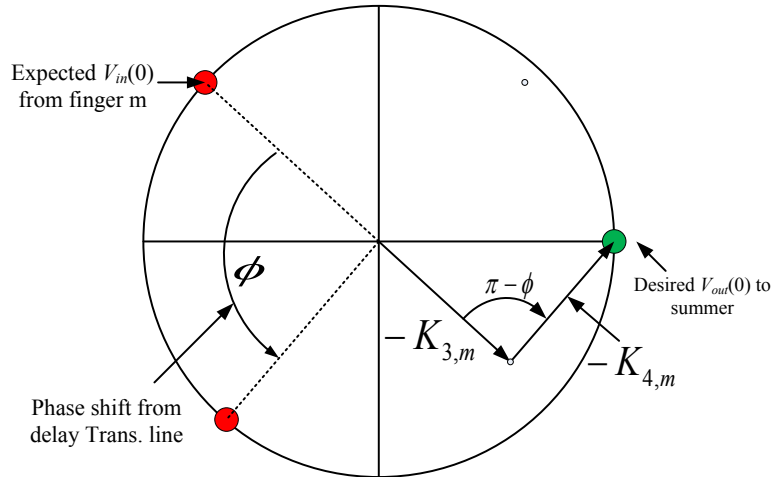


Figure 19. Method for adjusting gains to achieve desired receiver rotation.

An additional feature of this approach is that the IDTs become directional due to the phase shifting. When the PGA gains are properly chosen for a particular $f_0 = f_c + f_\Delta$ then the acoustic wave for a signal at frequency f_0 will be preferentially launched in the desired direction toward the receiving IDT. Conversely, if energy is supplied at frequency $f'_0 = f_c - f_\Delta$, the wave will be launched in the opposite direction. A similar directional preference exists with the receiver IDT. The result of this directionality is that the insertion loss at frequency f_0 is less than at frequency f_c as long as $|f_\Delta|$ is sufficiently large. As mentioned earlier, this feature would be present over a wider range of frequencies if the finger spacing in the IDTs were made to be non-uniform. More discussion of this phenomenon is found in section 5.4.

3.3 Practical Implementation Options

This section begins with an overview of geometry considerations for the SAW transducer. In Figure 20 the approximate maximum frequency is shown for three different propagation velocities as a function of the feature size used to create the transducer fingers. This plot assumes that the minimum finger width and inter-finger spacing is the feature size, which implies that the finger width is $\frac{\lambda}{4}$. Most materials exhibit a propagation velocity of 3 to 5 km/s for Rayleigh surface acoustic waves, with velocities up to 12 km/s for very hard (e.g. diamond) substrates.

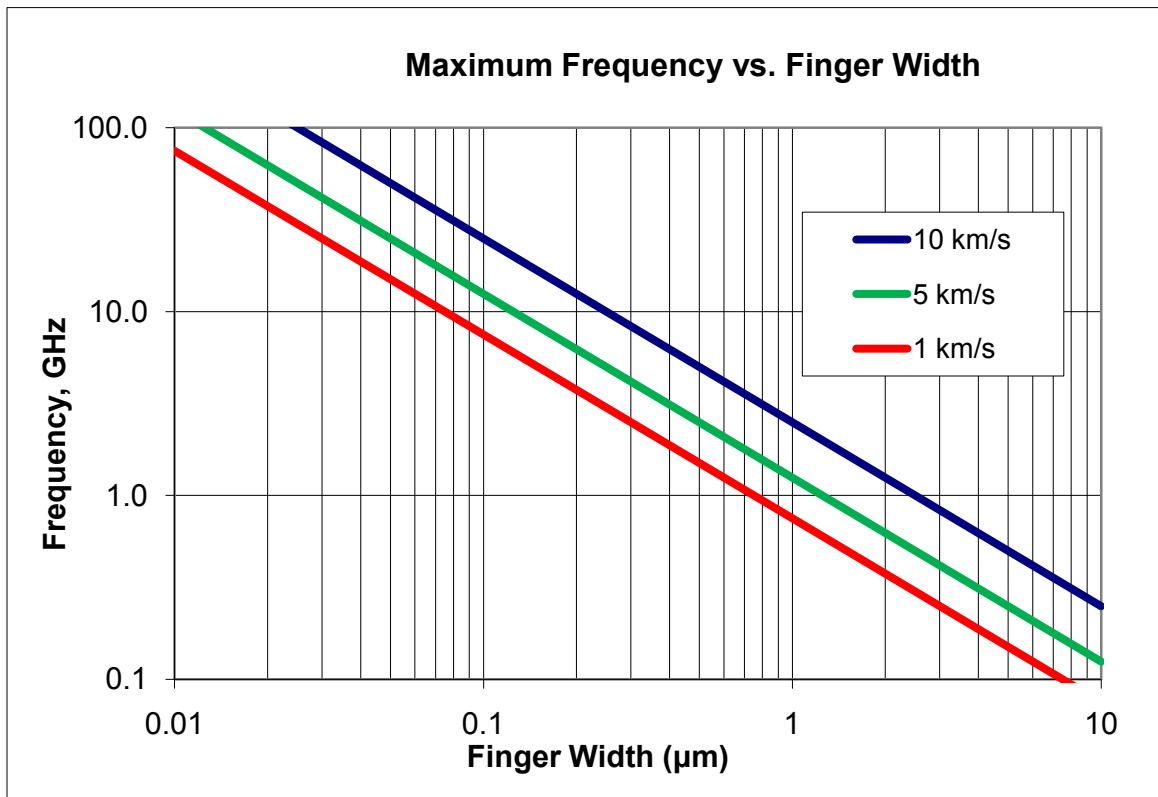


Figure 20. Maximum frequency vs. finger width.

A conclusion can be drawn from the data seen in Figure 20 that the feature size needs to be on the order of 1 μm or less for the device to operate in the vicinity of 1 GHz and a propagation velocity of 4 km/s. Since the finger spacing (or pitch) is generally no less than twice the feature size, this suggests a desired finger spacing of no more than 2 μm . Future applications of these devices for communication systems would likely call for operation up to the vicinity of 5 GHz for evolving communication systems. Further extension to reduce the finger width to 45 nm with a resulting frequency of 50 GHz using a high-speed substrate is also a strong possibility. With these constraints in mind, it becomes rapidly apparent that the limited area available for the circuits necessary to interface with fingers spaced by the required distance becomes very challenging. To make matters more difficult, bandwidth calculations suggest that the number of fingers should be in the range of 30 to 60 or more in each transducer for reasonable frequency selectivity. Clearly, this makes the notion of connecting two high-resolution variable-gain amplifiers to each finger very problematic.

These constraints provide motivation to explore lower-resolution options that are less ideal from a performance standpoint. An interesting starting point would be to consider a system which would support phase shifts of $\Delta\phi = \frac{N\pi}{4}$ radians with a total of eight phase possibilities as shown in Figure 21.

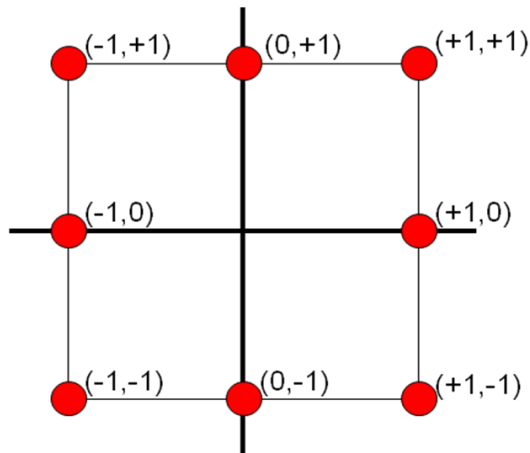


Figure 21. Phase rotation possibilities.

While these combinations (which can be controlled by a mere 3 bits of data per finger) are quite limited compared to the phase variations that could be achieved by a high-resolution variable-gain amplifier, it can be seen from Table 2 that within the range of the expected number of fingers to achieve the necessary selectivity, there are still many combinations available that should yield reasonably good frequency control. While this result does not necessarily verify that a proper combination will exist for every desired result, it suggests a strong likelihood that such is the case and this will be tested by the simulation results. This outcome perhaps supports the quote by Voltaire [45] that “The perfect is the enemy of the good.”

Table 2. Number of phase combinations vs. number of fingers.

M(#Fingers)	Combinations
32	1×10^{28}
64	7×10^{56}
128	5×10^{114}

Another way to view the tuning resolution with the finite number of phases is to consider that the total change in phase shift at the receiver due to the change of phase of a single finger would be approximately

$$\Delta\phi_T = \frac{\Delta\phi_F}{M_R} \quad (16)$$

where M_R is the number of receive fingers. Since

$$\frac{d\phi_T}{d\omega_{OSC}} \approx -\frac{\Delta\phi_T}{\tau_D} = -\frac{\Delta\phi_F}{\tau_D M_R} \quad (17)$$

it can be shown, for the example where $\tau_D = 100\text{ns}$, $\Delta\phi_F = \frac{\pi}{4}$, and $M_R = 32$, that

$$|\Delta\omega_{OSC}| \approx \frac{\pi}{4 \cdot 32 \cdot 10^{-7}} \approx 2\pi \cdot 39\text{krad/s} \text{ or } |\Delta f_{OSC}| \approx 39\text{kHz.}$$

Tuning to frequencies between these points can be accomplished using the fine tuning mechanism as shown in Figure 2.

There are several ways to accomplish these eight levels of phase rotation. One approach is to begin with a pair of signals, one being the input signal and other being a signal shifted by approximately 90° . These two signals can each be multiplied by -1 , 0 ,

or +1 and the results added to get any of the eight phases shown in Figure 21. Through logical control of gain elements, signals can be supplied to the sending fingers and extracted from the receiving fingers in a way that provides the desired phase shift in both cases. A variety of implementations to support this approach have been explored including both a transmission-gate switching approach and a source-follower switching approach. The source-follower-approach worked very well in simulations, but the layout showed that the space required was far in excess of the space available. The transmission-gate switching approach was closer to working in the available space. However, a layout attempt of the transmission gate approach using a 0.5- μm 3-metal layer process showed that the approach would not be feasible for reasonable finger spacing. However, a process that would support devices with 0.18- μm geometries and with a 6-metal process could work very effectively.

It is appropriate at this juncture to note approaches to generating the approximately quadrature phase shift. For the purposes of this discussion, it is assumed that the phase shift is generated by a simple delay transmission line. However, there is wide availability of a device generally referred to as a $-3\text{dB } 90^\circ$ hybrid coupler that could also provide this phase shifting. Either approach to generating the necessary quadrature phase shifting could be a suitable option. With either the transmission line or the hybrid coupler approach, all of the required eight phases can be derived from a combination of inverting and summing gain stages. It is also rather straightforward to develop four of the phases using three sections of transmission line with length $\frac{\lambda_c}{8}$ where λ_c is the

wavelength at the center frequency of operation. Once these four phases are available the remaining required four phases can be generated through simple inversion.

Another approach to managing the phase relationship at each finger is to create the eight individual phase busses and to connect the appropriate bus to each finger. This connection could be established using a variety of RF switching technologies. A conventional technology for doing this switching could be a CMOS transmission gate. Alternative, and perhaps much more interesting, technologies could include switching technologies based on phase-change switches utilizing chalcogenide materials. The chalcogenide technology would provide the benefit of non-volatile configuration and small geometry accompanied by the challenges of programming as well as uncertain RF switching characteristics.

3.4 Implementations Presented in this Dissertation

For the development of this dissertation, performance simulations have been done for a wide variety of cases. Results will be presented for two cases that are likely to be the most feasible to implement.

Case 1: Four phases are supplied to the control elements for each sending finger with approximately $\frac{\pi}{2}$ radians of phase separation between them. The signal for each phase is derived from a set of four transmission gates (TGs) acting as resistive switches,

each connected to one of the phases through buffer stages. Either one or two of the four transmission gates may be active for any finger at any time depending on the phase requirement. The buffer stages are required between the phase lines and the TGs to provide isolation so that the load on each of the incoming phase lines is relatively constant and independent of the switch settings.

Case 2: Eight phases are supplied to the control elements for each sending finger with approximately $\frac{\pi}{4}$ radians of phase separation between them. The signal for each phase is derived from a set of eight resistive switches where only one is active for any finger at any time. The benefit of this approach is that the buffer stages may not be necessary as the fact that only a single switch is active for each stage will reduce phase rotation of the incoming signal due to switch loading. The resistive switch in this case could be either a TG or an alternative switch design which could be constructed from a diode or an alternative material whose resistive state can be switched using either a volatile or non-volatile mechanism.

In both cases, the process is essentially reversed for the receiving fingers, where the desired phase rotation is collected from each finger, amplified, and summed to the appropriate node, and each of the resulting phases appropriately rotated and summed to form the output signal.

3.5 Material and Fabrication Options

The discussion up to this point supports the premise that a tight integration between the silicon-based interface elements and the fingers connected to the piezoelectric surface is essential. Approaches such as connecting wire bonds between a silicon circuit and the fingers incorporated in an IDT on a piezoelectric substrate are impractical because of the geometries necessary to support wire bonding. As a result of this limitation, it rapidly becomes apparent that the only reasonable approach to implementation is to find a way to integrate a piezoelectric substrate with a silicon substrate that contains the requisite electronic capabilities necessary for controlling the phase relationships between the adjacent fingers.

It is well-known that silicon does not have piezoelectric properties and most piezoelectric materials do not make good semiconductors. As mentioned earlier, GaAs is a material that has the dual property of being a good semiconductor and having piezoelectric properties, but its limited commercial use for either property is testimony to the design and processing challenges it presents.

The most common practice to address this issue is to deposit a thin film of crystalline piezoelectric material on a dielectric layer deposited on the silicon-based integrated circuit. In some cases the top metal layer may be exposed, either on top of this dielectric layer or co-planar with this layer. Exposing the top metal layer of the integrated circuit enables this layer to serve the function of providing the metal fingers that are in contact with the piezoelectric film as shown in Figure 22 where the metal

fingers are shown in cross section above the SiO_2 dielectric layer. In this simplified diagram the controlling circuits are buried in the substrate below the SiO_2 layer shown.

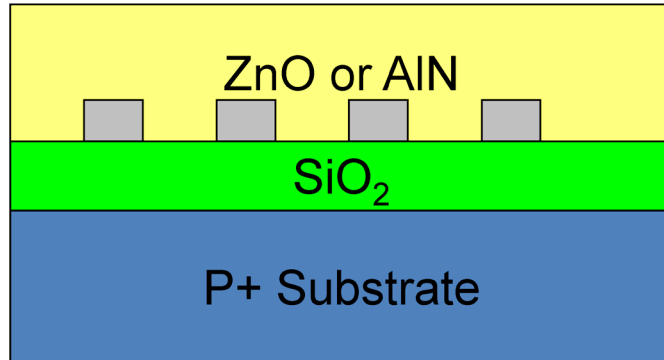


Figure 22 Cross-section view of a thin-film piezoelectric material on Si.

Alternatively, the dielectric layer may cover the top metal layer and the fingers can be deposited and patterned following the deposition of the piezoelectric film and connected to the circuitry through exposed vias. Using this approach the fingers would then be above the piezoelectric layer.

The dielectric layer can be a conventional material such as SiO_2 or Si_3N_4 . Harder dielectric materials such as diamond-like carbon (DLC) [46] may also be used and can support higher acoustic velocities in the piezoelectric film deposited on them with a resulting increase in the upper frequency capability of the SAW device (refer to Figure 20). Depending on the thin film structure and the crystal orientation of the piezoelectric film, various waves as described in Section 1.1 may dominate.

Two commonly used piezoelectric thin films [47] are Zinc Oxide (ZnO) on Si [48], [49] and Aluminum Nitride (AlN) on Si [50], [51] and on GaAs [52]. ZnO can be deposited by Electron Cyclotron Resonance (ECR) sputtering [53], Thermal evaporation[54], Atomic Layer Deposition (ALD) [55], Metal-Organic Chemical Vapor

Deposition MOCVD [56], DC Sputtering[57], RF Sputtering [58], Reactive RF Sputtering [59], Molecular Beam Epitaxy (MBE) [60], and spray pyrolysis [61].

All of the process listed above have apparently been able to achieve good results in terms of depositing films that exhibit good piezoelectric properties. Most of the process descriptions suggest that the substrate should be in the range of 200 – 400 °C for good crystal growth, and some of the processes show improved results from post-deposition annealing. Good results have been reported by Hickernell [62] using both DC sputtering and DC and RF Compound sputtering of ZnO. Hickernell reports that

“Transducer quality surface-wave films are characterized by their optical clarity, high density, smooth surface, small crystallite size, and well-oriented crystallite axes.”

Research has been done with a wide variety of orientations including (from top to bottom) a): IDT/Piezo/SiO₂/Si, b): Piezo/IDT/SiO₂/Si, c): IDT/Piezo/MGP/SiO₂/Si, and d); MGP/Piezo/IDT/SiO₂/Si, where Piezo represents a piezoelectric thin film and MGP represents a thin film metal ground plane. Wu *et al* reported results with all four combinations [63]. It appears that all of the listed orientations can be made to work, but orientation b) provides what appears to be both good performance as well as some processing benefits as it enables the use of the top metal layer in the IC process to serve as the IDC fingers. This approach avoids the need to perform a metal etch of the fingers on top of the piezoelectric thin film and the resulting damage that may occur to that film during the etch process.

Trolier-McKinstry and Murali [64] suggest that, while both wurtzites ZnO and AlN show good piezoelectric response along the [0001] axis, AlN has the advantages of

higher resistivity due to its larger band gap but requires more demanding vacuum conditions in order to avoid mechanical stresses. ZnO deposition is less demanding but since Zn is a fast-diffusing ion it creates incompatibilities with other semiconductor processes. With both films the underlying crystal structure and ion bias must be controlled in order to assure good selectivity between the (0001) and the (000 $\bar{1}$) orientations.

Finally, a simplified top view of a possible layout of a SAW device on a Si substrate is shown in Figure 23. In an actual layout it is likely that circuits would also reside under the SAW fingers and use all of the available space on the substrate.

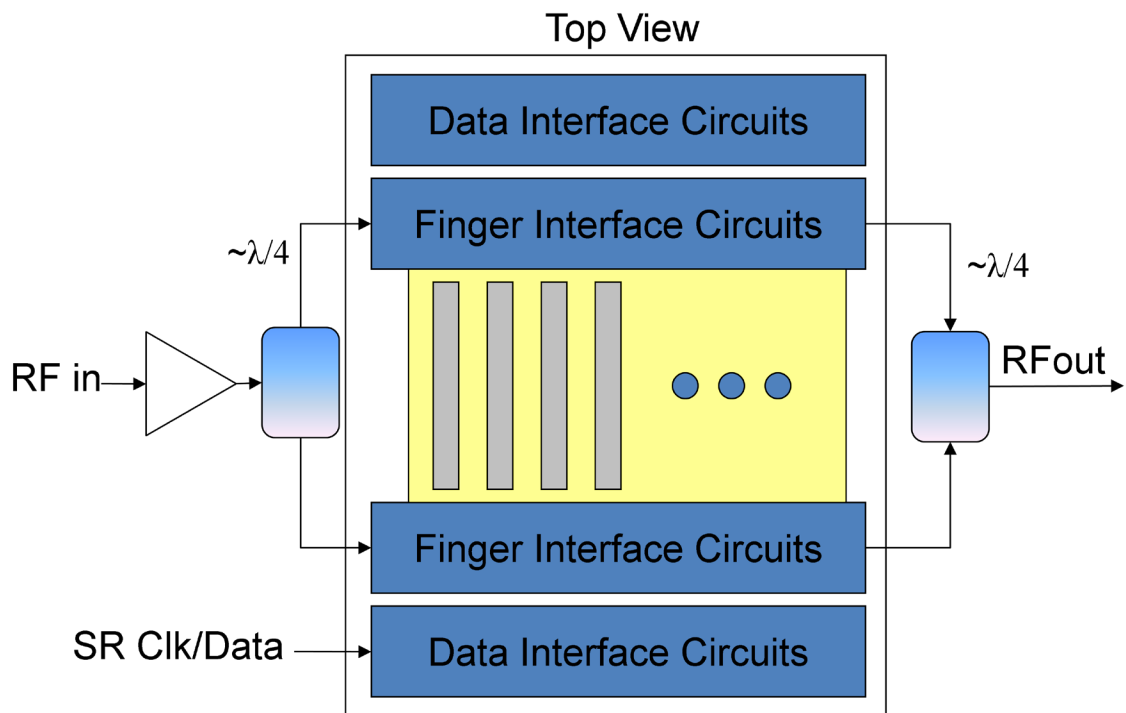


Figure 23 Top view of possible layout of circuits and SAW device.

3.6 RF Considerations

High frequency operation adds considerable complexity to a design.

Consideration must be given to RF issues such as mismatches, reflections, source, load, transmission line impedances, crosstalk, device impedances, and group delay effects.

Typically, a concern is raised when line lengths exceed a few percent of the RF wavelength. The approach of the RF designer would be to carefully match impedances when splitting an RF signal to multiple ports using standard designs such as a 3 dB hybrid splitter or a Wilkinson power splitter, both of which are designed to minimize the effect of reflections from one output port on the signal sent to a second output port.

This classical analog approach is rather different from the approach used in the digital design world regarding such challenges as clock distribution, which is achieved at multi-GHz rates without dealing with matching issues. The digital approach incorporates numerous active devices with relatively high input impedances to minimize loading effects on a signal commonly distributed to numerous nodes. In simulating and implementing these designs, it is important to understand the power of the MOSFET and CMOS buffer while also recognizing the limitations due to finite source impedances, device and transmission line parasitic effects, and the effects of reflections and group delays. Shrinking geometries continually move the design center toward the simplified digital approach, but increasing frequencies continue to present their analog challenges.

3.7 Additional Phase Noise Considerations

There are two issues related to phase noise that were not covered in the previous discussion which pertained to the conventional SAW device. These issues are the noise due to the tuning voltage and the noise related to the fact that there is a buffer amplifier for each receive finger compared to a single buffer amplifier for the entire receive IDT in the conventional SAW device.

The frequency control for a typical widely tunable oscillator uses an analog voltage that can tune the oscillator resonator over its entire frequency range. This is the case for a standard YIG or varactor-tuned resonator as shown in Figure 24. In the case of the CSAW oscillator the analog tuning range can be very limited

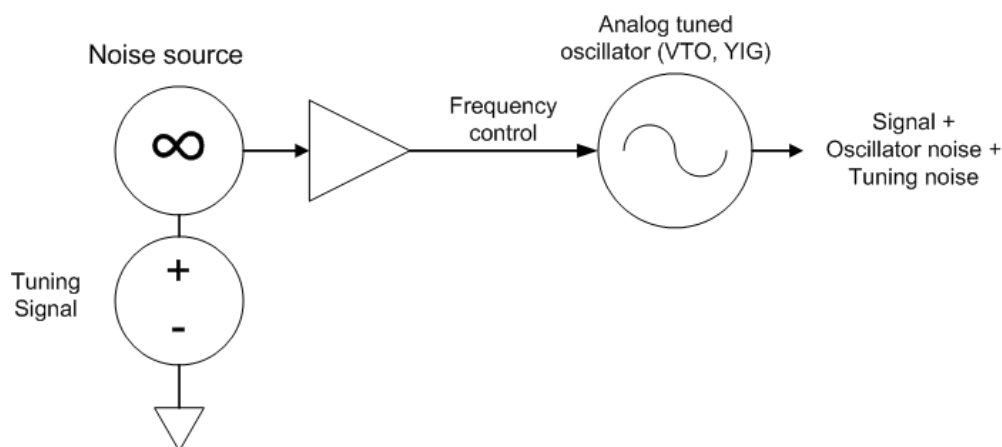


Figure 24 Tuning noise source for analog-tuned broadband oscillator.

The concern regarding the SNR at the output of multiple buffers is addressed in Figure 25. The important point shown here is that the signals from the outputs of the individual buffer amplifiers are added coherently while the noise from these buffers is added non-coherently. Thus the total SNR is the same for both the conventional and the configurable SAW configuration.

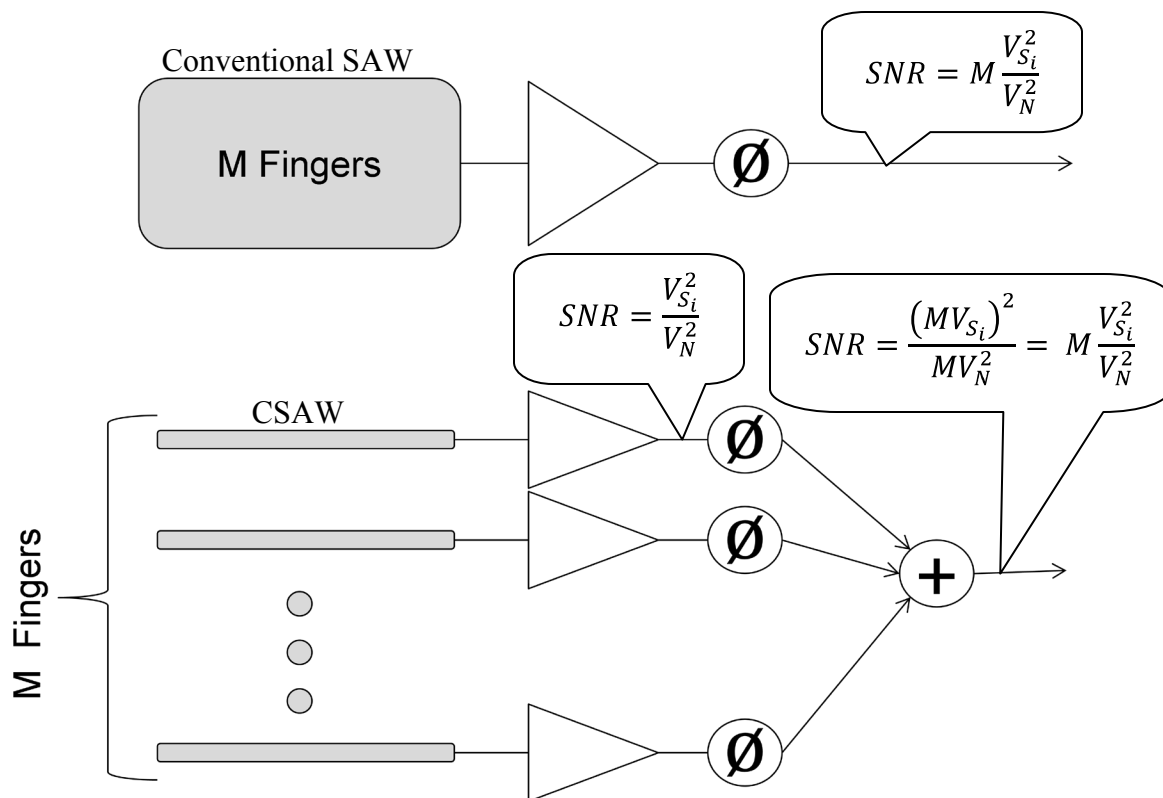


Figure 25 SNR comparison of conventional SAW vs. CSAW.

CHAPTER 4 PRIOR AND CURRENT ART

The unique aspects of this proposed concept include the use of digitally-controlled complex finger weighting for both the sending and receiving transducers to create a wide-band tunable SAW oscillator with a predictable oscillating frequency. The concept of connecting to individual fingers is not new. It was suggested by Tancrell in 1971:

“For surface wave devices, the restriction that the coefficients be real is related to the fact that the same voltage appears across every finger pair. Otherwise the need to supply a voltage of different amplitude or phase at each finger increases the difficulty of fabrication enormously. The restriction that the elements be uniformly spaced is only due to the fact that most of the work on digital filters and antennas has been concerned with this case.” [65]

Numerous discussions of tunable SAW resonators for filter and oscillator applications have appeared in the literature. Some use multiple IDTs on the same substrate to provide different filter responses [66]. Still others use an approach whereby the propagation velocity of the substrate is slightly modified through changes in electrical bias [67], [68], or through applying physical force by means such as magnetostrictive [69] or magnetoacoustic [70] materials. Others use an external phase shifting network with the capability to achieve a wide phase variation [71], [72]. An architecture was proposed by Amorosi and Campbell that used two different delay paths and a variable gain for each of the paths operating in parallel to create a variable effective delay [73].

Several papers have been published that discuss the concept of adjusting the gain (or tap) weights on individual fingers. Kenny *et al.* mentions the problem of the image passband mirrored about the center frequency f_C when not using complex gain terms [74]. Pastore *et al.* suggests that “Unambiguous frequency translation requires a complex multiplication ... along with broadband 90° splitters and combiners.” The authors then abandon that approach and discuss an approach using dissimilarly tuned input and output IDTs to avoid the image problem [75]. Kenny *et al.* discusses the simulation of a programmable SAW filter with variable gain and sign on the input and output fingers but no quadrature phase variation [76]. The results of a prototype with four weighted output taps were reviewed.

Panasik *et al.* [77],[78],[79] along with Zimmerman *et al.* [80] published papers in which various weighting designs were used to modify the frequency response of a SAW device but did not include any quadrature weighting. Duquesnoy *et al.* [81] published a paper using real weighting of the receiving fingers using a GaAs substrate. Oates *et al.* described methods of capacitively coupling RF signals [82] [83] [84] to a SAW delay line through an air gap and using biased MOS capacitors to control the real tap weights. Van Rhijn *et al.* [85] used switched JFETs on the receive fingers to control real tap weights. Hunsinger and Franck used programmable-current shunt diodes [86] to control receive finger real tap weights. That work was extended by inserting an Acoustic Charge Transfer (ACT) –based Programmable Tapped Delay Line (PTDL) using GaAs to receive and select the SAW signals by Guediri *et al.* [87]

Two patents on related concepts have been issued to J.A. Kosinski and R.A. Pastore. One was issued on October 1, 2002 on the topic “Programmable saw filter including unidirectional transducers” where the design focused on using a phased array of fingers in order to achieve directionality so as to reduce the “triple transit” effect [88]. This patent application supports the concept of individual interfaces to the IDT fingers but does not suggest an oscillator application. Additional attempts to date to find existing research on the topic of digitally tuning the SAW device to create a wideband oscillator have not yet yielded any evidence of existing work.

The other patent awarded to the same inventors was issued on April 1, 2003 entitled “Programmable surface acoustic wave (SAW) filter” [89] in which multiple IDTs were used along with different coupling resistance values for each to provide for adjustable weighting. This patent does not discuss individual control of fingers or quadrature weighting.

CHAPTER 5 SIMULATION

5.1 Simulation Approach

A common approach to simulating SAW devices is using the Coupling of Modes (COM) theory [90] [91] [92] [93]. These tools may be adaptable to future work, but they are designed to analyze classical multi-finger IDT structures and do not provide for integration with circuits such that the interaction between the circuits and SAW devices can be analyzed.

The research for this dissertation required a more system-oriented approach to simulation than could be supported by the existing COM tools and their derivatives. Future work will likely involve the COM tools to refine the design details, but the intent of this work was to demonstrate the described conceptual approach. After considering various options to build a system simulation tool to support this research, it was decided to develop SPICE models to simulate the SAW function. This approach offered the benefit of excellent integration with the semiconductor circuits necessary to interface with the SAW device. It is important to note that the SPICE transmission line is a “coupling of modes” model where the modes are the electric and magnetic fields. The electromagnetic transmission line, therefore, has a close functional resemblance to the electroacoustic transmission line created by the SAW structure.

While the use of SPICE to simulate SAW functions is uncommon, it has been done before. Early work was done by Bhattacharyya *et al.* [94] where SPICE transmission lines were used to simulate IDT elements and their interface with the transducers. Further work by Hohkawa *et al.* [95] included a more complete model using transmission lines based on an impulse model of the SAW filter[96]. These simulations all used lossless transmission lines. The work conducted for this research expanded considerably on this early SPICE work by incorporating lossy transmission lines to simulate the SAW functions and by developing a very tight integration between SPICE and MATLAB.

The simulations were performed using a combination of MATLAB®, available from The Mathworks, and LTspice, available from Linear Technology Corporation. The desired circuit is created using LTspice which can simulate the electronic devices using their SPICE parameters and which can simulate the SAW devices using appropriate lengths and parametric values of lossy transmission lines. The parameters for the lossy transmission lines were chosen to yield insertion loss results similar to those of published SAW devices.

The key to making this simulation tool pair useful is the structuring of the LTspice simulation files so that MATLAB code can read the critical SAW parameters, read and modify the control devices in the simulation file, launch the simulation, and read and analyze the simulation results. The MATLAB code is given a target frequency from which it determines, using appropriate algorithms combined with the SAW parameters in the simulation file, the desired phase offset for each finger of the sending and receiving

IDTs. These results are then used to determine the optimum control settings in the circuits of the simulation file.

The MATLAB code can cycle through a chosen set of target frequencies, run the desired AC analysis at each frequency, and interpret the resulting amplitude and phase response of the simulation result. The simulation time, which can take many hours for a wide range of target frequency samples, can be optimized by controlling the frequency range of analysis to cover a reasonable range of frequencies around the target frequency.

In practice this is accomplished by reading the LTspice netlist file for the prototype system, creating and saving a modified version of the file for a particular target frequency, launching an instance of LTspice in batch mode with that modified netlist filename as a command line parameter, waiting for the simulation to complete, then reading the LTspice data (.raw) file and interpreting the data. It is also quite useful if the MATLAB code can, in addition, create the resulting LTspice schematic files for the purposes of providing more detailed understanding about the circuit function. This is the approach used to create the simulation results described in the following section.

Numerous approaches to hardware implementation have been explored for this research. Some were rejected due to excess complexity or difficulty to implement in the available space given the required finger pitch. Two of the most promising architectures are discussed in section 5.2. The software algorithms used to control this hardware to achieve the desired frequency control is discussed in section 5.3.

5.2 Simulated Designs

Many simulations have been conducted in exploration of various approaches to this research. For the purposes of this dissertation the results for the two cases described in section 3.4 will be given. For these simulations the device parameters used were those of the AMIS 0.5 μ m C5N [97] process available through the MOSIS Fabrication Service [98]. The frequency ranges chosen for simulating these systems is an octave with a geometric center at approximately 200 MHz and 800 MHz. As the simulations will indicate, the C5N process has adequate performance for these frequency ranges, but a process with improved frequency response would be necessary to extend the operating frequency range. Most of the devices use the parameterized geometries listed in Table 3. Parameterizing the geometries simplifies the modifications necessary to adapt the design to a different process.

Table 3. General SPICE simulation device parameters

.param lm=.6u	minimum length
.param wm=20u	base NMOS channel width
.param wmin=10u	minimum channel width
.param k=2.45	ratio of PMOS channel width to NMOS channel width
.param VDD=5	supply voltage

A summary of the cases follows.

5.2.1 Design Case 1

Four phases are supplied to the control elements for each sending finger with approximately $\frac{\pi}{2}$ radians of phase separation between them. The process of generating

these four phases begins with the source shown in Figure 26 which creates the signal V_{inQ} having a nominal phase delay of $\frac{\pi}{2}$ radians at the center frequency of operation. In this figure the input AC voltage source V_{in} is swept as defined by the SPICE directive in the simulation.

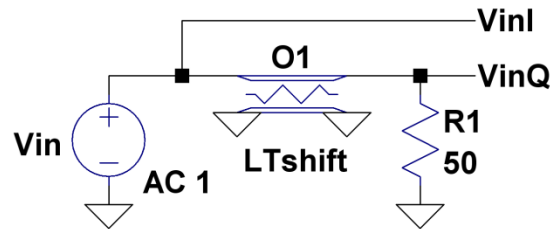


Figure 26. Input simulation source.

These two signals, V_{inI} and V_{inQ} are both sent to two inverting buffer pairs for each finger as shown in Figure 27 in order to make the signals I_{pos} , I_{neg} , Q_{pos} , and Q_{neg} available to the set of 4 transmission gates (TGs) shown in Figure 28. The buffer stages are required to provide isolation so that the load on each of the incoming phase lines is relatively constant and independent of the switch settings.



Figure 27. Inverters used to generate four phases from the two quadrature phases.

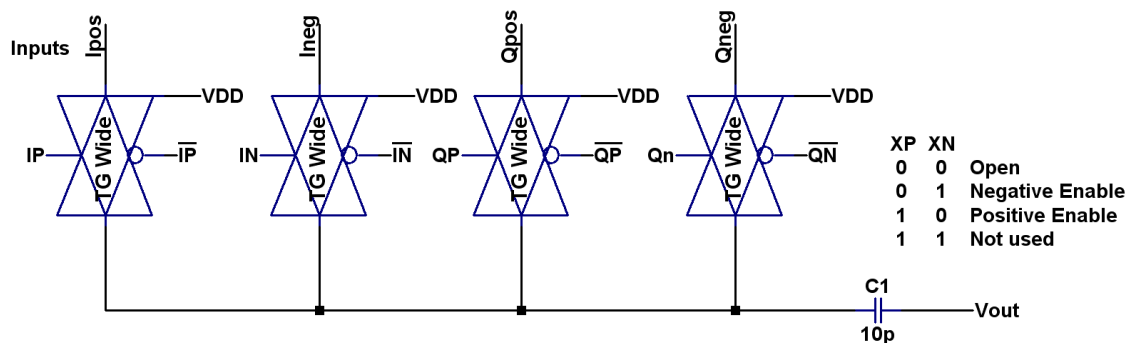


Figure 28. Sending finger control element.

The design of the inverters using devices from the C5N process previously mentioned is shown in Figure 29 where the component values are chosen to yield a gain over the range of operating frequencies of close to $A = -1$, and the capacitor C1 is chosen to compensate for the device capacitances and Miller effect in order to create a phase shift close to π radians over the range of operation.

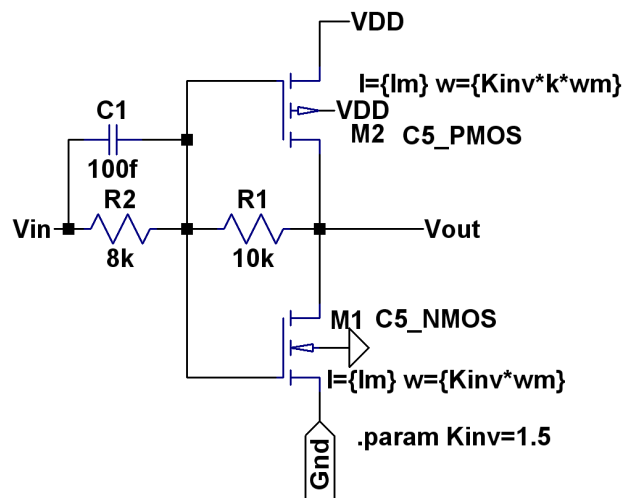


Figure 29. Inverter design.

As the simulation results will show, the values chosen will create in the system an increase of gain with frequency up to a point but will manage to maintain the phase requirements reasonably well.

The device parameters in Figure 29 (as are virtually all devices used in this simulation) are parameterized based on the technology. The globally-set terms l_m and w_m are minimum length and minimum width, respectively. The parameter k is set globally to compensate for the higher mobility of the N-channel devices relative to the mobility of the P-channel devices for the process technology and is set to a value of 2.45 for these simulations. This value was derived based on simulations of various inverter designs. The value of K_{inv} is chosen to provide suitable bandwidth for the given capacitive loads. The value of $C1$ is chosen to compensate for the gate capacitance of the devices and to improve the gain flatness and phase response.

The signal for each phase is derived from a set of four transmission gates (TGs) acting as resistive switches, each connected to one of the phases through the buffer stages. Either one or two of the four transmission gates may be active for any finger at any time providing one of 8 phases at approximately 45° increments.

In an actual circuit there will be no need for the DC blocking capacitor $C1$ shown in Figure 28 since the piezoelectric material should have very high DC resistivity. The circuit inside each of the TGs is shown in Figure 30 where the width and length of the MOS devices can be controlled parametrically. In an actual implementation the TGs will be controlled by a shift register, but for this simulation their state is controlled by the MATLAB code which modifies the SPICE netlist and can also create an LTspice .asc file with the digital values set to tune the resonator to the desired frequency.

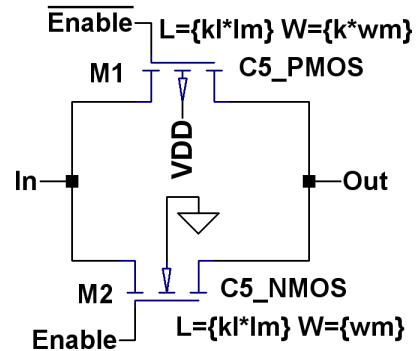


Figure 30. Transmission gate circuit.

The outputs of the drivers directly drive the array of lossy transmission line segments that comprise the simulated IDT as shown in Figure 31.

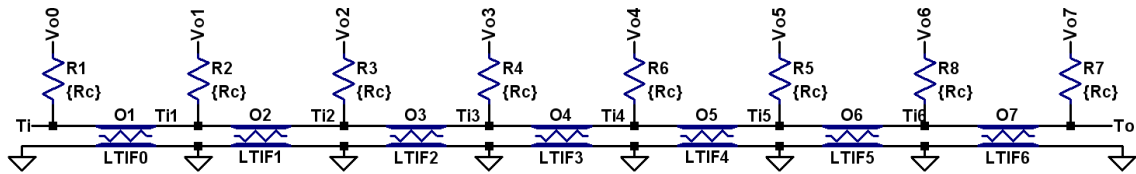


Figure 31. Lossy transmission line segments simulating IDT portion.

where the parameters of the transmission line segments are controlled by the SPICE directives shown in Table 4. In the simulation the parameter dl is set by the MATLAB code, and the parameter $Tiflen$ is set to be the length corresponding to a half wavelength at frequency f_c .

Table 4. SPICE directives for IDT transmission lines.

<code>.param TIFlen0=1.0*Tiflen</code>	<code>.model LTIF0 LTRA(len={TIFlen0} R=.05 L=1.25n C=500f)</code>
<code>.param TIFlen1=(1+1*dl)*Tiflen</code>	<code>.model LTIF1 LTRA(len={TIFlen1} R=.05 L=1.25n C=500f)</code>
<code>.param TIFlen2=(1+2*dl)*Tiflen</code>	<code>.model LTIF2 LTRA(len={TIFlen2} R=.05 L=1.25n C=500f)</code>
<code>.param TIFlen3=(1+3*dl)*Tiflen</code>	<code>.model LTIF3 LTRA(len={TIFlen3} R=.05 L=1.25n C=500f)</code>
<code>.param TIFlen4=(1+4*dl)*Tiflen</code>	<code>.model LTIF4 LTRA(len={TIFlen4} R=.05 L=1.25n C=500f)</code>
<code>.param TIFlen5=(1+5*dl)*Tiflen</code>	<code>.model LTIF5 LTRA(len={TIFlen5} R=.05 L=1.25n C=500f)</code>
<code>.param TIFlen6=(1+6*dl)*Tiflen</code>	<code>.model LTIF6 LTRA(len={TIFlen6} R=.05 L=1.25n C=500f)</code>
<code>.param TIFlen7=(1+7*dl)*Tiflen</code>	<code>.model LTIF7 LTRA(len={TIFlen7} R=.05 L=1.25n C=500f)</code>

The 32-finger sending system consists of 4 modules each of which contain 8 transmission gate sets as shown in Figure 28 that drive the 8 ports Vo0 through Vo7 of the segmented transmission line shown in Figure 31. For completeness, the eighth transmission line segment is between adjacent modules. The number of modules can be expanded arbitrarily. An example of a single 8-finger sending module is shown in Figure 32 where the data inputs *have* been set by the MATLAB code to 0 (represented by the ground symbol) or 5V (represented by the number “5”) to control the 32 internal TGs which adjust the phase sent to each of the 8 fingers. Note that the first sending module shown below (as well as the last receiving module) has the transmission line terminated in a matching load. These terminations are very important to prevent reflections from the end of the finger array from re-entering the system. In practice there will need to be an acoustically-absorbing material to be applied to the ends of the substrate to minimize these reflections. This is particularly important order to minimize the response of the system to image frequencies which are preferentially sent and received in the opposite direction from the desired frequency as will be seen in section 5.4.1. The limited accuracy from simulating the degree of acoustic reflection following mitigation for an

actual device may lead to errors in predicting the response to the image frequency. It is important to note that other factors such as gain variations vs. phase angle in both the signal generation in the sender or summation of the received signals can also lead to leakage at the image frequency.

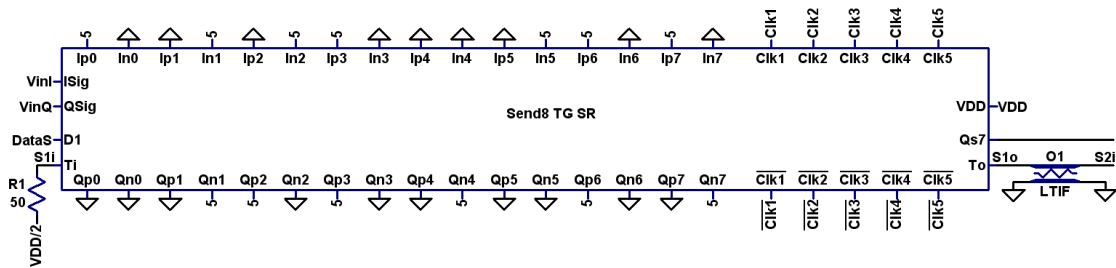


Figure 32. Eight-finger sending module.

The transmission line emerging from the last of the sending modules directly drives a special transmission line that simulates the relatively long delay between the sending IDT and the receiving IDT. In this simulation the length of this delay line was chosen to be 100ns, equivalent to 20 wavelengths at the center frequency of 200 MHz. Increasing the delay time would yield higher Q but would need to be accompanied by an increase in the number of fingers in each IDT in order to increase the selectivity of the filtering provided by the IDTs. This delay line along with the first of four eight-finger receiving modules are shown in Figure 33 where the digital inputs have again been programmed by the MATLAB code (in this case for a frequency of 280 MHz).

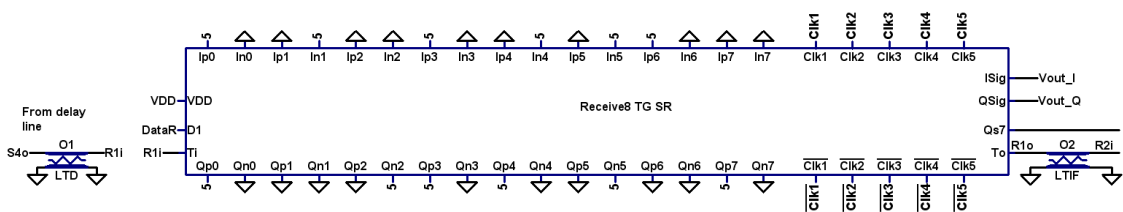


Figure 33. Eight-finger receiving module and intra-IDT delay line.

Further examination of a receive module shows another array of transmission line segments in Figure 34 that provide inputs to each of the receive finger control elements in Figure 35 consisting of 4 TGs per finger whose conductivity is controlled by shift registers in the actual circuit and which are controlled by the MATLAB code for the simulation. The TG design is as shown in Figure 30. Once again the capacitor in Figure 35 is necessary for simulation only as that DC blocking function will be provided by the piezoelectric dielectric properties.

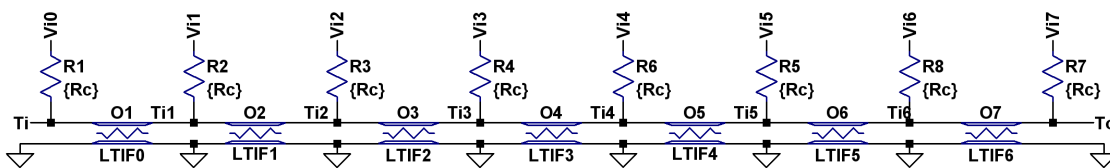


Figure 34. Lossy transmission line segments simulating receive IDT line.

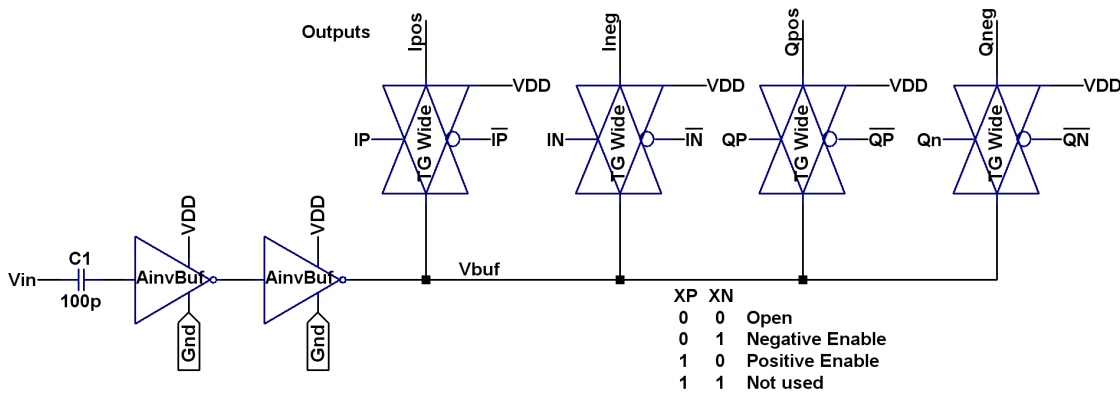


Figure 35. Receive finger control element.

The output of each of these control elements drives a set of inverting buffer elements shown in Figure 36 where each inverter is as shown in Figure 29.

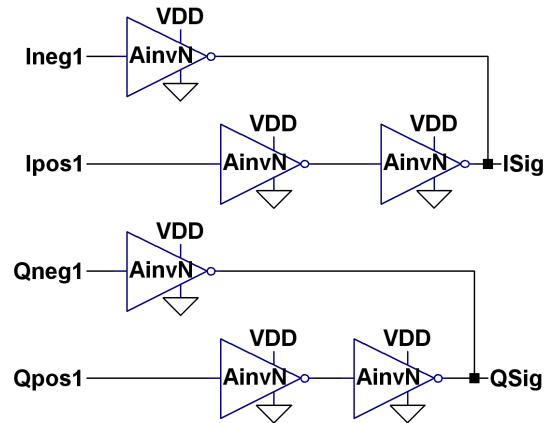


Figure 36. Buffer elements driven by the receive element signals.

The I and Q signals from the buffers for all of the 32 receive fingers are summed in the circuit in Figure 37 to form the final output. The passive components for this summing circuit will not be integrated into the IC, and the transmission lines and summing function will likely be replaced by an RF combiner.

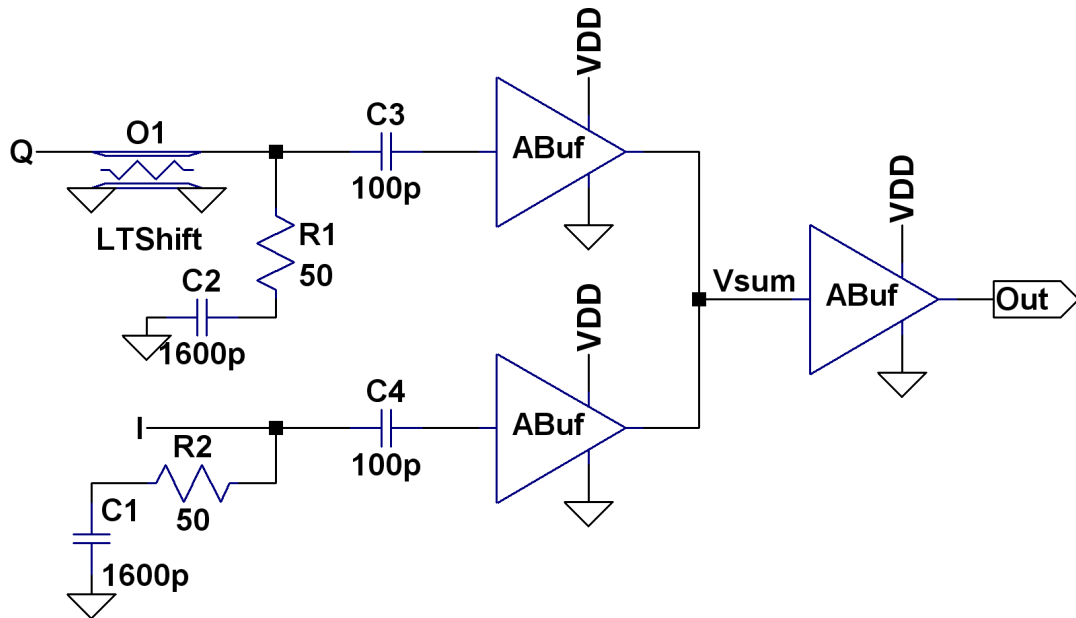


Figure 37. Quadrature combiner for the receive fingers.

5.2.2 Design Case 2

The intent of this design case is to support the potential for using solid-state switching mechanisms to select the phase relationships between the various fingers in a device. A very interesting approach would be to use a non-volatile switching element such as a chalcogenide-based resistive element as a switching device using an architecture similar to a crossbar switching matrix. This could lead to a device with a programmable frequency-response, and once programmed the response would be retained through the non-volatile nature of the switching elements. It could also be potentially used as a passive element in the operational mode. However, it is likely that there will need to be active devices integrated in the system to support the switch programming mode.

For this simulation the AMIS 0.5 μ m C5N devices were used as described earlier except that the switches used were SPICE behavioral switches that will be described later. At this time the RF parasitic characteristics of switches fabricated from the chalcogenide materials is not well understood, so it is not possible to construct a highly accurate model of these devices. This simulation model will, however, provide a good basis for further study of the capability of devices utilizing switches with various RF properties.

This design case requires that eight phases be supplied to the control elements for each sending finger with approximately $\frac{\pi}{4}$ radians of phase separation between them.

The signal for each phase is derived from a set of eight resistive switches where only one is conducting for any finger at any time. The benefit of this approach is that the buffer stages may not be necessary between the phase lines and the switches since there is no need to create intermediate phases by combining the signal from two phase lines. The resistive switch in this case could be either a TG or an alternative switch design which could be constructed from a diode or an alternative material whose resistive state can be switched using either a volatile or non-volatile mechanism. The circuit to generate the eight required phases is shown in Figure 38 where the passive devices would be located outside of any integrated circuit and may be replaced with RF coupler elements.

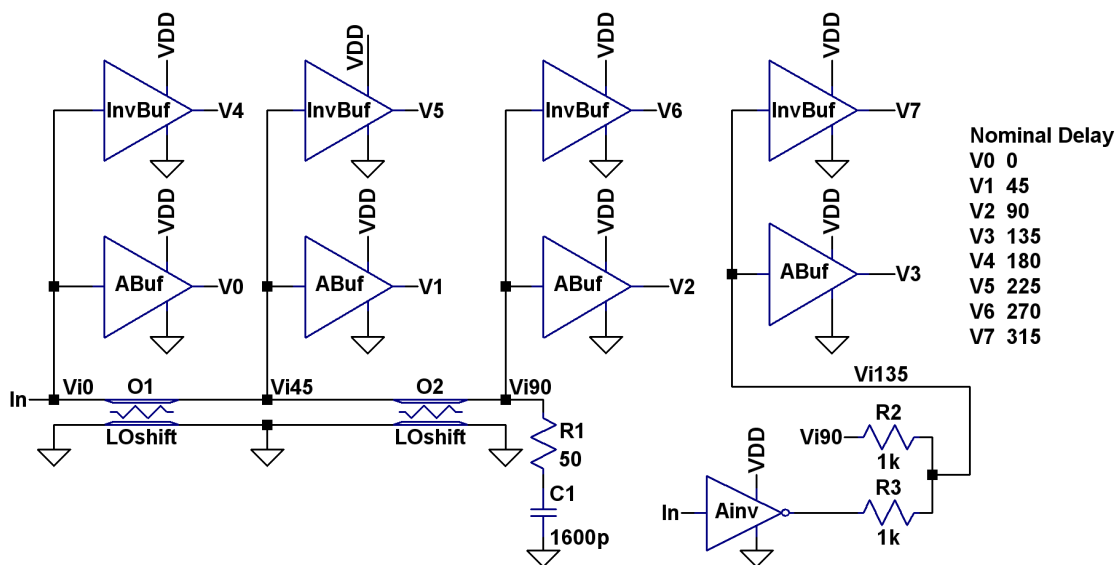


Figure 38. Signal Generation Circuit

The analog buffer ABuf is constructed as shown in Figure 39

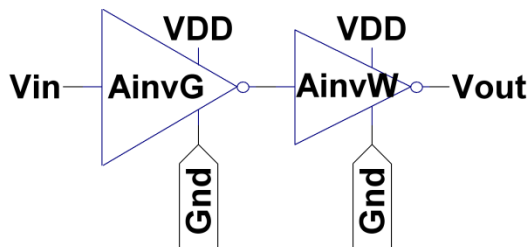


Figure 39. Analog buffer.

where the input analog inverter AinvG is constructed from minimum-geometry devices as shown in Figure 40, and the wide inverter AinvW is constructed of devices with triple the ordinary width as shown in Figure 41. The components for the wide inverter are chosen to provide a gain with unity magnitude and a phase shift of π radians.

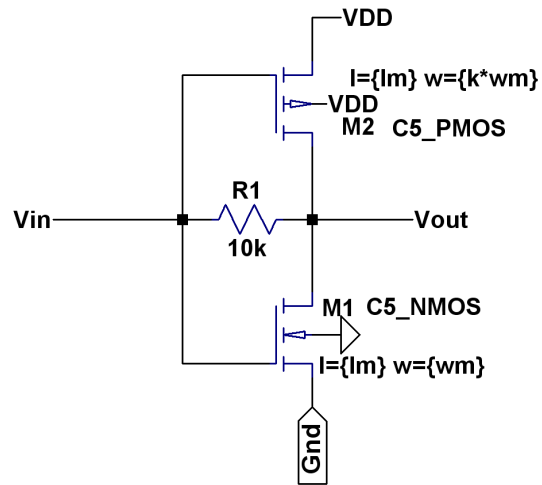


Figure 40. AinvG Input inverter.

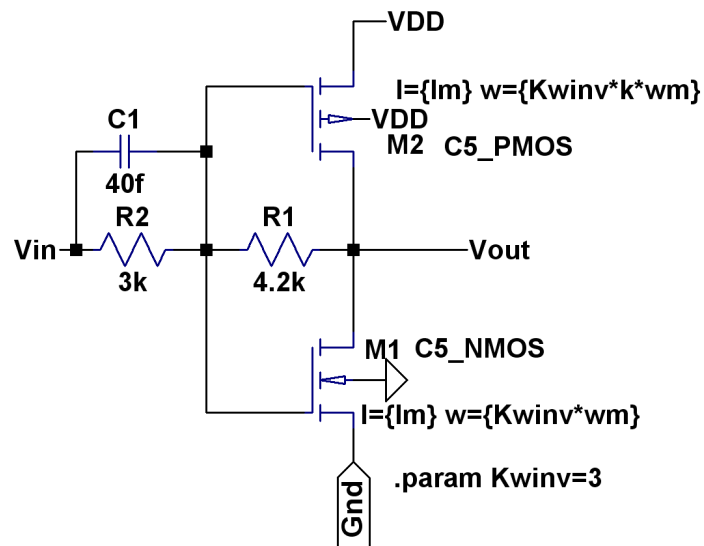


Figure 41. AinvW Wide analog inverter.

The design of this system does not, for this simulation, provide any buffers between the 8-phase signal generator and the switches controlling the signal to the

fingers. As a result, the number of finger loads on each phase of the generator can vary from 0 to half of the sending fingers. The wide inverter AnivW is needed to reduce the signal level variation due to load variation

The inverting buffer InvBuf of Figure 42 is similar to that of Figure 39 with the addition of an Ainv module that is identical to that shown in Figure 29.

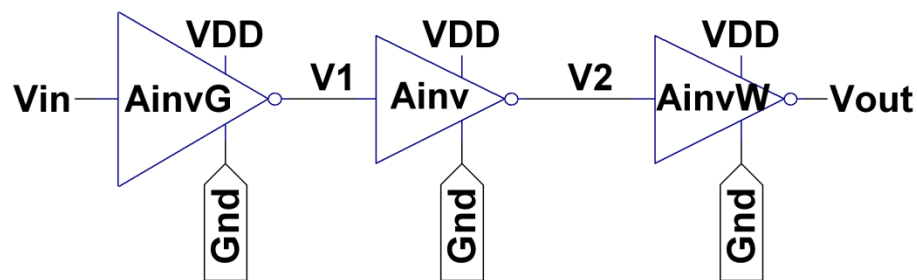


Figure 42. InvBuf Inverting buffer design.

The eight phases are supplied to each sending module as shown in Figure 43 where the eight inputs SPh0 through Sph7 are the eight sending phases. The nodes Ti and To are the transmission lines and, as previously, the input port of the transmission line is terminated with a matching resistor, and the output port To is connected to an eighth transmission line segment representing the space between IDT fingers. In this case there are eight fingers being controlled, and there are no decoders embedded in the module so that there are eight bits of control data for each finger with the resulting 64 bits of control data. The 0-0 through 7-0 represent the control bits for finger 0 in the module, and exactly one of these bits should be active as indicated by the number 5 on the line. It can be seen in the figure that the eight active control bits are associated with eight

different fingers. As with the previous simulation, the LTspice schematic file with the appropriate control bit assignment is created by the MATLAB code operating on the requirement for a given desired frequency.

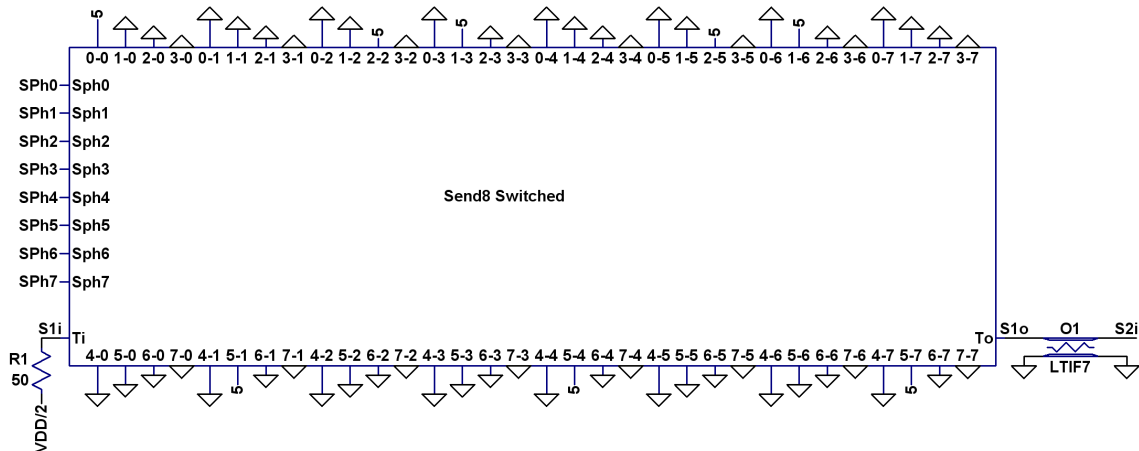


Figure 43. Eight-finger sending module.

The eight fingers in each of the sending modules are controlled by the eight switch sets shown in Figure 44 with each of the modules supplying a signal to one of the fingers Vo0 to Vo7. Each of the modules has eight signal phase inputs Sph0 through Sph7 and eight control inputs Ph0 through Ph7.

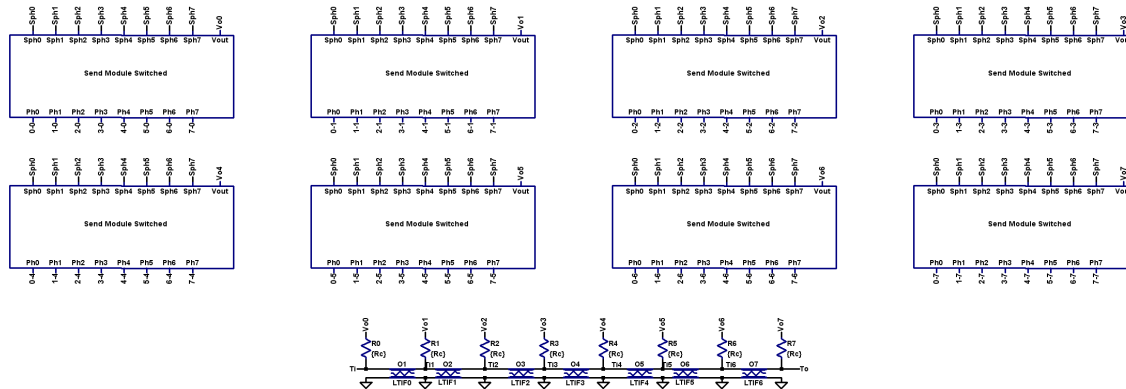


Figure 44. Switching modules controlling the fingers.

As mentioned earlier, the switching elements are behavioral SPICE switches with programmable on and off resistances as shown in Figure 45. The parameters listed for the switch model can be easily modified and additional parasitic elements can be easily added in parallel and series with these elements to simulate various solid state switching materials and geometries. It is also possible to use transmission gates in place of these switches, should that alternative provide some benefits over the architecture used in Design Case 1.

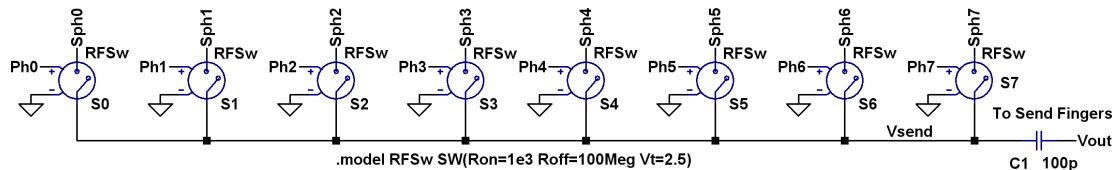


Figure 45. Detail of the finger control elements.

The output of the last sending finger module drives a transmission line that simulates the propagation between the sending and receiving IDTs. As in Design Case 1, the length of this line is set to 100 ns which corresponds to 20 wavelengths at the center frequency of 200 MHz.

The output of the delay line is sent to the array of receiving fingers where a similar set of switching elements connects the finger signal to the appropriate phase summing junction as shown in Figure 46. As with the sending module, further refinement of the switch parameters and parasitic elements can be easily added to simulate the actual switching device RF characteristics.

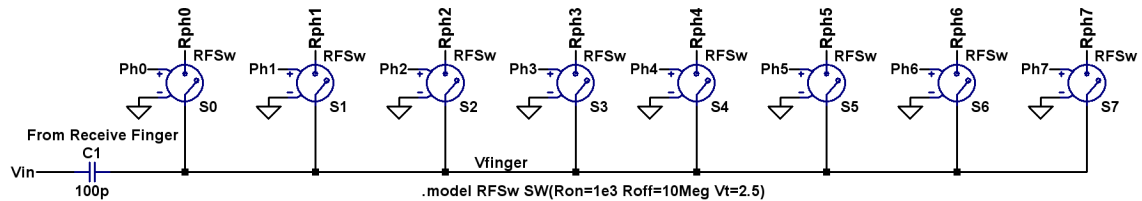


Figure 46. Receiving module switching array.

The outputs of these finger switches are sent to the receiver summing module shown in Figure 47. This module is designed to provide the appropriate phase shift to each of the finger signals. The simulation results suggest that this module design works reasonably well, but there is likely an opportunity for improvement in this design. Providing accurate signal summing capability over a large bandwidth at high frequencies is challenging. Using conventional transmission line combiners works well, but these devices are inherently bulky and tend to support a limited frequency range. Solid-state summers will generally utilize high impedance sources supplying signal currents to a low-impedance node serving as the input to a transimpedance amplifier that effectively translates input current into an output voltage with good gain.

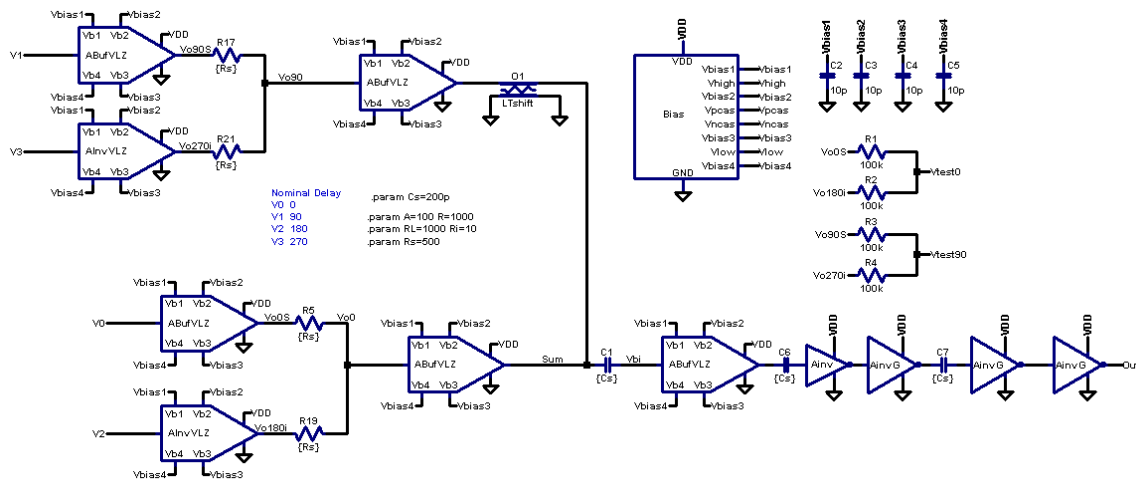


Figure 47. Receiving summing and shifting module.

The bias circuit in Figure 47 is derived from Baker [99] with minor modifications to parameterize the device geometries. The modules named AInvVLZ is shown in Figure 48 and the non-inverting version of it named ABufVLZ are identical except for the absence of the output inverter included in Figure 48. The devices AInvG and AInv are as shown in Figure 40 and Figure 29 respectively.

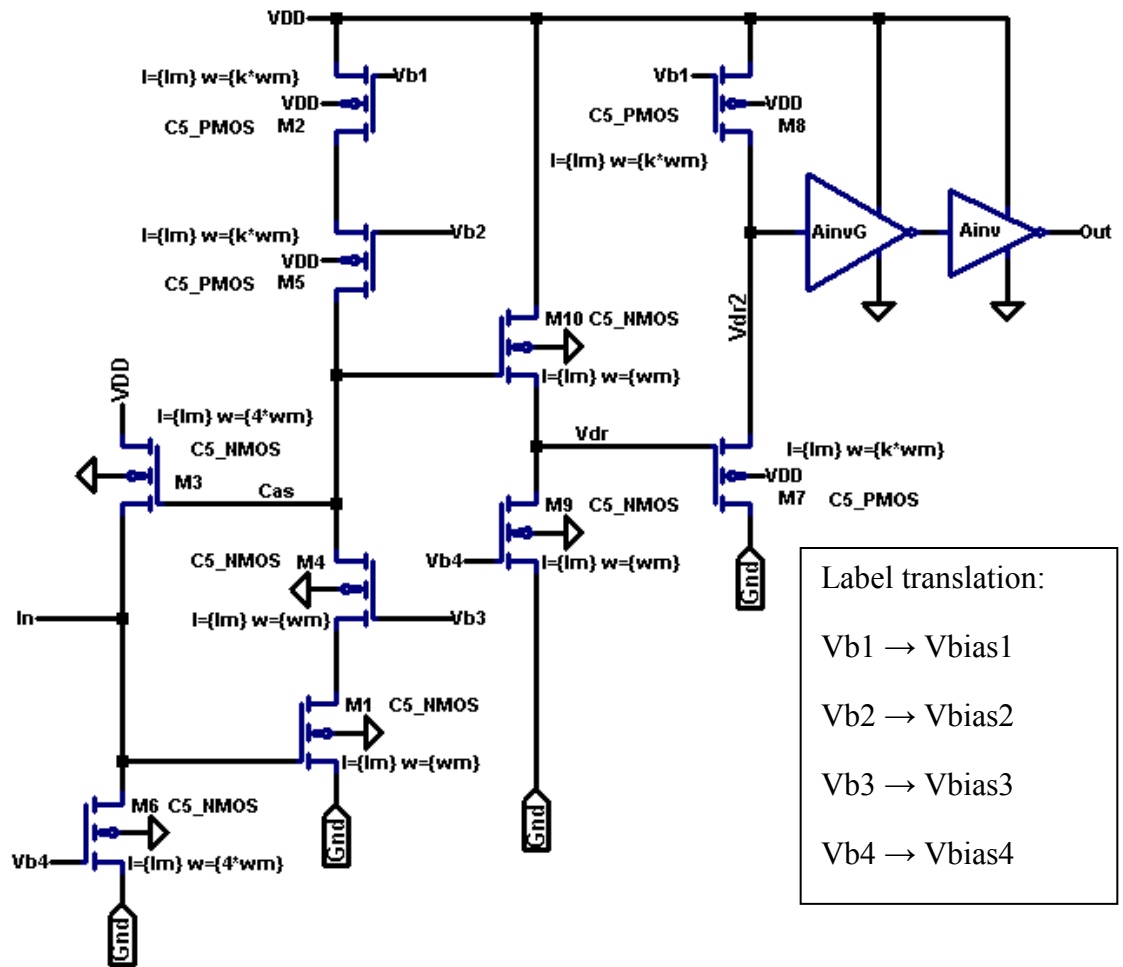


Figure 48. Low input impedance amplifier stage.

The gain of the non-inverting version of the device ABufVLZ is shown in Figure 49 where the magnitude is relatively flat. The phase delay is more than desired but can be compensated for in the algorithms described in the following section.

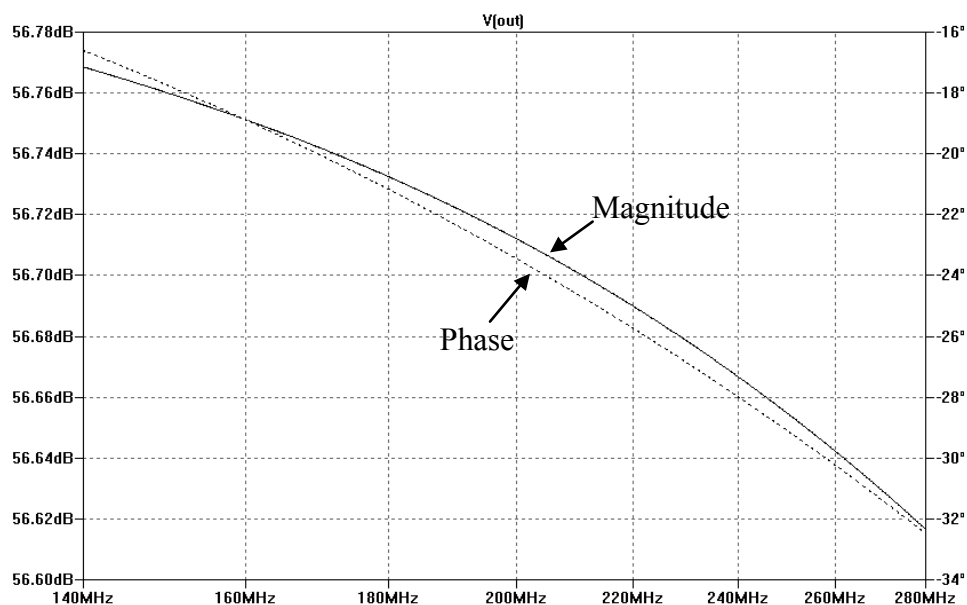


Figure 49. Gain of the amplifier in Figure 48

The interesting aspect of this design is that the low input impedance shown in Figure 50 can be achieved due to the feedback through device M3 combined with the relatively high gain of the input stage due to the dual cascode configuration. Stability tests show good margin and the power consumption is very low.

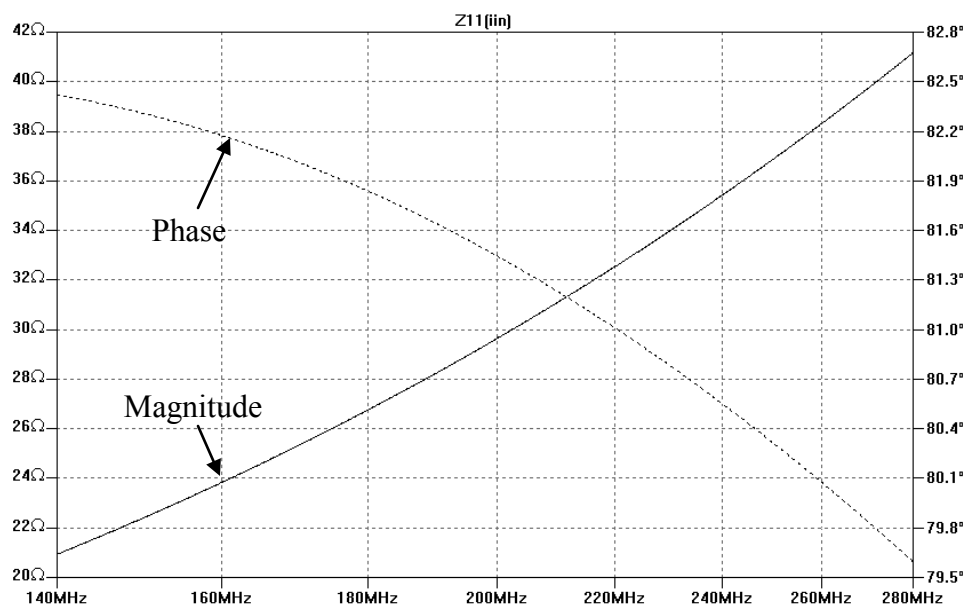


Figure 50. Input impedance of amplifier in Figure 48

The final output of the device is shown in Figure 47. This completes the description of the hardware component of the simulation.

5.3 Simulation Algorithms

This section describes the algorithms for computing the phase control parameters for the digitally controllable SAW resonator which meets the Barkhausen criteria at a desired frequency f_D . For this description it is assumed that the spacing of the fingers is constant.

5.3.1 Determining the phase shift between IDT fingers

The basic phase shift between fingers in an IDT is given by

$$\angle(IDT) = -2\pi \frac{T_F}{T_D} \quad (18)$$

where the transit time between fingers is

$$T_F = \frac{d_F}{v} \quad (19)$$

given d_F and v as defined in Equation (1) and the period of the desired frequency

$$T_D = \frac{1}{f_D} \quad (20)$$

5.3.2 Determining target phase of the signal to each finger

The target phase of the input signal that should be supplied to each of the sending fingers, converted using the standard modulus function so that it falls in a range of $[0:2\pi]$, is

$$\angle(target_i) = mod(\angle(IDT)(0:N_f - 1), 2\pi) \quad (21)$$

where N_f is the number of sending fingers and the operation $(0:N_f - 1)$ returns an array of N_f elements increasing uniformly from 0 to $N_f - 1$.

If the spacing is not uniform, then adjustments can be easily made to this equation where the phase shift angle between fingers depends on the finger pair. At this point the target phase angle is now known for the sending fingers.

5.3.3 Determining available phases of the input signal

If eight phase angles are used, the available angles would ideally be

$$\theta = \frac{\pi}{4} [0, 1, 2, 3, 4, 5, 6, 7] \quad (22)$$

One implementation of this system would be achieved by utilizing a conventional two-way 90° hybrid power splitter [100] combined with inverters and summers to provide the required phases. Four phases listed in Equation (22), $\theta =$

$\frac{\pi}{4} [0, 2, 4, 6,]$ can be developed by using the two outputs of the 90° hybrid power splitter (0° and 90°) and adding two inverter stages to produce the angles 180° and 270°.

The other four phases can be created by summing each pair of adjacent quadrature signals. The data sheet for the hybrid splitter shown in the reference suggests a phase imbalance, or difference between the phases of the two outputs, to vary by less than 7 degrees over a greater than octave frequency range as shown in Figure 51.

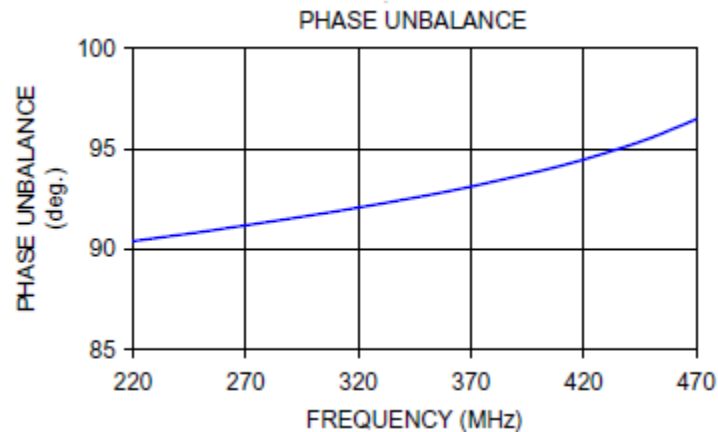


Figure 51. Mini-Circuits model “QCN-3+” 90° splitter “phase unbalance.”

While this appears to be a very useful component for generating the requisite phase shifts for both the sending and receiving process, there does not appear to be a satisfactory SPICE model available to support this device. Consequently the SPICE simulation used for this dissertation developed the phase delay with a conventional transmission line. With such a transmission line the phase characteristics will lead to a phase delay proportional to frequency. This provides manageable but not optimal performance over an octave of frequency range where the phase delay has a 2:1 range. A somewhat realistic work-around for this situation would be a delay line in SPICE the length of which was MATLAB controllable based on the desired resonator frequency. Since the intent of the simulation for this work was to evaluate the performance under conditions as realistic as possible, this approach was not pursued. However, it would be very easy to do and will be considered for future simulation of a system that might incorporate the hybrid splitter and combiner. For the purposes of this simulation, the assumed available phase shift angles are

$$\theta = \frac{1}{2} [0, \phi, 2\phi, \phi + \pi, 2\pi, \phi + 2\pi, 2\phi + 2\pi, \phi + 3\pi] \quad (23)$$

which are the angles available from inverting and summing components from an unshifted signal and a signal delayed by an angle ϕ which has a nominal value of $\frac{\pi}{2}$ at $f = f_c$.

5.3.4 Assigning input signal phases to the fingers

For the purposes of this discussion it is assumed that the available phases are distributed as specified in Equation (22). Obvious modifications to this discussion can be made to support the available phase distribution of Equation (23). For a conventional SAW device where $f_D = f_c$ (and $T_D = T_F$) the target phases are relatively easy to assign as they are limited to 0 and π (or 180°) as shown in Figure 52.

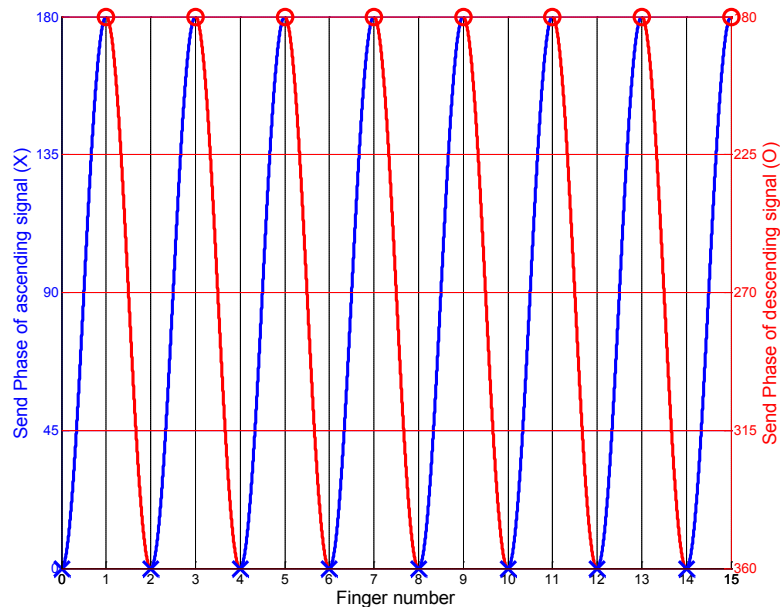


Figure 52. Phases of sending fingers for conventional SAW device.

However, for the devices described in this dissertation where the desired frequency may be significantly different from the center frequency of the device, the target sending finger phases are generally very different. An example of this case is shown in Figure 53. In this figure the angles of the ascending portion of the sinusoid, shown in blue, correspond to the left axis and the angles of the descending portion of the sinusoid, shown in red, correspond to the right axis. The marker “X” corresponds to places where the ascending portion of the sinusoid crosses a finger location while the marker “O” corresponds to the finger crossing of the descending portion. In Figure 53 the desired frequency is higher than the center frequency while in Figure 54 the desired frequency is lower than the frequency f_C .

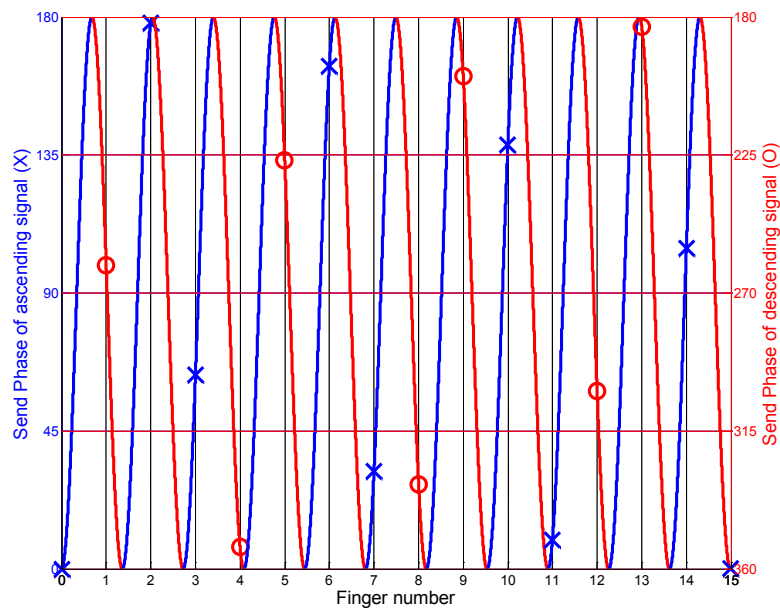


Figure 53. Sending finger phases for $f_D > f_C$.

In both cases the algorithm for determining the phase to supply to each of the sending fingers is identical. The phase of choice is the phase corresponding to the closest phase alternative among those listed in Equation (22) at the finger crossing. Using Figure 53, for example, the phases selected would be 0° , 270° , 180° , 45° , 0° , and 225° for the first six fingers, noting that 0° and 360° are the same phase.

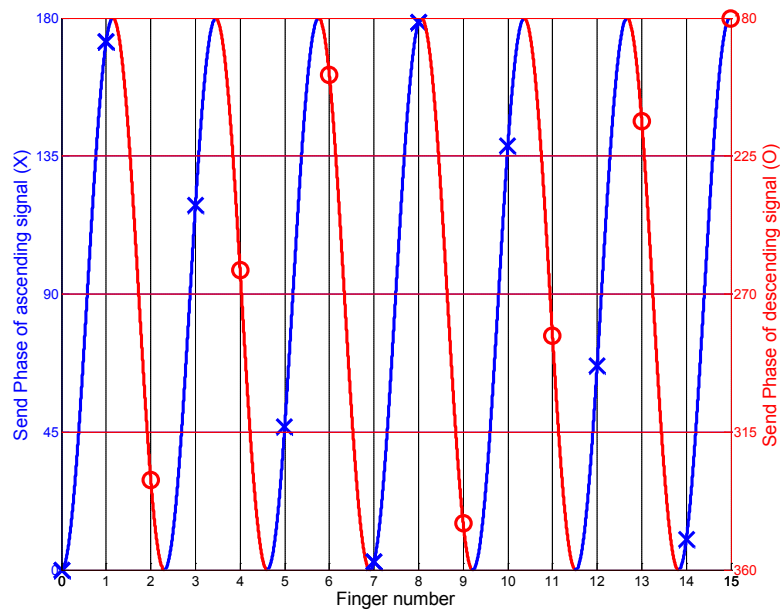


Figure 54. Sending finger phases for $f_D < f_C$.

5.3.5 Estimating the launch angle

Following the selection of the optimal available phase variation of the input signal, it is now necessary to estimate as accurately as possible the actual launch angle of the acoustic wave, defined as the phase of the acoustic signal at the last sending finger. The launch angle is ideally determined by the weighted mean of the contribution to the

launched signal by all sending fingers, where the weighting factor is a combination of the amplitude of the signal at each sending finger and the attenuation through the sending IDT. Phase distortion due to reflections is neglected in this estimate. Each finger is delivered a version of the input signal shifted by a known angle and the acoustic wave from each finger travels at an assumed velocity with a resulting phase shift to the end of the sending IDT. Ideally the signal contributed by each finger at that point should be identical, but because of the limited phase resolution there will be some variation in the phase of the signal contributed by each finger. In reality other non-ideal conditions will inject additional phase errors into the signal, most notably the reflections of the acoustic waves from the fingers they pass as they travel along the surface. To some extent this reflection phenomenon is incorporated in the SPICE model as a result of the impedance mismatch due to injecting the signal into the transmission line junction.

The array of signal phase angles supplied to the input finger array is

$$\angle(finger_i_sig) = \theta(min_i_indices) \quad (24)$$

where θ is an array selected either from Equation (22) or (23) and $min_i_indices$ is the index array selected for the array of sending fingers to yield the desired phases.

The angular finger delay array due to the transit time for each finger to the launch point is the target angle of each finger subtracted from the target angle of the last finger.

$$\angle(finger_i_delay) = \angle(target_i(N_i)) - \angle(target_i) \quad (25)$$

The contribution angle is then

$$\angle(finger_i_contribution) = \angle(finger_i_sig) + \angle(finger_i_delay) \quad (26)$$

The launch angle, assuming equal signal level at each finger and negligible attenuation through the sending IDT, is then determined by the mean of the angle of all the contributing signals

$$\angle(\text{launch}) = \text{mean}(\angle(\text{finger}_i\text{contribution})) \quad (27)$$

5.3.6 Estimating the receive angle

Given a launch angle, the expected phase angle at the first receiving finger, or the receive angle, is determined by the frequency, the propagation velocity, and the distance between the closest transmit and receive fingers. Once again, there are many factors in reality that distort the receive angle and lead to imperfections in the estimation. A typical cause of error is a phenomenon referred to as the triple-transit effect which is caused by an acoustic signal reflecting from the receiving fingers back toward the sending ones and the resulting reflection being sent back toward the receiving fingers at a different phase angle.

In the simulations used here the receive angle is estimated by

$$\angle(\text{receive}) = \angle(\text{launch}) - 2\pi f_D(T_D + T_P) - \Phi_E \quad (28)$$

where f_D is the desired frequency, T_P is the propagation delay through the electronics circuits, Φ_E is known phase errors due to internal reflections and mismatches, and

$$T_D = \frac{d_{TF}}{v} \quad (29)$$

where d_{TF} is the distance between the IDTs as measured by the closest finger pair and v is the acoustic velocity of the substrate.

5.3.6 Assigning phase delays to the receiving fingers

For the receiving IDT the algorithm is similar to the algorithm for the sending fingers. The first step is to determine the angle expected to be received at each finger given the frequency and the angle received at the first finger determined by the $\angle(receive)$ value. The available phase delays are, for this research, assumed to be similar to those available for the sending fingers. The objective is to rotate the angle of the received signal from each receiving finger to zero degrees using the available phase delays and add it to the total received signal.

An initial approach is to simply find the closest match to the target receive angle for each finger and assign it to a phase delay that generates the closest match to a zero-phase result. In the example shown in Figure 55 where $f_D > f_C$ and $\angle(receive) \cong 145^\circ$ the objective is to provide sufficient delay so that the signals from all fingers are rotated to 360° .

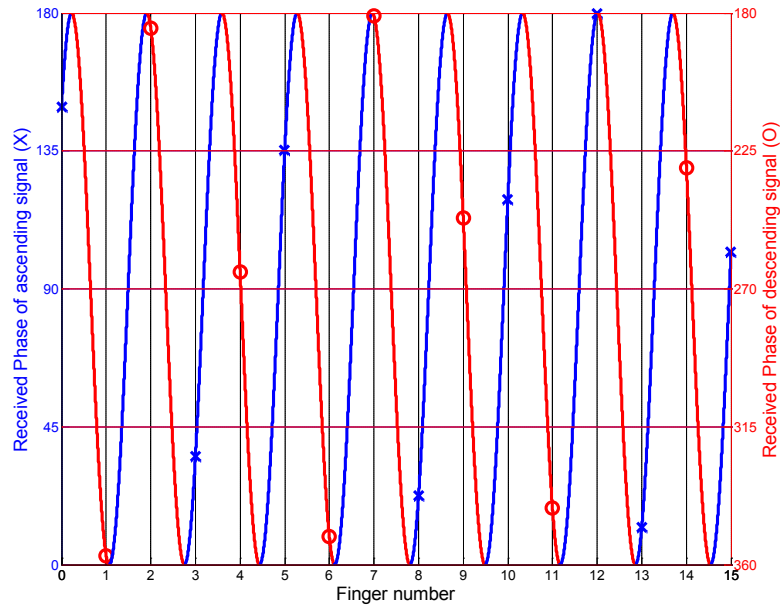
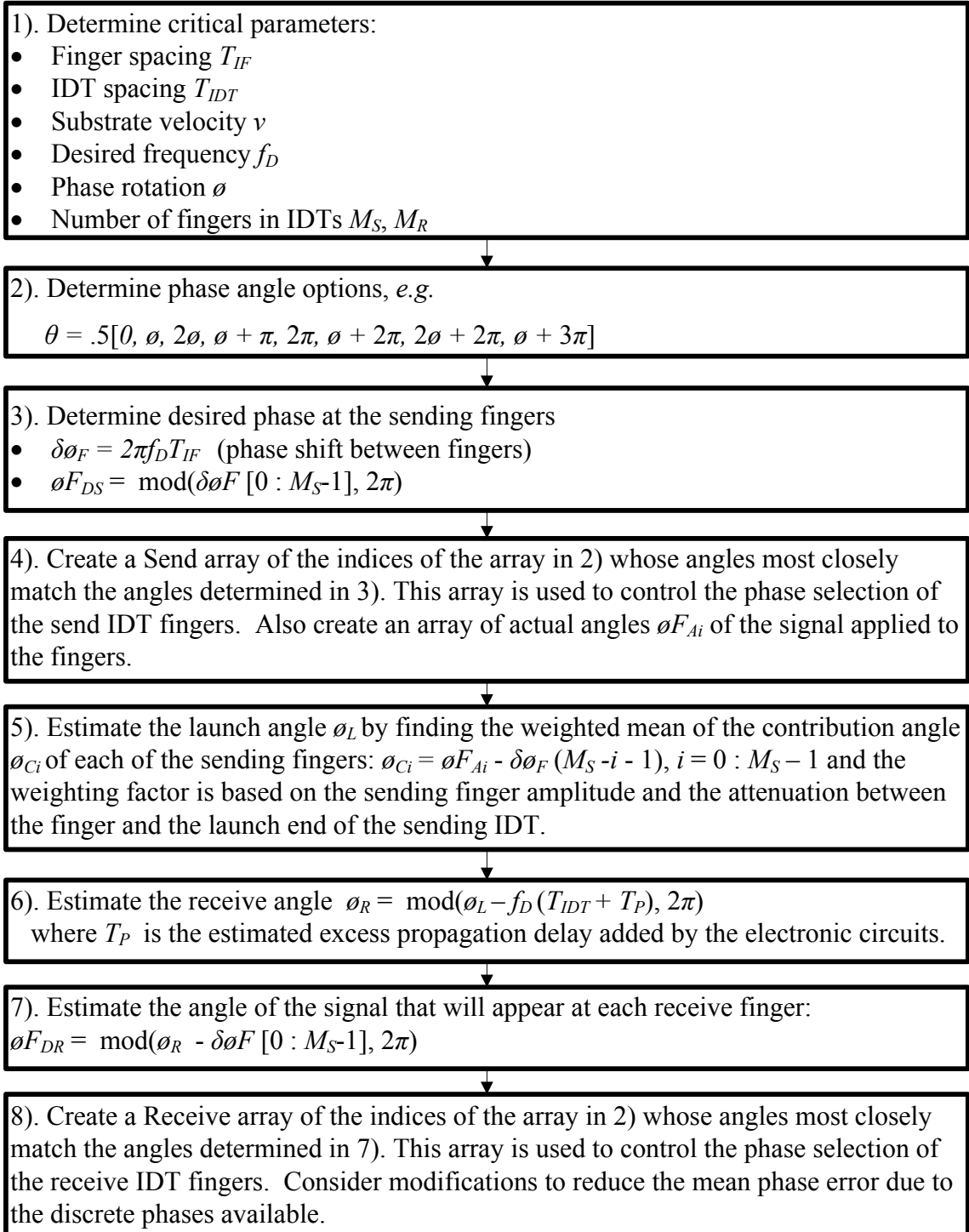


Figure 55. Receiving finger phases.

Thus the phase delay applied to the received signals from the first six fingers, for example, should be 225° , 0° , 180° , 315° , 90° , and 225° . This delay can be computed by subtracting the received angle from 360° or simply by using the opposite vertical axis.

While the approach as described is a good approach, it is not generally optimal because it does not necessarily lead to the minimum total phase error. It is quite possible that when each finger is connected to the phase that is closest to its desired phase the final output phase will have a bias and not be as close to a zero phase error as possible. Stated differently, if the phase errors for all fingers are of the same polarity, the total will not be as close to zero as desired. Various approaches exist to address this phase bias problem. One approach is to apply a dither to the phase selection. Another approach that may be slightly better would be to exhaustively search all reasonable alternatives of adjacent

phases to find the optimal outcome. The dither approach currently used in this research leads to good results. The simulation algorithm is summarized in Table 5.

Table 5. Algorithm to determine finger phases

5.4 Simulation Results

5.4.1 General Simulation Observations

The primary focus of the simulation is to determine how closely the frequency response and the phase shift of the SAW device and the associated electronics match the behavior predicted by the algorithm. This behavior is controlled exclusively by the digital data created by the algorithm and sent to the simulator where it adjusts the phase shifts applied to the fingers.

These frequency response and phase shift parameters are the dominant factors that control the tuned frequency of an oscillator controlled by the SAW resonator. Gain variation with frequency is of less concern as it can be compensated for with programmable variable-gain amplifier devices.

The results will show inconsistent and rapidly-fluctuating amplitude and phase performance in the vicinity of the center frequency as was discussed previously in section 3.2. This fluctuation is due to a variety of factors. One of the factors is inherent in the nature of the SAW device itself and is due to the fact that at their center frequency the sending fingers radiate equally well in both directions. Thus some of the radiated energy travels in the wrong direction and gets partially reflected back at various phases. Due to reciprocity, it can be shown that the receiving fingers are also less effective at picking up the proper signal. At frequencies away from the center frequency the signal is preferentially sent in the desired direction since the phase shifting of the fingers causes constructive interference in that direction and destructive interference in the opposite direction. This effect can be observed in Figure 56 where the LTspice input signal is

swept from 140 MHz to 280 MHz and the signals at five locations on the sending IDT and the final output are observed. In this case the finger phases are set to create a bandpass filter at 160MHz and as in all of these tests the finger spacing is set to be a half wavelength at 200 MHz. Finger 15 is at the midpoint of the sending array and it can be seen that the signal amplitude at that point is approximately the same when a 160 MHz signal is launched as when a signal with the image frequency of 240 MHz is launched. The solid lines in the figure are magnitude and the dotted lines are phase. The interesting characteristic about the phase is the increase in the magnitude of the slope at the

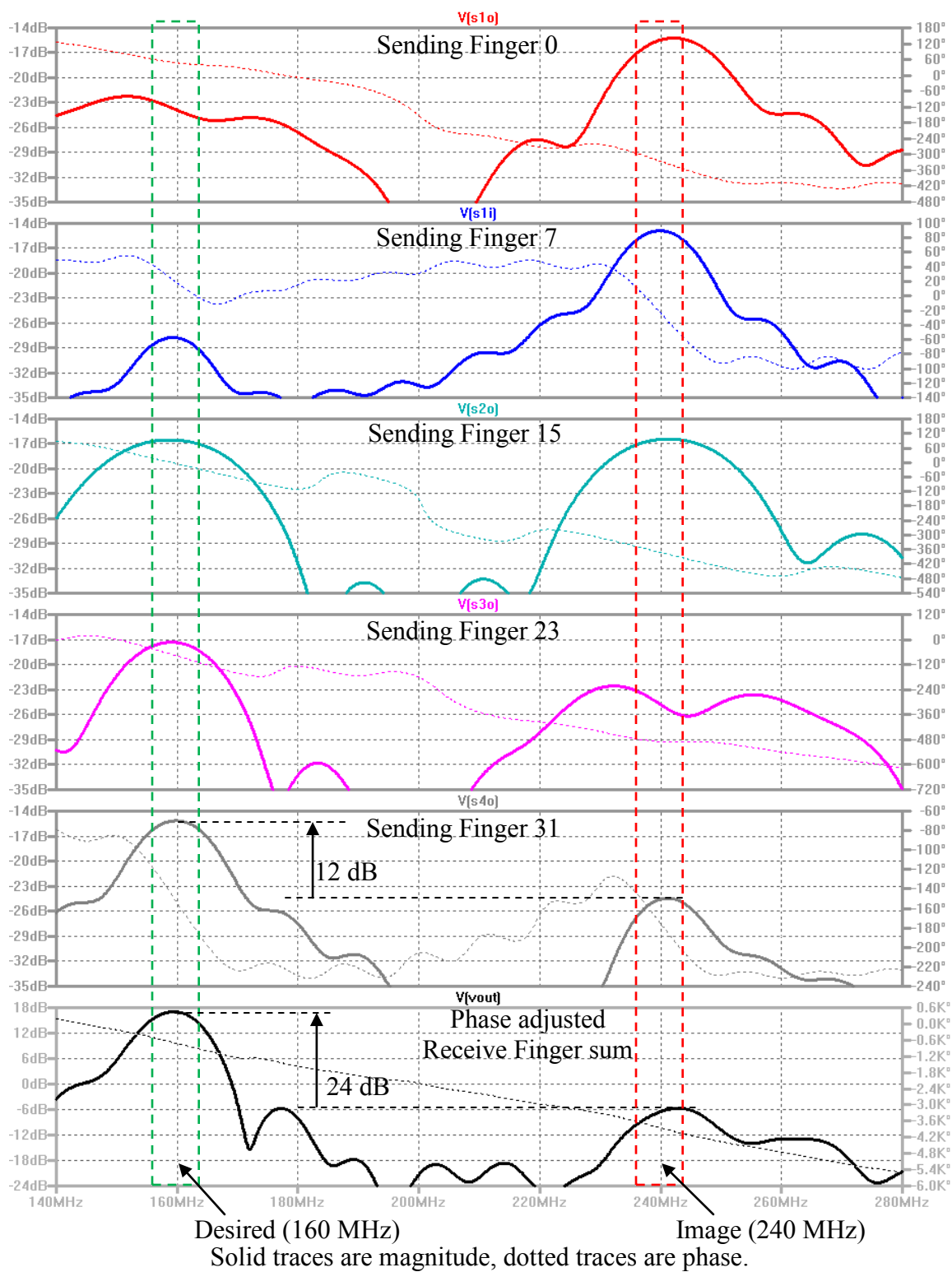


Figure 56. Acoustic amplitude of desired and image components vs. position

As the observation point moves toward Finger 0 the relative amplitude of the image signal increases and the opposite happens when the observation point moves toward Finger 31, the last of the sending fingers. It can also be observed that at Finger 31 the difference in amplitudes of the response at the desired frequency of 160 MHz is approximately 12 dB higher than the response at the undesired image frequency of 240 MHz. At the combined output of the phase rotated receive signal the response at the desired frequency is approximately 24 dB higher than the response at the image frequency. This increase in separation supports the reciprocity comment made previously.

The explanation for this phenomenon is simply that when the finger phases are set to provide constructive interference in the proper direction for the desired frequency they are inherently set to provide constructive interference in the opposite direction for the image frequency. This is the reason for taking care to minimize acoustic reflections from the edge of the piezoelectric surface. It also explains some of the anomalous behavior in the vicinity of the center frequency where this directionality is less effective.

There are several approaches available to address this issue. Various finger designs, generally referred to as Single Phase Unidirectional Transducers (SPUDTs) can significantly reduce this bidirectional response [101]. In some implementations of SAW devices the fingers are bifurcated to reduce their effective width, creating an effective SPUDT [102]. In general the drawback to SPUDT designs is that the increasing complexity of the finger geometry results in a larger effective finger pitch (and therefore a lower resonant frequency) for a given photolithographic process. The alternative of slight variations of finger pitch with a well-chosen pattern may also hold promise for

reducing this effect since there would no longer be a frequency that would support bidirectional transfer for all fingers.

5.4.2 Design Case 1 Simulation Results

Two types of simulations are run for each design. The initial type involves multiple simulations, each examining the response of the device over the entire frequency range of interest with the device configured for a specific desired resonant frequency. Starting with Design Case 1 (DC1) described previously, the simulation determines the frequency response at the arbitrarily chosen desired frequencies of 160 MHz, 200 MHz, and 240 MHz. The results are presented here graphically in Figure 57 through Figure 59. For each test the magnitude and phase of the response is plotted with the green circles on the phase plot appearing at increments of 360° showing the possible oscillation frequencies and the red dots on the amplitude plots appearing at the same frequencies but showing the amplitude of the response at that frequency. The title of the plot contains the target frequency and the frequency at which the phase is the multiple of 360° that is closest to the maximum amplitude response. The frequency at which this occurs is referred to as the Peak Phase Frequency and is the frequency at which an oscillator would typically find its resonant frequency.

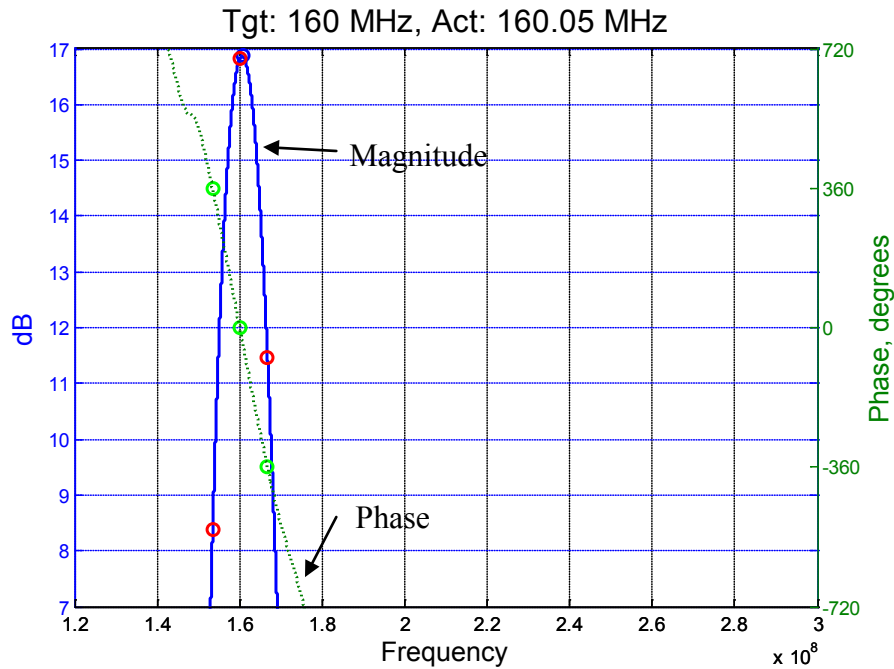


Figure 57. Results for a desired frequency of 160 MHz.

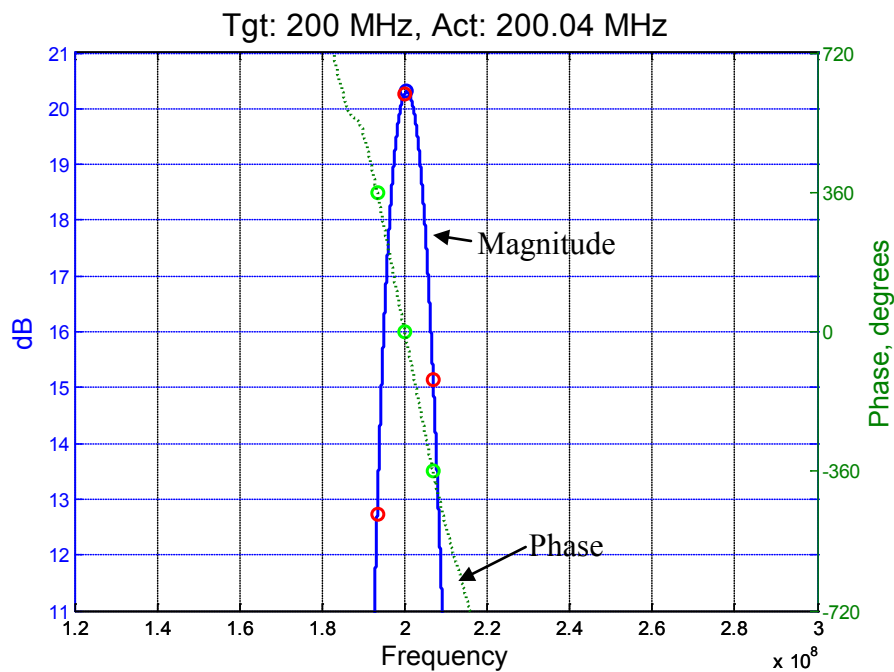


Figure 58. Results for a desired frequency of 200 MHz.

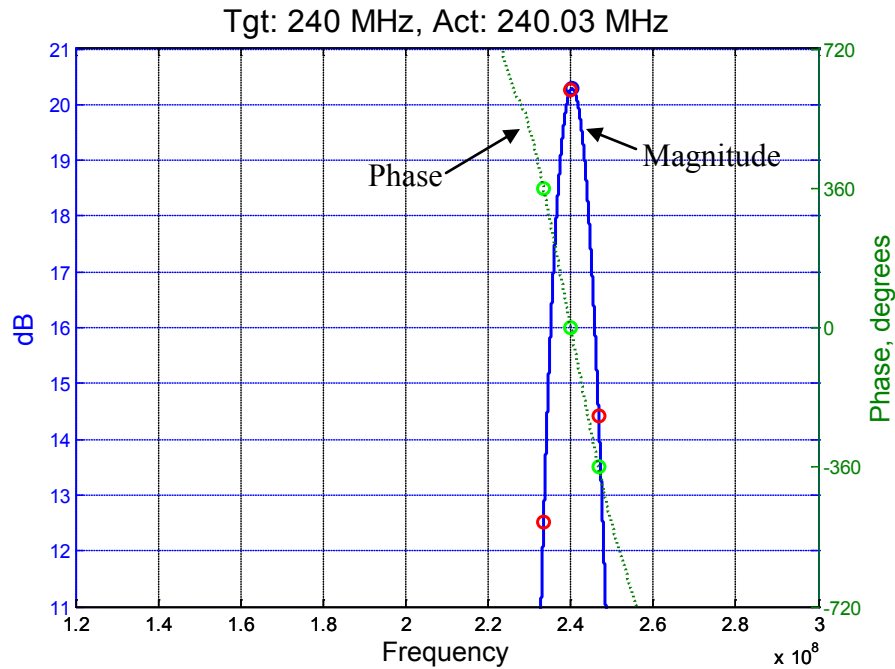


Figure 59. Results for a desired frequency of 240 MHz.

For each simulation run the simulator produces a variety of detailed results including the results shown in Table 6. The most important results are the “Peak Phase Frequency” and the “Phase at the Desired Frequency.” The phase at the desired frequency suggests the magnitude of the phase correction required to compensate for the phase error in order to tune an oscillator to the desired frequency in a phase-locked loop (PLL). Conversely, the Peak Phase Frequency suggests the frequency error that would be encountered without the appropriate phase correction. The Peak Amplitude result indicates the variation of gain required to achieve sufficient open-loop gain to initiate oscillation.

Table 6. Summary of simulation results.

Test Number	1	2	3
Desired Frequency:	160.00 MHz	200.00 MHz	240.00 MHz
Peak Amplitude:	16.88 dB	20.31 dB	20.29 dB
at frequency:	160.650 MHz	200.550 MHz	240.420 MHz
Peak Phase Frequency:	160.050	200.040 MHz	240.030 MHz
Phase at Desired Frequency:	2.61°	2.26°	1.85°

The simulation tool is easily adapted to produce a wide variety of analyses. Clearly, the results shown so far for this Design Case cover only three frequencies. The second type of simulation provides results similar to those shown in Table 6 for a wide variety of frequencies over the frequency range of interest. The simulation tool can also provide the results of this repetitive analysis. However, depending on the number of points of interest the simulation can take many hours or days to complete. An example of this analysis covering numerous frequency points is shown in Figure 60 through Figure 62. In Figure 60 the total phase shift through the SAW device and associated electronic circuit is shown at each analyzed frequency. Based on data from previous runs of similar simulations, certain system performance parameters such as excess propagation delay and phase shift through the electronics have been quantified. The values of these parameters are assigned to variables in the algorithm that determines the finger phases, resulting in precompensation for some of these global effects. The performance parameters shown in these plots are the results directly from the SPICE simulation of the entire device. The simulation can also analyze the statistics of this result. In this case the standard deviation of the phase is approximately 4 degrees. The simulations in this case were done at 100

kHz intervals over the 140 MHz operating frequency range, resulting in 1401 separate simulations.

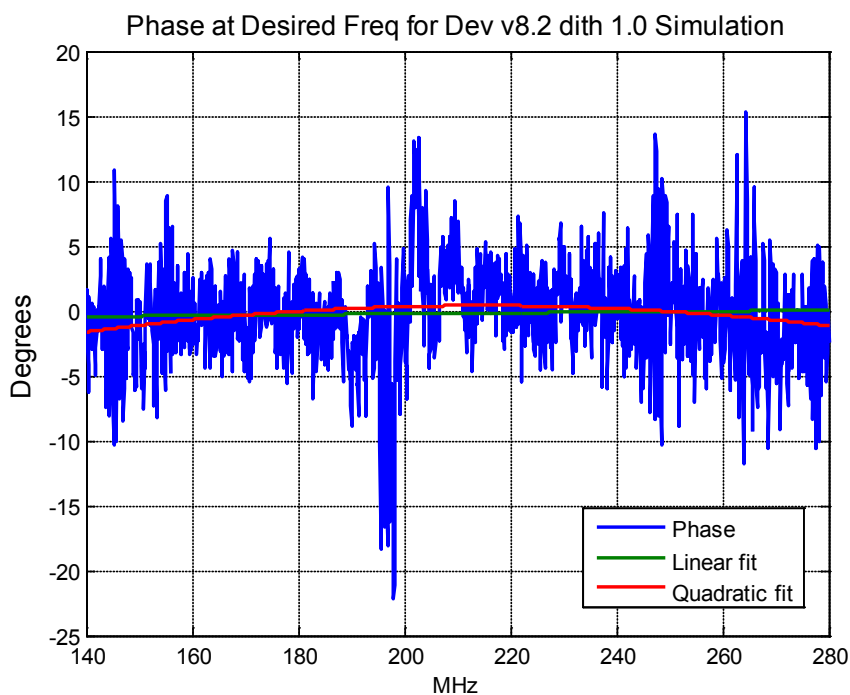


Figure 60. Phase at desired frequency for DC1.

The data in Figure 61 are similar to those of Figure 60 except the plot shows the simulated uncorrected resonant frequency of the device whereas Figure 60 shows the predicted phase correction that would need to be applied to achieve the desired frequency. In the three plots in Figure 60 through Figure 62 it is readily apparent that the results at the frequencies in the vicinity of 200 MHz fluctuate over a greater range than the results further from that center frequency. This fluctuation is due to SAW factors such as the increased triple-transit effect and the greater bidirectionality of the IDTs in

that frequency range, as well as a more uneven distribution of the phase shifts which results in poorer performance of the summing nodes.

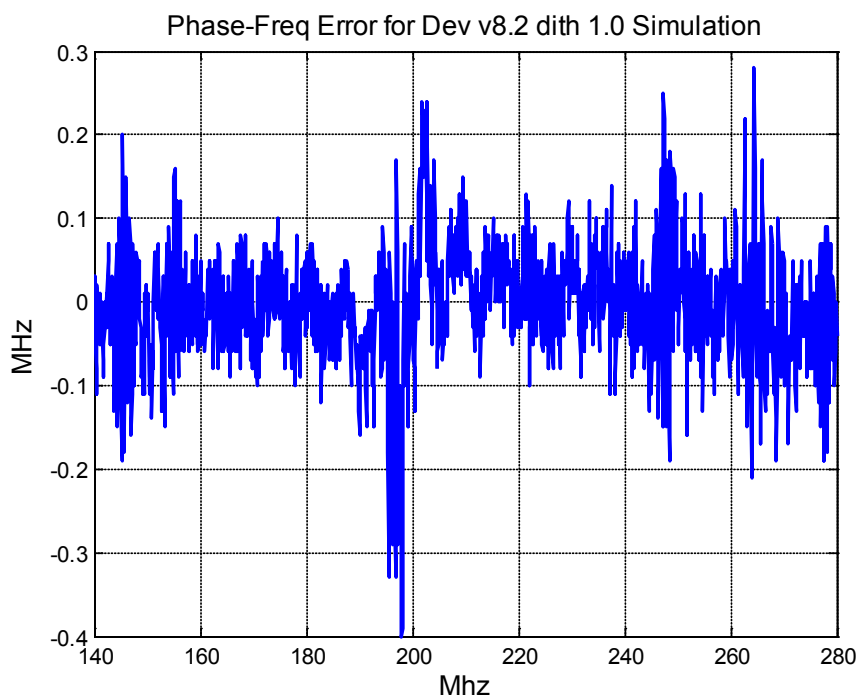


Figure 61. Frequency error for DC1.

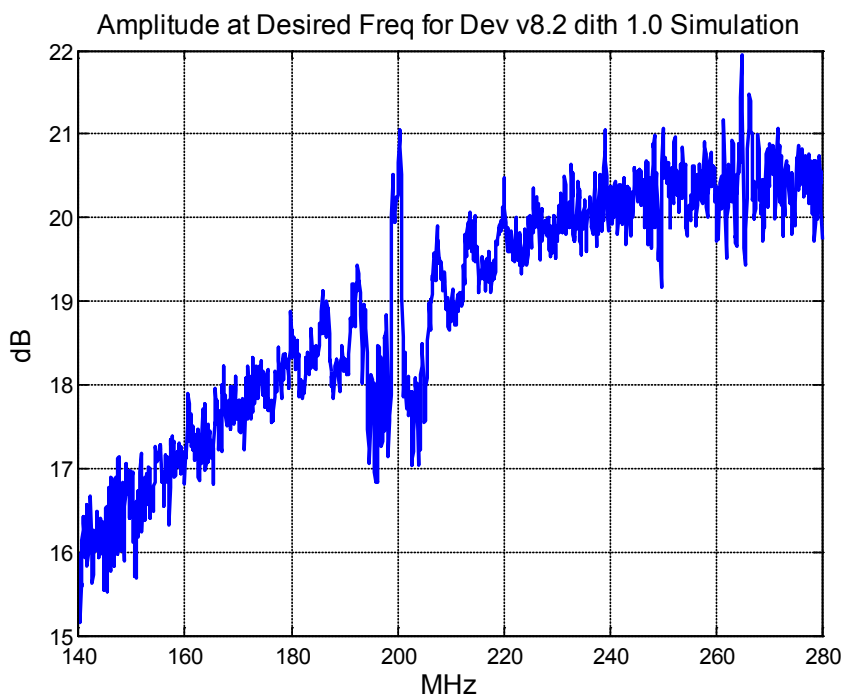


Figure 62. Amplitude response vs. frequency for DC1.

The results of Figure 62 show the amplitude at the desired frequency for each of the simulations. The gradual rise in the response is due largely to peaking capacitors, such as the capacitor C1 shown in Figure 41, added to the various inverters and buffers. Adjusting these values could result in a flatter amplitude response but result in a change in the phase response. The approximately 5 dB of variation can be easily compensated for with a variable gain RF amplifier.

5.4.3 Design Case 1a Simulation Results

Design Case 1a (DC1a) utilizes the same architecture and electronics as were used in DC1 except the finger spacing is changed by a factor of 4 to provide a center frequency of 800 MHz. The preliminary results from testing over a frequency range of 500 MHz to 1 GHz are very encouraging with the results from the end points of the

frequency range shown in Figure 63 and Figure 64. The primary limitation is the decrease of gain of about 8 dB over the octave which will require additional compensation to correct for. Based on Equations (7) and (9) the estimated Q for this configuration is $Q \approx 600$ at $f = 1\text{GHz}$.

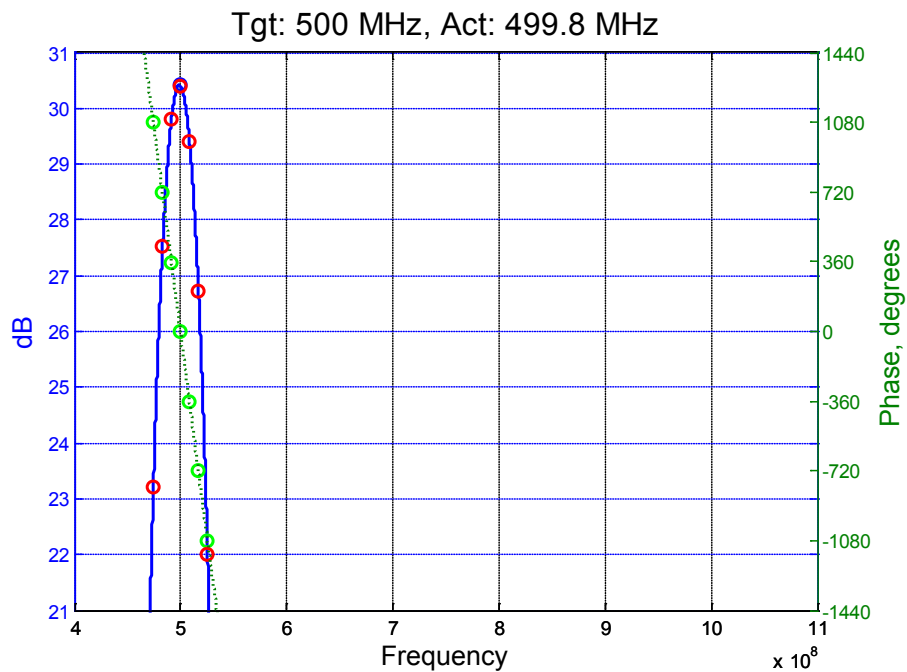


Figure 63. Results at 500 MHz for the high-frequency DC1a case.

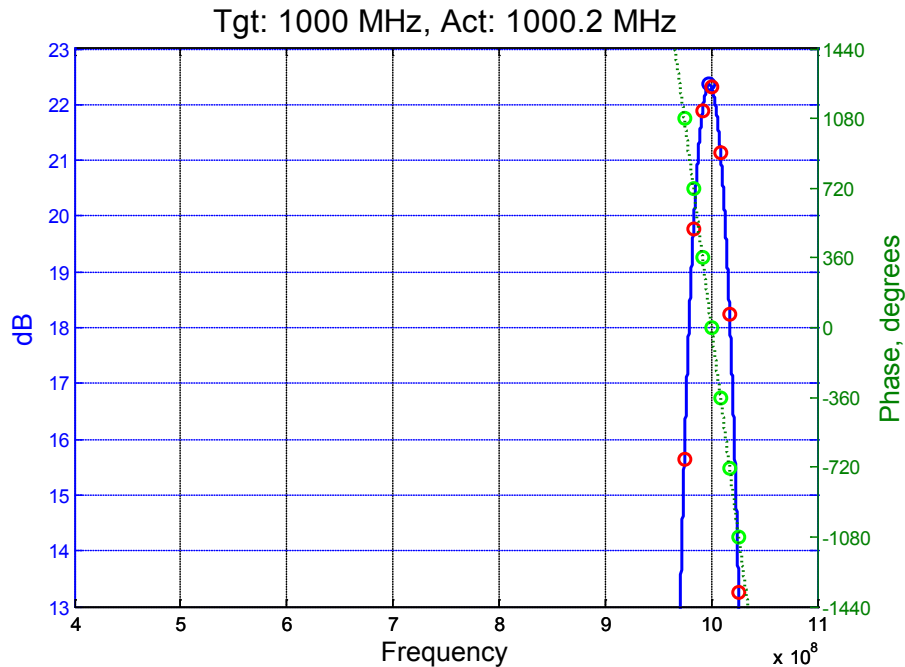


Figure 64. Results at 1 GHz for the high-frequency DC1a case.

5.4.4 Design Case 2 Simulation Results

Design Case 2 (DC2) can be simulated in a very similar manner. The results will show more phase variation than in DC1 because there is less isolation between fingers connected to the same phase and, therefore, more interaction. Consequently the phase relationships between the fingers are not as well controlled. The results for the same three frequencies are shown in Figure 65 through Figure 67.

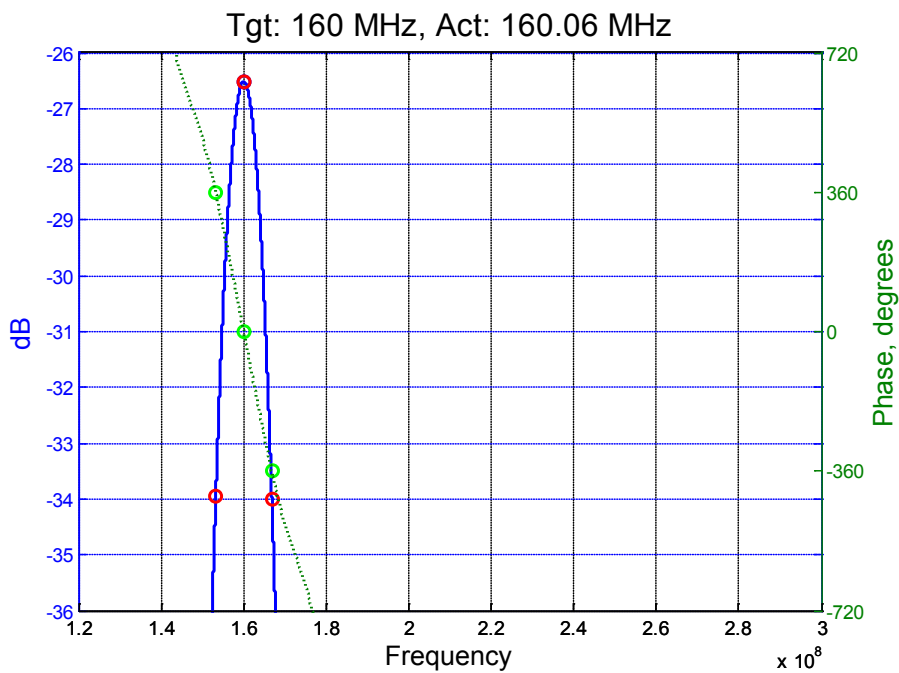


Figure 65. Results for a desired frequency of 160 MHz.

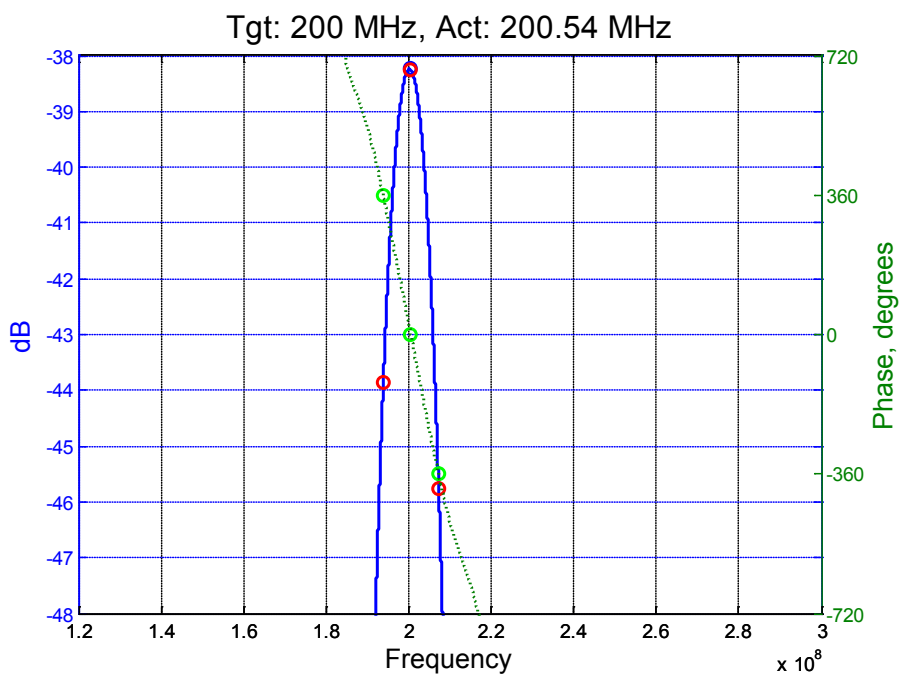


Figure 66. Results for a desired frequency of 200 MHz.

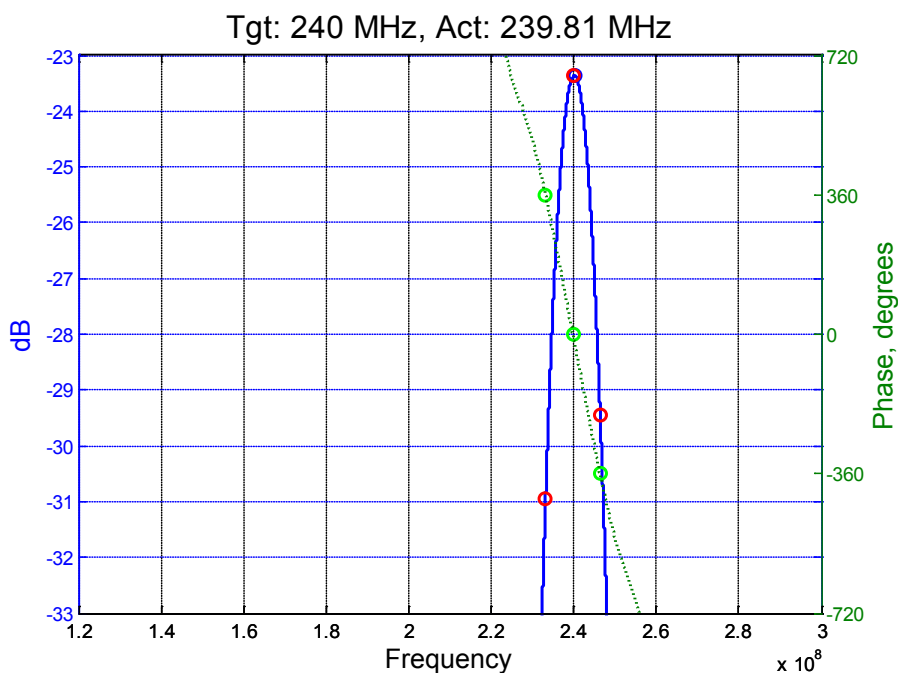


Figure 67. Results for a desired frequency of 240 MHz.

As with DC1, the same analysis can be performed with multiple frequencies. The results, as predicted, show less consistency. In this case the standard deviation of the phase is approximately 6.9° during a similar run of 1401 frequencies spaced at 100 kHz intervals. The largest phase error is approximately twice as large as with DC1. The performance of the DC2 design could probably be improved with additional buffering between fingers. Conversely, providing additional correction either through more sophisticated precompensation or additional loop phase compensation may provide very satisfactory performance with the benefit of lower power consumption and compatibility with non-volatile switching technology.

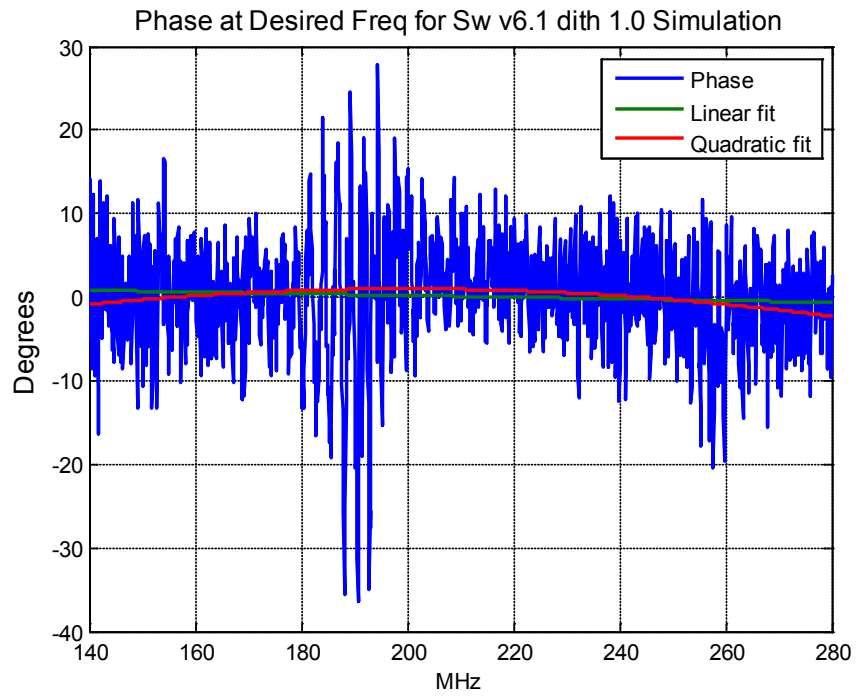


Figure 68. Phase at desired frequency for DC2.

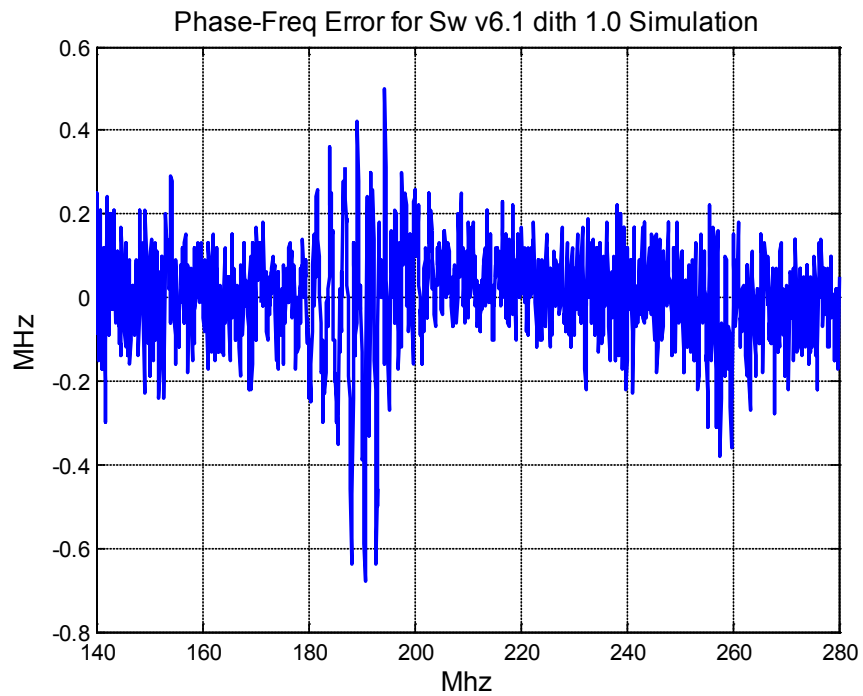


Figure 69. Frequency error for DC2.

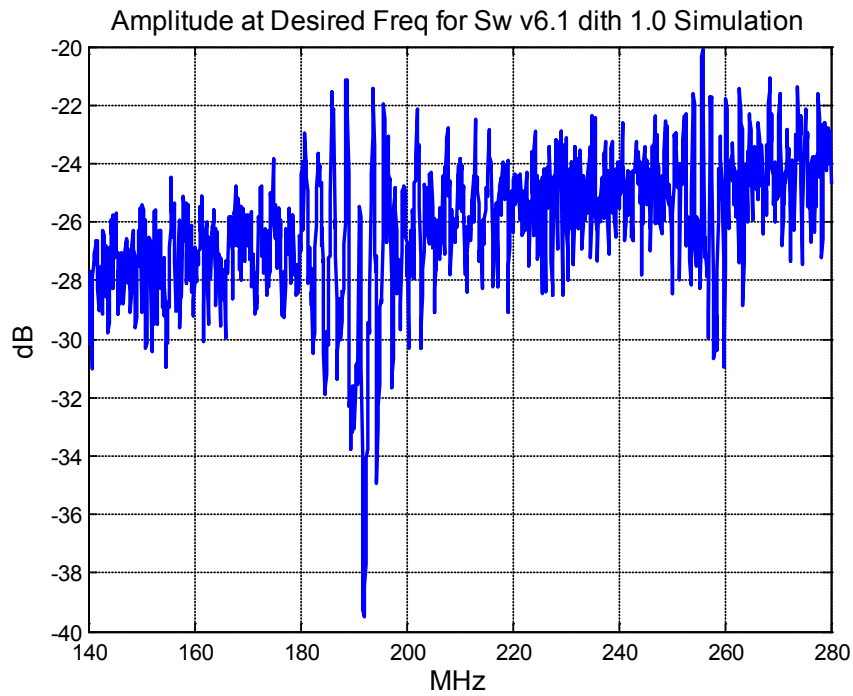


Figure 70. Amplitude response vs. frequency for DC2.

The data show that the overall performance of DC2 is less predictable than the performance of DC1. As with DC1, the greater fluctuation excursion in the frequencies around 200 MHz is due to SAW factors such as the triple-transit effect, increased bidirectionality of the IDTs, and the changes in phase shift distribution.

CHAPTER 6 CONCLUSIONS AND FUTURE WORK

6.1 Conclusions

The results of the design and simulations discussed in this dissertation support the premise that the techniques discussed offer a very viable approach to developing programmable SAW resonators. These devices can be used as resonators for high-Q oscillators, as programmable filters, correlators, convolvers, and in special applications such as programmable dispersive delay lines for chirp radar or as a device for detecting materials that may have frequency-sensitive properties. The simulations show that even with a limitation of eight levels of phase control per finger for each IDT the controllability of the resonant frequency is limited by the anomalies of the device physics and the process of accurately delivering the intended phase shifts to the fingers and not by the inherent resolution of the control process. The results suggest that there appears to be considerable opportunity to develop this technology further to extend the frequency range, to increase the Q of the resonator, and to extend the technology into additional application areas.

6.2 Future work

Future work can be focused initially on efforts to experimentally verify the theory presented in this dissertation. This work can include:

- Prototype the concept on a piezoelectric substrate with several pre-programmed frequency responses.
- Characterize approaches to developing the phase shifts and switching the phases to the fingers.
- Develop thin-film processes for depositing and patterning piezoelectric materials on an integrated circuit with the SAW fingers integrally connected to the appropriate circuits.
- Determine appropriate integrated circuit processes and lay out a test chip to use for the integration.

The second focus will be to improve simulation capability, particularly in the area of developing or acquiring tools to characterize finger impedances, along with the SAW attenuation and reflection properties.

REFERENCES CITED

-
- [1] S. Kati, *The Beginnings of Piezoelectricity: A Study in Mundane Physics*, Springer-Verlag, 2006, p 15
- [2] L. Rayleigh, "On Waves propagated along the Plane Surface of an Elastic Solid," *Proceedings of the London Mathematical Society*; 17-1, 1885, pp. 4-11.
- [3] D. Morgan, "A History of Surface Acoustic Wave Devices," *Advances in Surface Acoustic Wave Technology, Systems, and Applications*, edited by C. Ruppel and T. Fjeldly, World Scientific, 2000, pp. 1-39.
- [4] M.G. Holland, L.T. Claiborne, "Practical Surface Acoustic Wave Devices," *Proc IEEE*, Vol 62, No 5, May 1974, pp 582 – 611.
- [5] A. Hachigo, D. Malocha, "Apodization Design Technique for Layered Structure SAW Devices," *1997 IEEE Ultrasonics Symposium*, Oct 5-8, 1997, pp. 205-209.
- [6] M. P. da Cunha, E. L. Adler, "High Velocity Pseudosurface Waves (HVPSAW)," *IEEE Trans o Ultrasonics, Ferroelectrics, and Frequency Control*, Vol. 42, No. 5, Sept. 1995, pp. 840 – 844.
- [7] C. Campbell, Applications of Surface Acoustic and Shallow Bulk Acoustic Wave Devices,; *Proceedings of the IEEE*, Vol 77, No. 10, October 1989, pp. 1453 – 1484.
- [8] Y. Fusero, S. Ballandras, J. Desbois, J. Hode, P. Ventura, "SSBW to PSAW Conversion in SAW Devices Using Heavy Mechanical Loading," *IEEE Transactions on Ultrasonics, Ferroelectrics, and Frequency Control*, Vol. 49, No. 6, June 2002, pp. 805 – 814.
- [9] M. P. daCunha, "Effects of Layer Thickness for SAW, PSAW, and HVPSAW Devices," *IEEE Trans Ultrasonics, Ferroelectrics, and Freq Control*, Vol 48, No. 1, Jan. 2001, pp. 93 – 99.
- [10] J. G. Gualtieri, J. A. Kosinski, and A. Ballato, "Piezoelectric materials for surface acoustic wave applications," in *Proc. 1992 IEEE Ultrasonics Symp.*, Oct. 1992, pp. 403-412.

-
- [11] J. G. Gualtieri, J. A. Kosinski, and A. Ballato, "Piezoelectric materials for acoustic wave applications," *IEEE Trans Ultrasonics, Ferroelectrics, and Freq Control*, Vol 41, No. 1, January 1994 pp. 53 - 59.
- [12] M. Kadota, T Kimura, "High-Frequency Resonators with Excellent Temperature Characteristics using Edge Reflection," *IEEE Frequency Control Symposium*, 2007, May 29, 2007-Jun 1, 2007, pp 154-159.
- [13] E. Papadakis, *Ultrasonic Instruments and Devices*, Academic Press, 1999, p. 580.
- [14] V.M. Hietala, S.A. Casalnuovo, E.J. Heller, J.R. Wendt, G.C Frye-Mason, A.G. Baca, "Monolithic GaAs Surface Acoustic Wave Chemical Microsensor Array," *IEEE MTT-S Digest*, 2000, pp. 1965 – 1968.
- [15] T. W. Grudkowski, G.K. Montress, M. Gilden, J.F. Black, "Integrated Circuit Compatible Surface Acoustic Wave Devices on Gallium Arsenide," *IEEE Trans. Microwave Theory and Techniques*, vol. 29, pp. 1348-1356, 1981.
- [16] M. Feldmann, J. Henaff, M Kirov, "SAW and SSBW Propagation in Gallium-Arsenide," *IEEE Ultrasonics Symposium*, 1981, pp. 264 – 267.
- [17] D. Morgan, "A History of Surface Acoustic Wave Devices," *Advances in Surface Acoustic Wave Technology, Systems, and Applications*, edited by C. Ruppel and T. Fjeldly, World Scientific, 2000, p. 7.
- [18] Phonon Corporation Web Site, "Introduction to SAW," <http://www.phonon.com/sawintro.asp>.
- [19] V. Mortet, O. Elmazria, M. Nesladek, M.B. Assouar, G. Vanhoyland, J. D'Haen, M. D'Olieslaeger, P. Alnot, "Surface acoustic wave propagation in aluminum nitride-unpolished freestanding diamond structures," *Appl. Phys. Lett.*, Vol 81, No.9 (Aug. 26, 2002), pp. 1720 – 1722.
- [20] P. Kirsch, M.B. Assouar, O. Elmazria, and P. Alnot, "5GHz SAW devices based on AlN/diamond layered structure," *IEEE Ultrasonics Symposium*, Oct. 2-6 2006, pp 2293 – 2296.
- [21] A. Rukhlenko, "Iterative WLS Design of SAW Bandpass Filters," *IEEE Trans on Ultrasonics, Ferroelectrics, and Frequency Control*, Vol 54, October 2007, pp. 1930 – 1935.
- [22] R. H. Tancrell, M. G. Holland, "Acoustic Surface Wave Filters," *Proceedings of the IEEE*, Vol 59, March 1971, pp. 393 – 409.

-
- [23] M. F. Lewis, "Triple-Transit Suppression in Surface-Acoustic-Wave devices," *Electronics Letters*, Vol 8, Number 23, November 16, 1972, pp. 553 – 554.
- [24] A.R. Reddy, "Design of SAW Bandpass Filters Using New Window Functions," *IEEE Trans Ultrasonics, Ferroelectrics, and Frequency Control*, Vol. 35, January 1988, pp. 50 – 56.
- [25] J. Lamperski, "Saw Filters With Weighted Tapered Interdigital Transducers," *IEEE Ultrasonics Symposium*, 2003, pp. 203 – 206.
- [26] T.E. Parker, "Precision Surface-Acoustic-Wave (SAW) Oscillators," *IEEE Trans Ultrasonics, Ferroelectrics, and Frequency Control*, 35/3, May 1988, pp.342-364.
- [27] G.K. Montress and T.E. Parker, "Design and Performance of an Extremely Low Noise Surface Acoustic Wave Oscillator," *IEEE International Frequency Control Symposium*, 1994, pp 365-373.
- [28] T.E. Parker, G.K. Montress, "Spectral Purity of Acoustic Resonator Oscillators," *IEEE Frequency Control Symposium*, 1992, pp. 340 – 348.
- [29] R. Rhea, *Oscillator Design and Computer Simulation*, Second Edition, Noble Publishing, 1995, pg. 60.
- [30] A.J. Budreau and P.H. Carr, "Temperature Dependence of the Attenuation of Microwave Frequency Elastic Surface Waves in Quartz," *Applied Physics Letters*, V 8, N.6, March 1971, pp 239 – 241.
- [31] A. Das, S. Das, *Microwave Engineering*, McGraw Hill, 2000, pp 240 ff
- [32] M. Lewis, "Some aspects of SAW oscillators," *IEEE Conference on Sonics and Ultrasonics*, Monterey, CA, 1973, paper C8.
- [33] D. Morgan, *Surface Acoustic Wave Filters With Applications to Electronic Communications and Signal Processing*, Elsevier, Second Edition, 2007, p. 15.
- [34] C. E. Shannon, "A Mathematical Theory of Communication," *The Bell System Technical Journal*, Vol. 27, pp. 379 – 423, 623 – 656, July, October, 1948.
- [35] D. B. Leeson, "A Simple Model of Feedback Oscillator Noise Spectrum," *Proceedings of the IEEE*, February 1966, pp. 329 – 330.
- [36] T. E. Parker, G. K. Montress, "Spectral Purity of Acoustic Resonator Oscillators," *IEEE Frequency Control Symposium*, 1992, pp. 340 – 348.

-
- [37] T. H. Lee, *The Design of CMOS Radio-Frequency Integrated Circuits*, Cambridge University Press, Second Edition, 2004, pp. 667ff.
- [38] E. EerNisse, "Calculations on the Stress Compensated (SC-Cut) Quartz Resonator," *30th Annual IEEE Symposium on Frequency Control*, June 1976, pp. 8-11
- [39] Crystek Corporation CVCSO-914-1000 Data Sheet, available at <http://www.crystekcrystals.com/crystal/spec-sheets/vcxo/CVCSO-914-1000.pdf>, Fall 2008
- [40] G.K. Montress, T.E. Parker, D. Andres, "Review of SAW Oscillator Performance," *IEEE Ultrasonics Symposium*, 1994, pp. 43 – 54.
- [41] Micro Lambda Wireless, Inc.
http://www.microlambdawireless.com/YIG_Oscillators/EMYTOs/MLOS-P_Series.htm .
- [42] Bliley Technologies, Inc.
http://www.bliley.com/datasheets/Bliley_NV47AG_1.1x1.4_OCXO.pdf .
- [43] Agilent Technologies E5500 Series
<http://cp.literature.agilent.com/litweb/pdf/5965-7589E.pdf> .
- [44] Agilent Technologies E8663B Analog Signal Generator
<http://cp.literature.agilent.com/litweb/pdf/5989-4866EN.pdf> .
- [45] C. Voltaire, *Dictionnaire Philosophique*, 1764
- [46] H. Nakahata, A. Hachigo, K. Itakura, S. Fujii, S. Shikata, "SAW Resonators of SiO₂/ZnO/Diamond Structure in the GHz Range," *Proceedings of the 2000 IEEE/EIA International Frequency Control Symposium and Exhibition*, June 9, 2000.
- [47] F. Hickernell, "Thin-Films for SAW Devices," *Advances in Surface Acoustic Wave Technology, Systems, and Applications*, edited by C. Ruppel and T. Fjeldly, World Scientific, 2000, pp. 51 ff.
- [48] L. Le Brizoual, F. Sarry, O. Elmizria, P. Alnot, "GHz Frequency ZnO/Si SAW Device," *IEEE Ultrasonics Symposium*, 2005, pp. 2174-2177.
- [49] E.Ntagwirumugara, T.Gryba, V. Zhang, J. Carlier and J.E. Lefebvre, "Fabrication of 945 MHz Band Film Surface Acoustic Wave Resonators Using ZnO Thin Film with Si Substrate," *IEEE Frequency Control Symposium*, 2007, pp. 176-180.

-
- [50] F.S. Hickernell, H.M. Liaw, "The Structural and Acoustic Properties of Sputtered Aluminum Nitride on Silicon," *Proceedings of the Ninth IEEE International Symposium on Applications of Ferroelectrics*, 1994, ISAF '94, Aug. 7-10 1994, pp 543-546
- [51] H.M. Liaw, F.S. Hickernell, "The Characterization of Sputtered Polycrystalline Aluminum Nitride on Silicon by Surface Acoustic Wave Measurements," *IEEE Transactions on Ultrasonics, Ferroelectrics, and Frequency Control*, Vol 42, No. 3, May 1995, pp 404 – 409.
- [52] H.M. Liaw, F.S. Hickernell, "SAW Characteristics of Sputtered Aluminum Nitride on Silicon and Gallium Arsenide," *IEEE Ultrasonics Symposium*, 1994, pp. 375 – 379.
- [53] M. Kadota, T. Kasanami, M. Minakata, "Deposition and Piezoelectric Characteristics of ZnO Films by Using an ECR Sputtering System," *IEEE Transactions on Ultrasonics, Ferroelectrics, and Frequency Control*, Vol 41, No. 4, July 1994, pp 479 – 483.
- [54] O. Fouad, A. Ismail, Z. Zaki, R. Mohamed, "Zinc Oxide Thin Films Prepared by Thermal Evaporation Deposition and its Photocatalytic Activity," *Applied Catalysis B Environmental*, Vol 62, No. 1-2, pp. 144 – 149, Jan. 10, 2006.
- [55] S. Lee, Y. Im, Y. Hahn, "Two-Step Growth of ZnO Films on Silicon by Atomic Layer Deposition," *Korean J. Chem. Eng.*, Vol 22, No. 2, Feb. 2005, pp. 334 – 338.
- [56] G. Du, Y. Chang, Y. Zhang, Y. Ma, X. Yang, B. Zhao, "ZnO Thin Films Growth, Characteristics, and Applications," *Proceedings of the 7th International Conference on Solid-State and Integrated Circuits Technology*, 2004, Oct. 18-21, 2004, pp. 2361 – 2365.
- [57] J. Visser, M. Vellekoop, A. Venema, E. van der Drift, P. Rek, A. Nederlof, M. Nieuwenhuizen, "Surface Acoustic Wave Filters in ZnO-SiO₂-Si Layered Structures," *1989 Ultrasonics Symposium*, Oct 3 – 6, 1989, pp 195 – 200.
- [58] W. Shih, R. Huang, "Fabrication of high frequency ZnO thin film SAW devices on silicon substrate with a diamond-like carbon buffer layer using RF magnetron sputtering," *Vacuum*, Vol 83, 2009, pp. 675 – 678.
- [59] F. Moeller, T. Vandahl, D. Malocha, N. Schwesinger, W. Buff, "Properties of Thick ZnO Layers on Oxidized Silicon," *1994 Ultrasonics Symposium*, Nov 1-4, 1994, pp. 403 - 406

-
- [60] K. Iwata, P. Fons, S. Niki, A. Yamada, K. Matsubara, K. Nakahara, T. Tanabe, H. Takasu, "ZnO Growth on Si by Radical Source MBE," *Journal of Crystal Growth*, Vol. 214-215, 2 June 2000, pp. 50-54.
- [61] H. Kim, Y. Lee, Y. Roh, J. Jung, M. Lee, and H. Kwon, "Development of ZnO Thin Films for SAW Devices by the Ultrasonic Spray Pyrolysis Technique," *1998 IEEE Ultrasonics Symposium*, Oct. 1998, pp. 323 - 326
- [62] F. Hickernell, "Zinc-Oxide Thin-Film Surface-Wave Transducers," *Proceedings of the IEEE*, Vol 64, No. 5, May 1976, pp. 631 - 635.
- [63] H. Wu, N. Emanetoglu, G. Saraf, J. Xhu, P. Wu, Y. Chen, Y. Lu, "SAW Analysis of the $Mg_xZn_{1-x}O/SiO_2/Si$ System," *2003 IEEE Ultrasonics Symposium*, Oct 2003, pp. 897 - 900
- [64] S. Trolrier-McKinstry, P. Murali, "Thin Film Piezoelectrics for MEMS," N. Setter, ed., *Electroceramic-Based MEMS: Fabrication-Technology and Applications*, Ch. 10, Springer Science+Business Media, Inc., 2005, pp 205 - 207.
- [65] R. Tancrrell, "Analytic Design of Surface Wave Bandpass Filters," *IEEE Trans. on Sonics and Ultrasonics*, Vol Su-21, No. 1, Jan 1974, pp 12-21.
- [66] J. Zhu, N. W. Emanetoglu, Y. Lu, J. A. Kosinski, R. A. Pastore, "A Multi-IDT Input Tunable Surface Acoustic Wave Filter," *IEEE Transactions on Ultrasonics, Ferroelectrics, and Frequency Control*, Vol 48, No. 5, Sept 2001, pp. 1383 - 1388.
- [67] M. Elkordy, "Study of Voltage Tunable SAW Hybrid Devices," *IEEE Symposium on Antennas, Propagation, and EM Theory*, Nov. 2003, pp. 750 - 753.
- [68] M. Rotter, W. Ruile, A. Wixforth, J. Kotthaus, "Voltage Controlled SAW Velocity in GaAs/LiNbO₃-Hybrids," *IEEE Trans on Ultrasonics, Ferroelectrics, and Frequency Control*, Vol 46, No. 1, Jan. 1999, pp. 120 - 125.
- [69] D.C. Webb, D.W. Forester, A.K. Ganguly, C. Vittoria, "Applications of Amorphous Magnetic-Layers in Surface-Acoustic-Wave Devices," *IEEE Trans on Magnetism*, Vol Mag-15, No. 6, Nov. 1979, pp. 1410 - 1415.
- [70] V. Ermolov, M. Luukkala, "Tunable SAW Comb Filter," *Electronics Letters*, Vol 27, No. 18, August 29, 1991, pp. 1670 - 1671.
- [71] G. K. Montress, T. E. Parker, D. W. Kress, J. A. Kosinski, "Design and Performance of a Low Noise, Wide Tuning Range AWP SAW Delay Line VCO," *IEEE Frequency Control Symposium*, 1992, pp. 356 - 370.

-
- [72] J. Lin, Y. Kao, "A Low Phase-Noise Voltage-Controlled SAW Oscillator With Surface Transverse Wave Resonator for SONET Application," *IEEE Trans on Microwave Theory and Techniques*, Vol 55, No. 1, Jan. 2007, pp. 60 – 65.
- [73] R.I. Amorosi, C.K. Campbell, "Studies of a Tunable SAW Oscillator Using a Differential SAW Delay Line with MOSFET Control," *IEEE Trans on Sonics and Ultrasonics*, Vol. SU-32, No. 4, July 1985, pp 574-582.
- [74] T. Kenny, Y.C. Park, W.D. Hunt, J.S. Kenney, J. Kosinski, R. Pastore, "Wideband Programmable SAW Filters," *2001 IEEE Ultrasonics Symposium*, pp 89-92.
- [75] R. Pastore, J.A. Kosinski, H.L. Cui, "An Improved Tunable Filter Topology for HF Preselection," *1998 IEEE International Frequency Control Symposium*, pp 575-579.
- [76] T. Kenny, Y. Park, W. Hunt, J. Kenney, "Wideband Programmable SAW Filters," *2001 IEEE Ultrasonics Symposium*, Oct. 10, 2001, Vol 1, pp. 89-92.
- [77] C. Panasik, "250 MHz Programmable Transversal Filter," *1981 IEEE Ultrasonics Symposium*, pp. 48-52.
- [78] C. Panasik, "SAW Programmable Transversal Fiter for Adaptive Interference Suppression," *1982 IEEE Ultrasonics Symposium*, pp. 100 – 103.
- [79] C. Panasik, J. Toplicar, "Adaptive Interference Suppression using SAW Hybrid Programmable Transversal Filters," *1983 IEEE Ultrasonics Symposium*, pp. 170 – 174.
- [80] D. Zimmerman, C. Panasik "A 16-Tap Hybrid Programmable Transversal Filter using Monolithic GaAs Dual-gate FET Array," *IEEE MTT-S Digest*, 1985, pp. 251 – 254.
- [81] J. Duquesnoy, J. Poncot, H. Gautier, J. Do Huu, J. Uro, M. Peltier, "A Monolithic 7 Tap-programmable Transversal Filter on Gallium Arsenide," *1984 IEEE Ultrasonics Symposium*, pp. 303 – 307.
- [82] D. Oates, D. Smythe, J. Green, R. Ralston, A. Anderson, "Wide-BAND SAW/FET Programmable Transversal Filter,:" *1984 IEEE Ultrasonics Symposium*, pp. 312 – 317.
- [83] D. Oates, D. Smythe, J. Green, "SAW/FET Programmable Transversal Filter with 100-MHz Bandwidth and Enhanced Programmability," *1985 IEEE Ultrasonics Symposium*, pp. 124 – 129.

-
- [84] E. Oates, J. Green, P. Grant, "SAW-Based 100 MHz-Bandwidth Adaptive Filter," *Electronics Letters*, September 11, 1986, No. 19, pp. 998 – 999.
- [85] A. van Rhijn, G. Lubking, J. Haartsen, "A fully silicon integrated SAW programmable transversal filter with programming/read-out circuitry," 1991 IEEE Ultrasonics Symposium, pp. 89 – 94.
- [86] B. Hunsinger, A. Franck, "Programmable Surface-Wave Tapped Delay Line," *IEEE Transactions on Sonics and Ultrasonics*, Vol. SU-18, No. 3, July 1971, pp. 152 – 154.
- [87] F. Guediri, R. Martin, B. Hunsinger, F. Fliegel, "Performance of Acoustic Charge Transport Programmable Tapped Delay Line," 1987 IEEE Ultrasonics Symposium, pp. 11 – 14.
- [88] J.A. Kosinski, R.A. Pastore, "Programmable saw filter including unidirectional transducers," U.S. Patent 6,459,345, issued October 1, 2002.
- [89] J. Zhu, Y. Lu, J. Kosinski, R. Pastore, "Programmable surface acoustic wave (SAW) filter," U.S. Patent 6,541,893, issued April 1, 2003.
- [90] K. Hashimoto, *Surface Acoustic Wave Devices in Telecommunications, Modeling and Simulation*, Springer-Verlag, ISBN 3-540-67232, 2000, Ch 7, pp. 191 ff.
- [91] V. Plessky, J. Koskela, "Coupling-of-modes Analysis of SAW Devices," *Advances in Surface Acoustic Wave Technology, Systems, and Applications (Vol 2)*, Ed. By C. Ruppel, T. Fjeldy, World Scientific, 2001, pp 1 – 81.
- [92] D. Morgan, *Surface Acoustic Wave Filters With Applications to Electronic Communications and Signal Processing*, Elsevier, Second Edition, 2007, pp. 238 – 260.
- [93] K. Hashimoto, "Fast Determination of Coupling-of-Modes Parameters Based on Strip Admittance Approach," 1999 IEEE Ultrasonics Symposium, Vol. 1, October 17-20, 1999, pp. 93 – 96.
- [94] A. Bhattacharyya, S. Tuli, S. Majurndar, "SPICE simulation of surface acoustic wave interdigital transducers," *IEEE Transactions on Ultrasonics, Ferroelectrics, and Frequency Control*, v. 42, n. 4, pp 784-6, July 1995.
- [95] K. Hohkawa, T. Suda, Y. Aoki, C. Hong, C. Kaneshiro, K. Koh, "Design on semiconductor coupled SAW convolver," *Proceedings of the 2000 12th IEEE International Symposium on Applications of Ferroelectrics*, Vol 1, July 21 – Aug 2 2000, pp. 325-328.

-
- [96] C. Hartmann, T. D. Bell, Jr. R. Rosenfeld, “Impulse Model Design of Acoustic Surface-Wave Filters, *IEEE Transactions on Microwave Theory and Techniques*, Vol. 21, No. 4, April 1973, pp. 162 – 175.
- [97] Information is available at <http://www.mosis.com/products/fab/vendors/amis/c5/> .
- [98] The MOSIS Service, Marina del Rey, CA. <http://www.mosis.com/> .
- [99] R. Jacob Baker, *CMOS Circuit Design, Layout, and Simulation*, John Wiley and Sons Publishers, Revised Second Ed., 2008, pg 650, Figure 20.47.
- [100] Many such devices are available from various suppliers. An example can be found at <http://minicircuits.com/pdfs/QCN-3+.pdf>.
- [101] D. Morgan, *Surface Acoustic Wave Filters with Applications to Electronic Communications and Signal Processing*, Elsevier, Ltd, Second Ed., 2007, Ch 9, pp. 263 – 292.
- [102] H. Nakamura, T. Yamada, T. Ishizaki, K Nishimura, “A New Design Concept for Low-Loss SAW Filters Based on Different-Width Split-Finger SPUDT,” *IEEE Trans on MTT*, Vol 49, No. 4, April 2001, pp 761-768.